



**UNIVERSITÀ DI PARMA**

**UNIVERSITÀ DEGLI STUDI DI PARMA**

DOTTORATO DI RICERCA IN  
“Scienza e tecnologia dei materiali”  
CICLO XXXIV

**FUNCTIONAL POLYMERIC MICRO- AND  
NANO-CONTAINERS FOR DRUG DELIVERY: IMAGE  
RECONSTRUCTION FROM COHERENT X-RAY  
DIFFRACTION, ENCAPSULATION OF BIOACTIVE  
COMPOUNDS AND MULTICOMPOUND TARGETED  
DELIVERY**

Coordinatore:  
Chiar.mo Prof. Enrico Dalcanale

Tutore:  
Dr. Victor Erokhin

Dottoranda:  
Adeliia Faizullina

Anni Accademici 2019/2022

---

## **ABSTRACT**

Drug delivery is a promising field, directed for a transfer of desirable chemical or therapeutic substances to a certain point. For this case different systems can be used and capsules synthesized by *layer-by-layer* technique are among the most promising ones.

These capsules can be synthesized using different polymers for the shell formation and different templates, where this shell will be formed. It is quite important to study the structure of these objects. Moreover, it is necessary to study the capsules in their natural surroundings, in a liquid one. For the first time these types of objects were studied in a liquid medium by Coherent X-ray Diffraction imaging. There is a significant difference in images that were obtained for dried and liquid samples.

When hollow capsules are synthesized, they can be loaded with different substances. In this work the capsules were loaded with such biologically active compounds as aquacobalamin (Vitamin B12) and dimeglumine chlorin E6. These compounds were encapsulated for the first time into this type of microcontainers. For a better and more precise delivery the shell of the capsules can be functionalized. For this reason, magnetite nanoparticles were incorporated into the shell. This allows to use external magnetic field for targeted delivery. Moreover, this

incorporation of magnetite nanoparticles made it possible to bring two types of capsules, loaded by different substances, in one zone. After the targeted delivery, encapsulated substances were released in this targeted zone by varying the pH of surrounding solution.

# TABLE OF CONTENTS

<b>ABSTRACT</b>	<b>i</b>
<b>LIST OF FIGURES</b> . . . . .	<b>v</b>
<b>LIST OF TABLES</b> . . . . .	<b>x</b>
<b>LIST OF ABBREVIATIONS</b> . . . . .	<b>xi</b>
<b>1 INTRODUCTION</b>	<b>1</b>
1.1 <i>DRUG DELIVERY SYSTEMS</i> . . . . .	2
1.2 <i>LAYER-BY-LAYER TECHNIQUE</i> . . . . .	5
1.2.1 <i>Polymeric drug delivery system</i> . . . . .	5
1.2.2 <i>Polyelectrolyte self-assembling technique</i> . . . . .	6
1.2.3 <i>Layer-by-layer capsules for drug delivery</i> . . . . .	9
1.2.4 <i>Templates for capsule assembly</i> . . . . .	10
1.2.5 <i>Polymers</i> . . . . .	12
1.2.6 <i>Stimuli for encapsulation and release</i> . . . . .	15
1.3 <i>COHERENT X-RAY DIFFRACTION IMAGING</i> . . . . .	21
1.4 <i>MAGNETIC NANOPARTICLES</i> . . . . .	31
1.4.1 <i>Magnetic nanoparticles in drug delivery</i> . . . . .	33
1.4.2 <i>NP in layer-by-layer technique</i> . . . . .	35
<b>2 MATERIALS AND METHODS</b>	<b>37</b>
2.1 <i>Materials</i> . . . . .	38
2.2 <i>Methods</i> . . . . .	39
2.2.1 <i>Fabrication of capsules by layer-by-layer technique</i> . . . . .	39
2.2.2 <i>Sample preparation for CXDI</i> . . . . .	42
2.2.3 <i>Synthesis of magnetite</i> . . . . .	45
2.2.4 <i>Fabrication of capsules with MNP</i> . . . . .	46
2.2.5 <i>Transmission and fluorescent optical microscopy</i> . . . . .	46
2.2.6 <i>Scanning Electron Microscopy (SEM)</i> . . . . .	46

2.2.7	<i>Transmission electron microscopy (TEM)</i>	47
2.2.8	<i>Atomic force microscopy (AFM)</i>	47
2.2.9	<i>Spectrophotometric experiments</i>	47
2.2.10	<i>Red Green Blue (RGB) color model</i>	47
<b>3</b>	<b>RESULTS and DISCUSSION</b>	<b>49</b>
3.1	<i>Synthesis of microcapsules by LbL technique</i>	50
3.2	<i>Coherent X-Ray diffraction Imaging</i>	57
3.3	<i>Magnetite nanoparticles characterization</i>	63
3.4	<i>Energy-dispersive X-ray analysis</i>	69
3.5	<i>Ultraviolet–visible spectroscopy (UV-VIS)</i>	70
3.6	<i>Loading and delivery of capsules. Release of inner substance</i>	73
3.7	<i>Loading of capsules with aquacobalamin (vitamin B12) and dimeglumine chlorin E6 inside capsules</i>	84
<b>4</b>	<b>GENERAL CONCLUSIONS</b>	<b>88</b>
	<b>REFERENCES</b>	<b>91</b>
	<b>LIST OF PUBLICATIONS</b>	<b>126</b>
	<b>ACKNOWLEDGEMENT</b>	<b>128</b>

## LIST OF FIGURES

1.1	Schematic representation of the adsorption process .	7
1.2	Schematic representation of layer-by-layer technique	9
1.3	Schematic illustration of stimuli for capsules opening and closing. . . . .	15
1.4	Schematic layout of five main CDI methods and iterative phase retrieval algorithms. (A) Plane-wave CDI. (B) Bragg CDI. (C) Ptychographic CDI. (D) Fresnel CDI. (E) Reflection CDI. (F) Phase retrieval algorithms. From (Miao et al., 2015). . . . .	29
2.1	Scheme of shell formation. 1) Polyanion solution was added to the templates. 2) Centrifugation. 3) Supernatant is removed. Washed at least 3 times. 4) Adding of polycation solution. 5) Centrifugation. 6) Supernatant is removed. Washed at least 3 times. These steps are repeated till the required number of layers are received. . . . .	40
2.2	The formation of a Ca-EDTA complex . . . . .	42
2.3	Scheme of the experiment: NPC solution is placed between 100-nm-thick silicon nitrate membranes, during the acquisition it is rotated around the vertical axis and shifted along the height for the position adjustment, when necessary. Diffraction patterns were acquired at each rotation angle. Reconstruction of the capsules structure was done according to the protocol on ID-10 beamline (ESRF). . . . .	44

2.4	The typical representation of the diffraction pattern acquired from a sample. The two-dimensional projection. . . . .	45
3.1	$CaCO_3$ particles. Images captured by optical microscope. . . . .	50
3.2	Size distribution of $CaCO_3$ particles in $\mu m$ . . . . .	51
3.3	SEM images of $CaCO_3-(PSS - PAH)_3$ surface. . . . .	52
3.4	Images of $CaCO_3-(PSS - PAH)_3$ from optical microscope. . . . .	52
3.5	SEM images of $CaCO_3-(PSS - PDADMAC)_3$ particles. . . . .	53
3.6	Images of $CaCO_3-(PSS - PDADMAC)_3$ from optical microscope. . . . .	53
3.7	Atomic force microscopy (Peak Force Tapping mode) of $(PSS - PAH)_3$ capsules. (A) Sensor height (topography); (B) Peak Force Error map; (C) the logarithm of the elastic modulus based on the Young's Modulus; (D) adhesion. . . . .	55
3.8	Height profile of a single capsule obtained using atomic force microscopy. . . . .	56
3.9	SEM images of NPCs where is HEK cells used as templates. Left - the single particle. Right - the complex of particles . . . . .	56
3.10	Reconstructed images of 5- $\mu m$ NPC loaded by 50-nm gold nanoparticles under dry conditions. . . a, b, c – are the cross sections, d, e, f – are the plane projections. a, d are top views; b, e are front views; c, f are side views. The same analogy is for subsequent images. . . . .	58
3.11	Reconstructed images of 5- $\mu m$ NPC loaded by 50-nm gold nanoparticles in liquid medium. . . . .	59
3.12	Reconstructed images of 6 PSS/PAH layers NPC loaded by 5-nm gold nanoparticles at pH 6.5 in liquid medium. . . . .	60

3.13	Reconstructed images of 6 PSS/PAH layers NPC loaded by 5-nm gold nanoparticles at pH 4 in liquid medium. . . . .	60
3.14	Reconstructed images of 12 PSS/PAH layers NPC loaded by 50 nm gold nanoparticles at pH 4 in liquid medium. . . . .	61
3.15	Reconstructed images of 12 PSS/PAH layers NPC loaded by 50-nm gold nanoparticles at pH 6.5 in liquid medium. . . . .	62
3.16	Reconstructed images of 12 PSS/PAH layers NPC loaded by 50-nm gold nanoparticles at pH 8.5 in liquid medium. . . . .	62
3.17	Magnetic separation of the prepared black product suspended in water without (left) and with (right) a magnetic field. . . . .	64
3.18	SEM images of MNP's. . . . .	64
3.19	SEM images of MNP's after filtration. Top – overall picture. Bottom – overall picture with signed particles' dimensions. . . . .	65
3.20	TEM images of MNP's. Left – more concentrated zone, right – less concentrated zone. . . . .	66
3.21	Size distribution of FeNPs in nm. . . . .	67
3.22	SEM images of $CaCO_3-(PSS-PAH)_2-(PSS-MNP/PAH)-PSS$ particles. . . . .	67
3.23	TEM images of MNP's after filtration. Top – overall picture. Bottom – overall picture with signed particles' dimensions. . . . .	68
3.24	SEM images (upper panels) and EDX spectra (bottom panels) of $CaCO_3-(PSS-PAH)_2-(PSS-MNP/PAH)-PSS$ (left) and $(PSS-PAH)_2-(PSS-MNP/PAH)-PSS$ (right). . . . .	70
3.25	UV-VIS spectra of the magnetite nanoparticles. . . . .	71
3.26	UV-VIS spectra of the utilized reagents: black – pure MNPs, red – MNPs stabilized with PEI. . . . .	72



3.27 UV-VIS spectra of the MNPs stabilized with a PAH: the green is diluted solution 1 to 1, the violet is 1 to 2. . . . .	73
3.28 Optical fluorescent microscope image of $CaCO_3$ particles with associated fluorescein sodium salt using FITC filter. . . . .	74
3.29 General scheme of the experiment. . . . .	74
3.30 Optical fluorescent microscope image of $CaCO_3$ /Fluorescein sodium salt $-(PSS - PDADMAC)_2 - (PSS - MNP/ PDADMAC)$ using FITC filter. . . . .	75
3.31 Optical fluorescent microscope image of $CaCO_3$ /Rhodamin B $-(PSS - PDADMAC)_2 - (PSS - MNP/ PDADMAC)$ using TRITC filter. . . . .	76
3.32 Schematic view of the experiment. 1) Two different drops with loaded dyes in the core of containers are placed on the glass. The drops are placed near each other. 2) With an external magnet the particles are moved to one point. 3) Two types of containers are mixed between each other. . . . .	76
3.33 Mixture of $CaCO_3$ /Fluorescein sodium salt $-(PSS - PDADMAC)_2 - (PSS - MNP/ PDADMAC)$ and $CaCO_3$ /Rhodamin B $-(PSS - PDADMAC)_2 - (PSS - MNP/ PDADMAC)$ , delivered to the focus area by external magnet . . . . .	77
3.34 Optical fluorescent microscope images of mixture of $CaCO_3$ /Fluorescein sodium salt $-(PSS - PDADMAC)_2 - (PSS - MNP/ PDADMAC)$ and $CaCO_3$ /Rhodamin B $-(PSS - PDADMAC)_2 - (PSS - MNP/ PDADMAC)$ . Top- using FITC filter. Bottom - using TRITC filter. . . . .	78
3.35 Optical image of the sample after the core dissolution by adding EDTA solution. . . . .	80

3.36	Optical fluorescent microscope images of the mixture of two types of capsules loaded with different dyes after core dissolution. Top – FITC filter, bottom – TRITC filter. . . . .	81
3.37	$CaCl_2 \cdot 2H_2O$ crystal formed after drying of the surrounding water. . . . .	82
3.38	$CaCl_2 \cdot 2H_2O$ crystal. Left – FITC filter, right – TRITC filter. . . . .	83
3.39	SEM images of: top – $(ALG - CHI)_2 - (ALG - MNP/CHI) - ALG - B_{12}$ ; bottom – $(ALG - CHI)_3 - B_{12}$ . . . . .	86
3.40	SEM images of: top – $(ALG - CHI)_2 - (ALG - MNP/CHI) - ALG - E_6$ ; bottom – $(ALG - CHI)_3 - E_6$ . . . . .	87

## LIST OF TABLES

1.1	Templates used for the preparation of hollow capsules	12
1.2	Some polyelectrolytes that are used as the shell in capsule fabrication . . . . .	14
3.1	Quantitative distribution of elements for $CaCO_3-(PSS-PAH)_2-(PSS - MNP/PAH) - PSS$ . . . . .	69
3.2	Quantitative distribution of elements for $(PSS - PAH)_2-(PSS - MNP/PAH) - PSS$ . . . . .	70
3.3	The distribution of dyes in the core and in the solution by comparison RGB values. . . . .	79
3.4	The distribution of dyes in the core and in the solution by comparison RGB values after dissolving the core with EDTA . . . . .	80

---

## **LIST OF ABBREVIATIONS**

<b>CaCO<sub>3</sub></b> calcium carbonate . . . . .	vi, vii, 11, 39, 50–53, 67
<b>AFM</b> atomic force microscopy . . . . .	vi, 28, 53, 55
<b>ALG</b> alginate . . . . .	ix, 15, 38, 40, 84–87
<b>CCD</b> charge-coupled device . . . . .	23, 24
<b>CHI</b> chitosan . . . . .	ix, 15, 38, 40, 41, 84–87
<b>CXDI or CDI</b> coherent X-Ray diffraction imaging . . . . .	22, 89, 91
<b>DDS</b> Drug delivery systems . . . . .	2–6, 13
<b>EDTA</b> ethylenediaminetetraacetic acid . . . . .	viii, x, 12, 38, 41, 42, 51, 79, 80, 84
<b>EDX</b> energy-dispersive X-ray analysis . . . . .	69
<b>ESRF</b> European Synchrotron Radiation Facilities . . . . .	v, 42, 44
<b>FFT</b> fast Fourier transform . . . . .	23, 29
<b>HCl</b> Hydrochloric acid . . . . .	12, 38, 41, 42
<b>LbL</b> layer-by-layer . . . . .	iv, 5, 6, 8–10, 12, 17, 35, 36, 39, 50, 89
<b>MF</b> melamine formaldehyde . . . . .	9–12, 16, 18
<b>MNPs</b> magnetic nanoparticles . . . . .	vii, viii, 18, 32, 33, 35, 36, 45, 46, 63, 70–73
<b>MRI</b> magnetic resonance imaging . . . . .	32
<b>NP</b> nanoparticle . . . . .	18, 19, 35
<b>NPCs</b> nanoengineered polymeric capsules . . . . .	vi, 2, 39, 43, 50, 53, 56–59, 63
<b>PAH</b> poly(allylamine hydrochloride) . . . . .	vi–viii, x, 9, 10, 13, 14, 16–18, 38, 40, 42, 46, 50, 52, 55, 67, 69, 70, 72, 73
<b>PDADMAC</b> poly(diallyldimethylammonium chloride) . . . . .	vi, 13, 16, 38, 40, 46, 50, 53
<b>PE</b> pectin . . . . .	14, 38, 40
<b>PEI</b> Polyethylenimine . . . . .	vii, 13, 14, 38, 40, 46, 71, 72, 84

<b>PEM</b> polyelectrolyte multilayer film . . . . .	8, 11, 17
<b>PSS</b> poly(4-styrenesulfonic acid) vi, vii, x, 9, 10, 13, 14, 16–18, 38, 40, 42, 50, 52, 53, 55, 67, 69, 70, 84	
<b>RGB</b> Red Green Blue . . . . .	47, 48, 80
<b>SAXS</b> small-angle X-ray scattering . . . . .	21
<b>SEM</b> scanning electron microscope vi, vii, 28, 51–53, 56, 57, 63, 66, 67, 89	
<b>TEM</b> transmission electron microscopy . . . . .	65
<b>USAXS</b> ultra small-angle X-ray scattering . . . . .	21
<b>UV-VIS</b> ultraviolet–visible spectroscopy . . . . .	iv, vii, viii, 70–73
<b>WAXS</b> wide-angle X-ray scattering . . . . .	21
<b>XRR</b> X-ray reflectivity . . . . .	21

---

## CHAPTER 1

---

# **INTRODUCTION**

The human or animal body is a complicated system. In some moments of life, when the organism is not able to resolve appeared problems by itself, it needs help, e.g., that is treatment with external therapeutical compounds. This happens when our immune system can't resist any infection or it need an external help. In this case different drugs can be used. The problem appears when we are facing with some grave situations, because this cases requires more concentrated, harmful, considerable quantity of the pharmaceuticals. However almost all pharmaceuticals can have some undesirable effects. For example, in the case of the serious illness, the used drugs not only help to repair desired zones of the organism but also make harms on other areas. That is why nowadays different systems are invented in order to reduce this harmful effect, to reduce the concentration of the drug, to develop a more targeted delivery system. As one of the options nanoengineered polymeric capsules (NPCs) can be used. This system is unique due to the fact that different compounds can be used for their preparation, we can functionalize it with different substances, we can deliver them easily to the certain zone, we can control release of the drug, etc. (Pastorino et al., 2013)

---

**1.1. DRUG DELIVERY SYSTEMS**

Drug delivery systems (DDS) is based on recently developed technologies which allows the targeted delivery and/or controlled release of chemical substances, e.g., drugs. It is a kind of smart interface between the patient and the drugs. In the field of drug delivery, it's important to find a perfect system that can behave itself like a vehicle in the circulatory system and move through cells and tissues. The other important thing in DDSs is that during drug delivery some therapeutic agents can influence on the healthy tissues that are not the target of

the drug. These side effects limit the ability to make optimal drugs for many diseases such as cancer, infectious diseases, etc. (Patra et al., 2018)

Usually in DDSs not only the drugs themselves are important but also the container for their delivery. This container should be stable during the delivery. It can be fabricated from a plenty number of polymers. However, considering the fact that these containers would be used in a body, the polymers should respond to some requirements like biocompatibility and biodegradability. Moreover, if we are speaking of the operation inside the human body, the size of a DDS should correspond to micro- or even nano- sizes. The synthesis of a such system that corresponds to all necessary requirements is a complicated task. (Zhang et al., 2013)

Some drugs are only effective if their bioactivity is within the therapeutic window. Bioavailability is the portion of the administered dose that enters the systemic circulation unchanged. The bioavailability of a drug is largely determined by the properties of the dosage form, which partly depend on its design and production. Differences in bioavailability between dosage forms of a given drug may be of clinical significance; therefore, it is important to know whether the dosage forms are optimal. (Hebert, 2013) Therapeutic window is the time range between wound and treatment during which the drug is still effective. (Danton and Dietrich, 2005)

To calculate the proper amount of the drug it is necessary to know the therapeutic index (TI), which is the ratio of the drug's amount that gives therapeutic effect to amount that causes toxicity. (Trevor et al., 2010) For almost all therapeutic agents, this range is wide enough. The maximum concentration of the drug in plasma is high enough above the minimum



therapeutic dose and sufficiently below the toxic concentration. (Reiffel, 2000) The larger therapeutic index, the safer is drug. Conversely, a drug with a narrow therapeutic index usually has a strong concentration dependence. There is only a narrowly defined range of doses of a drug in which the drug has a beneficial effect without causing serious consequences. In other words, small fluctuations in concentration values can have a toxic effect on the body or insufficient therapeutic effect. (Tamargo et al., 2015)

In addition, it is clear that the need for DDS is important. Since many drugs have already been invented, the attempts and the dose of their usage is already known. The remain problem was in their safety and less toxic lateral effects. Moreover, the synthesis of a new drugs which would be more “friendly” to the human’s body is more expensive and takes more time because of clinical tests. Therefore adequate design of “smart” containers is an easier solution of this task.

DDSs can be capable to control the rate of drug delivery, the frequency of drug releasing, can sustain the duration of therapeutic action, can be placed to specific, necessity points. (Lankalapalli and Kolapalli, 2009)

So, the main requirements to DDS are:

- Should protect from degradation in the bloodstream.
- Should provide controlled release.
- Should enhance drug stability.
- Should provide targeted drug delivery.
- Should decrease toxic side effects.
- Should improve pharmacokinetic and pharmacodynamic drug properties.

- Should be biodegradable and biocompatible.
- Should be scalable according to required volume of the encapsulated drug. (Lankalapalli and Kolapalli, 2009)

Recently, there was an important breakthrough in the field of DDS realization. Various container types have been developed and, moreover, many of them have been tested clinically. These systems are layer-by-layer (LbL) capsules (Sukhorukov et al., 1998a), liposomes (Allen and Cullis, 2013), polymersomes (Lee and Feijen, 2012), Particle Replication In Nonwetting Templates (PRINT) (Rolland et al., 2005), gels, prodrugs, cyclodextrins (Tiwari et al., 2012), etc.

The ability to control physico-chemical properties such as size, shape, surface functionality, and release mechanisms strongly supports the prospects of the particle design for a wide range of biomedical applications. (Si et al., 2016; Wang et al., 2016) In the future, it is expected that new types of containers, as well as drugs, will be improved and developed, allowing to establish new, more effective methods of treatment. Moreover, thanks to the development of DDSs, it is possible to realise new drugs that will be synthesized for a certain type of container, thereby increasing the effectiveness of the action and reducing toxic effects on the body. However, there is still a significant gap in knowledge, since understanding of all the features of interactions between particles and biological systems is far from complete. (Gai et al., 2017; Yan et al., 2012)

---

## 1.2. **LAYER-BY-LAYER TECHNIQUE**

---

### 1.2.1. **Polymeric drug delivery system**

Polymeric drug delivery systems can be divided into biodegradable and non - biodegradable ones. In general, there is no rigid

borders between these two classes of polymers. The difference is in the time of degradation, matter of degradation degree, conditions. Biodegradable polymers mostly are water-soluble or natural biopolymers, non - biodegradable are water-insoluble polymers, and the rate of their degradation is much slower. (Steinbüchel, 2005) Moreover, almost all carbon-based polymers are biodegradable. (Kyrikou and Briassoulis, 2007)

At the same time, it has been reported that there are some polymers with a controlled lifetime have been synthesized. These polymers should be stable during their usage and should biodegrade at the end of the experiment. (Lucas et al., 2008)

Drug release from a polymeric system is influenced by multiple factors such as drug properties, polymers properties and the type of DDS. Each case requires a consideration which DDS, polymers and drugs should be used. We should remember about DDS shape, morphology and porosity of its surface, type of polymers that are used, stability, charge, and solubility of a drug. Moreover, in the case of polymers we should remember about biodegradation mechanisms, such as hydrolysis and oxidation, and the rate of biodegradation. (Silverman et al., 2002) These types of reactions can be caused by water, acids, bases, salts, enzymes. The rate of biodegradation depends on molecular weight, hydrophilic or hydrophobic character of the polymers, crystallinity, glass transition temperature. Additionally, the external factors like, for example, pH and temperature can influence on DDS.

---

### 1.2.2. ***Polyelectrolyte self-assembling technique***

Polyelectrolyte self-assembling technique, also known as a layer-by-layer (LbL) technique, is a powerful deposition method that allows to fabricate thin films on substrates. (Decher, 1997) This technique is easily reproducible. It does not require any

specific, inaccessible reagents and does not require any special equipment. These films are formed by deposition of oppositely charged objects from solutions with washing between each deposited layer. In 1966 this method was applied for the first time by Iler. (Iler, 1966) He used oppositely charged colloidal particles - silica and aluminium - and deposited them on the glass surface. Afterwards this method was supplemented by Prof. Gero Decher. (Decher and Hong, 1991) He synthesized cationic and anionic amphiphile molecules. Then a solid support with positively charged surface was immersed in negatively charged amphiphile solution. A monolayer is adsorbed, the surface charge is reversed. Then the surface was washed in pure water and after the sample was immersed into the solution of positively charged amphiphiles. The second monolayer is adsorbed, and the surface charge returned to its initial sign. By repeating these steps one after the other, multilayered film is fabricated. These steps are schematically shown in the Fig. 1.1.

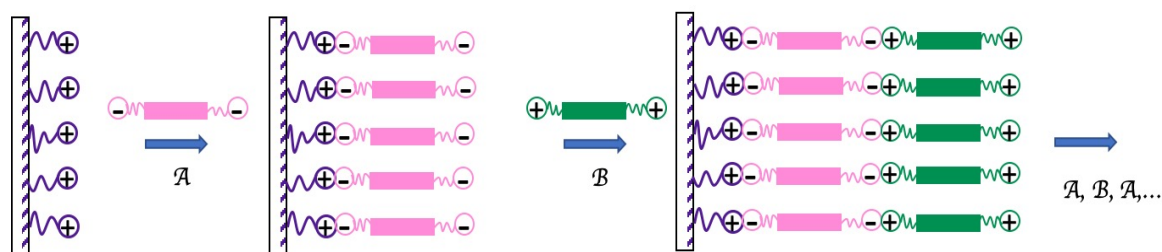


**Fig. 1.1** Schematic representation of the adsorption process

Due to the fact, that the technique is rather simple to use and repeat, it was quickly spread to diverse scientific communities. In particular, for the synthesis of regular assemblies of multiple materials including polymers (Fujii et al., 2010; Lvov et al., 1999), biomaterials (Caruso et al., 1998b; Lvov et al., 1994, 1995a, 1998), inorganic substances (Ariga et al., 1999; Lvov et al., 1996, 1997), and supramolecular assemblies. (Ariga et al., 1997, 2011; Katagiri et al., 2002a,b)

Later, the process of the film formation was mainly based on the attraction of oppositely charged objects (e.g., polymer-polymer, polymer-drug, polymer-drug-polymer, etc.) instead of the use of amphiphile molecules. (Lankalapalli and Kola-palli, 2009) At least two polyelectrolytes, which were oppositely charged, were used within the process. (Decher et al., 1992) The adsorption of a polyelectrolyte on a charged surface occurs due to comparatively high concentrations of polymers in solution. This fact results in the excessive adsorption of substances where charge neutralization and resaturation leads to reversal of a charge. The alternation of the surface charge leads to a formation of continuous complexes between differently charged polyelectrolytes, forming layers of oppositely charged films. (Ariga et al., 2011)

Polyelectrolytes, biological compound, magnetic nanoparticles, metal nanoparticles, dyes, aluminosilicates, zirconium phosphates, etc., are used as molecules that form layers in LbL technique. (Kotov, 1999) The driving forces for the LbL assemblies are not only electrostatic interactions, but also metal coordination (Lee et al., 1988; Wanunu et al., 2005), hydrogen bonding (Stockton and Rubner, 1997; Sukhishvili and Granick, 2000), covalent bonding (Chen et al., 1999; Such et al., 2006), supramolecular inclusion (Ikeda et al., 2001), bio-specific recognition (Hoshi et al., 2002; Lvov et al., 1995b), charge transfer complex formation (Shimazaki et al., 1998), and stereo-complex formation. (Serizawa et al., 2004, 2000)

The main steps of the method are illustrated in the Fig. 1.2: adsorption of one polyelectrolyte, washing, adsorption of second polyelectrolyte, that is oppositely charged to the previous one and final washing. The repetition of these steps allow to fabricate a polyelectrolyte multilayer film (PEM).

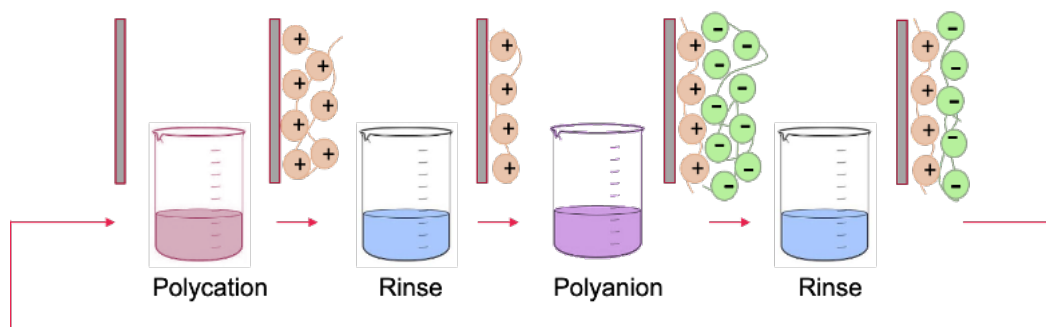


**Fig. 1.2** Schematic representation of layer-by-layer technique

Synthesis of films by LbL technique does not require special equipment, there are no special requirements on the physico-chemical properties of the surface, the size and shape of the substrate, the nature and topology of the surface, because the process involves adsorption from an aqueous solution. In addition, this technique allows to use a wide range of reagents.

Later, a very important step in using this technique was done in 1998. G. Sukhorukov and his colleagues had used LbL assembly for covering a colloidal particles. They had used manganese (II) carbonate  $MnCO_3$  as a core, PSS and PAH as a polyelectrolyte for the shell. Subsequent dissolution of the core leads to formation of hollow shells. (Caruso et al., 1998a; Donath et al., 1998; Qiu et al., 2001; Sukhorukov et al., 1998a, 1999)

These experiments had shown that LbL assemblies can be used for non-planar substrates thus opening great opportunities for further development and study of this objects.

---

### 1.2.3. *Layer-by-layer capsules for drug delivery*

As it was stated above, in 1998 the LbL technique was used for hollow capsule preparation. Melamine formaldehyde particle (MF particles) with 3  $\mu\text{m}$  diameter were used as a core. It was possible to dissolve these core particles when the pH of the solution was lower than 1.6. Polyanion and polycation molecules

(PSS and PAH respectively) were used in the process of adsorption on the colloidal particles. (Sukhorukov et al., 1998b, 1999) After the deposition of the layer, unadsorbed solution was removed after the centrifugation of the sample in the tube. The dispersed microparticles were washed with a water at least 3 times.

This method was the starting point for many studies, because after it became possible to synthesize hollow capsules of various shapes and sizes, as well as their use in medicine and pharmacology. Subsequently, variants of cores and polyelectrolytes were studied. Both organic and inorganic materials can be used for synthesis of such objects.

---

#### 1.2.4. ***Templates for capsule assembly***

For templates the main requirements are:

- They should be stable during LbL deposition process.
- During the dissolution of the template, the stability and the structure of the multilayer shell should not be interrupted.
- The dissolved template should exit from the hollow capsule without any problem.
- For easier characterization, it is better that the templates should have spherical shape and should be monodisperse. (De Cock et al., 2010; Peyratout and Daehne, 2004)

Polystyrene (PS) (Déjugnat and Sukhorukov, 2004; Elsner et al., 2004), MF (Sukhorukov et al., 1998a), erythrocytes (Moya et al., 2001; Neu et al., 2001) and polylactic acid (PLA) (Shenoy et al., 2003) particles were used as organic templates. The difficulty of using organic templates is that there is a problem in dissolving the core. Unlike organic materials, inorganic materials are easier to use. In addition, the cores can be dis-

solved easily. In case of MF as a core, during dissolving MF templates turn into protonated MF oligomers (Andres and Kotov, 2010). Because of their slow diffusion, the osmotic pressure arises, the shell of PEM is subjected to high mechanical stress that leads to the capsule rupture. Moreover, some part of oligomers remains inside the capsule. In the case of PS and PLA, these cores are dissolved in organic solvents, that can change the structure and stability of PEM. (Déjugnat and Sukhorukov, 2004) In addition, it was observed for these templates that the particles swell due to osmotic pressure. If erythrocytes are used as a core, capsules inherit a wide variety of different shapes and sizes. (Neu et al., 2001) In order to dissolve these cores, they are incubated in a basic hypochlorite solution. Due to these reasons, polyelectrolytes in the shell can be oxidized. (Moya et al., 2001)

On the other hand, there are inorganic cores such as silica nanoparticles, gold nanoparticles, cadmium carbonate, calcium carbonate, manganese carbonate. They can be dissolved in aqueous solution, and due to this, the resulting products of dissolution can easily leave the interior part of the capsule. Unfortunately, these templates do not always have spherical shape and they have high polydispersity; in addition, they can aggregate. There is different types of the inorganic cores. Some of them are more porous, respect to others, e.g.,  $CaCO_3$ . Due to this, it is possible to insert some active molecules into the capsules before the formation of the shell by adsorption of polyelectrolytes. (Petrov et al., 2005; Volodkin et al., 2004b) At the same time,  $SiO_2$  are smooth, spherical, monodisperse and available in various sizes. But they can be dissolved only in HF. (Adalsteinsson et al., 2004; Itoh et al., 2004; Schneider and Decher, 2004; Schuetz and Caruso, 2003) Gold nanoparticles are only available in nanoscale size and the only way to dissolve



them is to use hazardous potassium cyanide solution. (Delcea et al., 2011)

More typically used templates and some of their properties are shown in the table 1.1. (Delcea et al., 2011; Peyratout and Daehne, 2004; Skirtach and Kreft, 2009)

**Table 1.1** Templates used for the preparation of hollow capsules

Parameter	MF	PLA/PLGA	PS	SiO <sub>2</sub>	Carbonates
Size (μm)	0.5-12	0.2-20	0.1-1000	0.15-8	1-8
Shape	spherical	spherical	spherical	spherical	crystalline, porous
Monodispersity	excellent	low	excellent	Good-excellent	medium
Template solvents	HCl, DMSO	NMP, acetone	THF	HF	EDTA, HCl
Template dissolution	Incomplete	Incomplete	Incomplete	Complete	Complete
Drawbacks	Toxic residues	Residues	Toxic residues, aggregation	No problems	Aggregation
Biocompatibility of encapsulation	Low/medium	Very good	Low/medium	Medium	Very good

MF = melamine formaldehyde; PS = polystyrene; PLA = polylactic acid; PLGA = poly(lactic-co-glycolic acid); DMSO = dimethylsulfoxide; THF = tetrahydrofuran; HF = hydrofluoric acid; EDTA = ethylenediaminetetraacetic acid; NMP = 1-methyl-2-pyrrolidinone.

### 1.2.5. Polymers

Multifunctionality of LbL technique is also determined by the variety of materials that can be used for the capsule preparation, namely the numerous substances for the shell, such as biocompatible polyelectrolytes (Itoh et al., 2004; Shenoy et al., 2003), charged nanoparticles (Bédard et al., 2008; Caruso et al., 1998c; Kotov et al., 1995; Skirtach et al., 2005, 2006), proteins (Caruso and Möhwald, 1999), lipids (An et al., 2005; Moya

et al., 2000), small dye molecules (Dai et al., 2001) etc.

Non-biodegradable or biodegradable polymers can be used as a polyelectrolyte. Non-biodegradable polymers are known as stable ones for an experiment time. (Kyrikou and Briassoulis, 2007) These polymers should be chemically inert. The main advantage of biodegradable polymers that are used for DDS is that after their usage they didn't have to be removed from an organism. These polymers protect the drug until its release and sometimes can control the release rate. (Leja and Lewandowicz, 2010) However there is a stricter selection of these types of polymers due to their biocompatibility and possible toxicity in comparison to non-biodegradable ones. In the case of biodegradable polymers we can distinguish natural and synthetic ones. As an example of natural polymers we can list: chitosan, pectin, alginate, cellulose; as a synthetic polymers – polylactides (PLA), poly(amino acids), polycaprolactone (PCL), etc. (Ngwuluka et al., 2014; Uhrich et al., 1999)

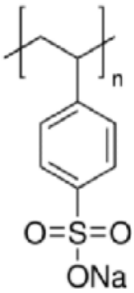
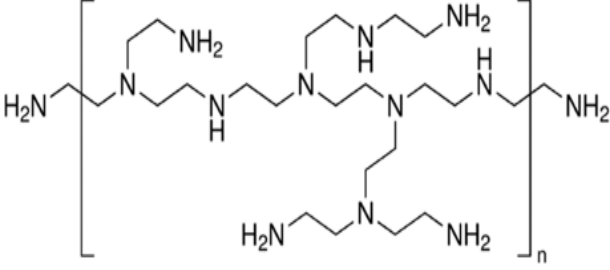
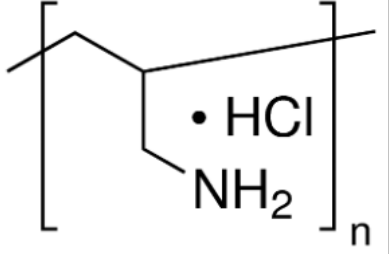
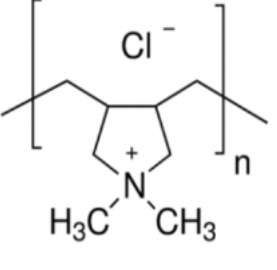
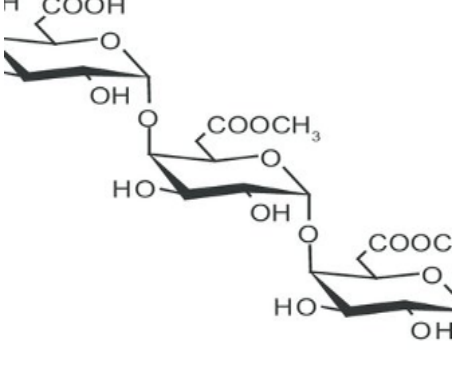
Polysaccharides are widespread in nature and can occur in plants (e.g., pectin), animals (e.g., chitosan), algae (e.g., alginate), microbes (e.g., dextran). (Sinha and Kumria, 2001) The main reason why these types of polymers are widely used in drug delivery is their safety, non-toxicity, stability, hydrophilicity, and biodegradability. (Anwunobi and Emeje, 2011)

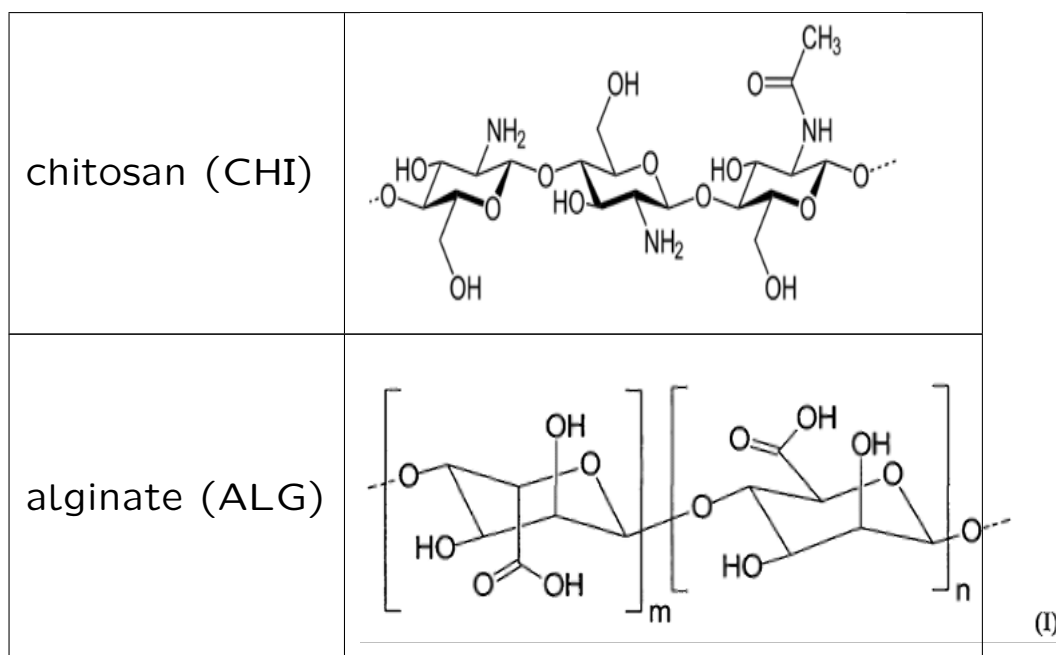
Up to date, the most often used non-biodegradable polyelectrolytes for the shell formation are PAH, PSS, PEI and PDADMAC. Due to the potential use of capsules in the pharmaceutical industry, there is a lot of studies of the applying natural polyelectrolytes such as polysaccharides, for example, dextran sulfate (Georgieva et al., 2002), chitosan (Berth et al., 2002), sodium alginate, carboxymethyl cellulose. (Qiu et al., 2001)

Frequently used polyelectrolytes for fabrication of capsules

are shown in the table 1.2.

**Table 1.2** Some polyelectrolytes that are used as the shell in capsule fabrication

poly(4-styrenesulfonic acid) (PSS)	
Polyethylenimine (PEI)	
poly(allylamine hydrochloride) (PAH)	
poly(diallyl dimethyl ammonium chloride) PAH	
pectin (PE)	



### 1.2.6. Stimuli for encapsulation and release

External stimuli play a role of trigger parameters that can influence the permeability of the shell of the capsules. There are three types of external stimuli: physical (light, ultrasound, magnetic field, mechanical deformation), biological (receptors, enzymes) and chemical (pH, solvent, ionic strength). They are schematically illustrated by the Fig. 1.3. (Delcea et al., 2011)

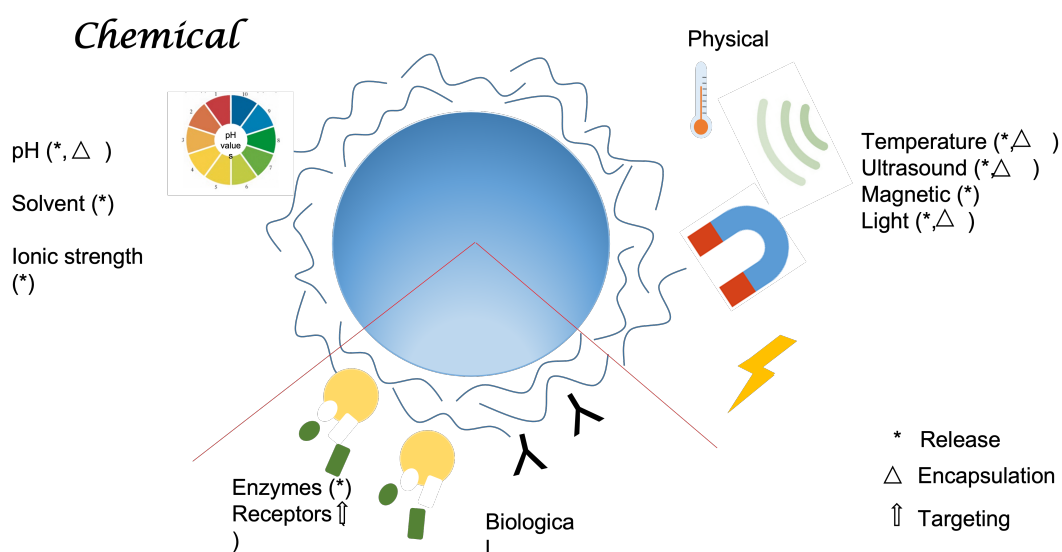


**Fig. 1.3** Schematic illustration of stimuli for capsules opening and closing.

These types of stimuli can be associated with properties of polymers, interaction with external fields or actions, functions of molecules, etc.

### ***Chemical stimuli***

Chemical stimuli like pH are often used. If weak polyelectrolytes are used for the shell fabrication, it is possible to open capsules by pH through protonation or deprotonation of polyelectrolytes' charged groups. Namely, the usage of such polyelectrolytes like PAH, poly(acrylic acid) (PAA) and poly(methacrylic acid) (PMAA) allows to apply variation of pH for changing of the capsule shells' permeability. In the case of protonation, capsules swell, resulting in the increase of their permeability. Contrariwise, during deprotonation, the permeability is decreased due to the reduction of polymers interactions. (Adalsteinsson et al., 2004; Burke and Barrett, 2003; Sui and Schlenoff, 2004)

In terms of ionic strength, salt ions screen the electrostatic interaction of oppositely charged polyelectrolytes in the shell. Due to this, the capsules can be loaded with a substance and then released in the presence of salt. However, the loading efficiency is low. Due to reduced electrostatic attraction inside the polyelectrolyte layers of the shell, the salt-induced permeability alterations are described. (Antipov et al., 2003b) Also, addition of salt can influence on the permeability, especially if one of the polyelectrolytes has hydrophobic groups. If the ionic strength is accrued, electrostatic interaction between oppositely charged polyelectrolytes is reduced that leads to the compression of capsules hydrophobic groups. This principle was used by Gao et al. for encapsulation of dextran molecules inside the capsule made of PSS and poly(diallyldimethylammonium chloride) (PDADMAC) on MF particles. (Antipov et al., 2003b; Delcea et al., 2011; Gao et al., 2004)

The capsule permeability can vary by the use of organic solvents. Lvov et al. had used the mixture of ethanol and water (1:1) in order to encapsulate urease into PSS/PAH capsules. The ethanol was removed from the sample and it allowed to close the pores of the capsule. But the role of this solvent is not completely studied in the question of shell permeability. (Delcea et al., 2011; Lvov et al., 2001)

### ***Physical stimuli***

***Temperature*** Temperature is one of the external stimuli. It can affect the properties of the material and the formation of multilayer PEM. (Büscher et al., 2002) For the first time, the effect of temperature on microcapsules synthesized by the LbL method was reported by Köhler et al. (Köhler et al., 2005) PEMs are kinetically stable. In this regard, the temperature increase can provide enough thermal energy to surpass the barrier necessary for polymer film rearrangements. In the case of capsules, the decrease in their shell's permeability is due to the interaction of electrostatic and hydrophobic forces. Accordingly, the same mechanism of opening the pores was considered to be the same as in the case when encapsulating with salt. (Delcea et al., 2011; Gao et al., 2004)

Another requirement for this type of stimulation is that the temperature must be higher than the glass transition temperature of the polyelectrolytes. (Köhler et al., 2005) The consequent response to thermal shrinking occurs in conjunction with the hardening of the shells and, consequently, an increase in the mechanical strength of the microcapsules. (Déjugnat et al., 2007) Such shrinkage can also be controlled by the number of bilayers in the shell or the balance of their charges. Capsules with an odd number of layers swell, and with an even number-shrink. (Köhler et al., 2005)

Bedard and his colleagues have demonstrated that the introduction of gold nanoparticles into the layers further increases the rigidity of microcapsules. (Bédard et al., 2008) It was found that microcapsules containing gold NPs' need higher temperatures to shrink to the same diameter as microcapsules without gold NPs'. (Bédard et al., 2009)

The external stimuli mentioned above (pH, ionic strength, solvent, and temperature) are useful for encapsulation, but cannot be applied for drug delivering and release, since these parameters must be kept constant under physiological conditions. Therefore, remote triggers or stimuli, based on external fields, become relevant. (Timko et al., 2010)

**Magnetic fields** The key benefit of usage magnetic nanoparticles (MNPs) in capsules is the possibility of targeted delivery. Besides, the therapeutically efficiency of such containers can be increased in the case of release due to magnetic field. However, MF templates cannot be used in this case. Lu and coworkers (Lu et al., 2005) have demonstrated the influence of MNPs aggregates by magnetic field on the shell permeability. The PSS/PAH capsules were used. Ferromagnetic cobalt nanoparticles, covered with a layer of gold, were inserted into the layers of these capsules.

Due to the paramagnetic properties of magnetite nanoparticles, it is possible to incorporate them into the shell of capsules and move them by the external magnetic field. (Dyab et al., 2009; García-Alonso et al., 2010)

**Laser light** For biomedicine, the use of a laser to open capsules must be carefully considered. It is necessary to load the capsules with nanoparticles, that must absorb incident light in the desired wavelengths range. In this case, the laser must meet two main requirements: the light should have minimal

absorption by cells/tissues and the maximum absorption of the nanoparticles. This can be achieved by selecting such a laser wavelength, called a biologically "friendly window", which uses the near-IR part of the spectrum (near-IR). (Roggan et al., 1999) The choice of this range is due to the fact that near IR is less harmful to skin tissues and can penetrate deeper into them, compared to visible light. (De Geest et al., 2007) Due to this, light-sensitive capsules have the potential to release drugs in vivo. This is possible by direct laser action, but only if the microcapsules are located close to the surface. If the capsules are located at a distance of more than a few millimeters from the surface, this can be done using optical fibers.

This stimulus is universal for both release and encapsulation. Encapsulation is caused by the rearrangement of polymers and changes in the permeability of the shell due to exposure to light. The efficiency of optical encapsulation increases with increasing irradiation time. (Koo et al., 2010)

Light, magnetic field, and other physical stimuli can also be used for the completely breaking the shell. (Delcea et al., 2011; Radt et al., 2004; Skirtach et al., 2004)

**Ultrasound** In order to use this type of stimulation, it is desirable to incorporate ZnO NPs into the capsule shell. This makes it possible to open the capsules under ultrasound. (Kolesnikova et al., 2010) By changing the number of layers with ZnO NPs, it is possible to control the mechanical properties and high sensitivity to ultrasound processes. Additional layers with ZnO NPs influence on the thickness and roughness of the shell, increase the fragility of microcapsules and their sensitivity to ultrasound, and reduce the rigidity of the shell.

In addition to the fact that ultrasound is often used to release the reagent from the capsule, it also has potential in



the field of encapsulation. (Han et al., 2010) However, in order to be effectively applied in medicine the approach must consider a necessity to reduce significantly its intensity. (Yashchenok et al., 2010b)

***Mechanical deformation*** Mechanical properties of microcontainers were studied by applying structural and mechanical characterization techniques. (Bédard et al., 2009; Dubreuil et al., 2003; Fery and Weinkamer, 2007; Tzvetkov et al., 2008) Due to the fact that capsules are often deformed upon intracellular uptake, the capsules should be mechanically stable. (Muñoz Javier et al., 2008) Also, there are losses in total amount of delivered drugs because of the deformation. If carbon nanotubes (Yashchenok et al., 2010a) or gold NPs (Bédard et al., 2009) are used for the functionalization of the capsules, the mechanical strength on the capsule shell is enhanced. Nanotubes or gold NP can be released upon mechanical rupture. (Caruso et al., 2009; Delcea et al., 2011)

### ***Biological stimuli***

***Enzyme-triggering release*** Another option for varying the shell permeability for the release of chemical substances from the core is the use of biological stimuli caused by the presence of enzymes. The use of various enzymes to open the pores in the capsules shell is of wide practical importance. (Zelikin et al., 2006) In this case, instead of using of polycations for the shell formation, the oligonucleotide sequences were used. The biggest advantage of this type of capsule is that it does not require an external trigger for intracellular drug delivery. (He et al., 2009) However, there is a problem with a delivery of such type of capsules and it is impossible to predict the release time of the drug. (Pavlov et al., 2011)

***Receptor-implementing targeting*** This method is used

only for the delivery of capsules. Basically, it is necessary to properly functionalize the capsules shell in order to use them for a targeted delivery. The simplest class of receptors are antibodies that allow specific targeting. (Cortez et al., 2007)

---

### 1.3. **COHERENT X-RAY DIFFRACTION IMAGING**

Nowadays a huge part of a new materials is consisted as nanomaterials. (Cao and Wang, 2011) It is necessary to observe and evaluate their structure. In this case the advanced design of nanomaterials is required. (Richman and Hutchison, 2009) For the structural investigation of these materials X-ray scattering methods are widely used. Moreover, these materials can be studied both in bulk and at the interfaces. The scattering contrast occurs due to the spatial difference of the electron density. The electron density is directly connected to the atomic number of component elements. Small-angle X-ray scattering (SAXS) gives structural resolution in the range from 1 to 100 nm (Narayanan, 2014) and is usually used for the determination of sizes and shape of macromolecules in solutions, as well as for determining spacing parameters of supramolecular systems. Wide-angle X-ray scattering (WAXS) allows to obtain structural elucidation at the atomic and molecular levels in systems where there is no perfect crystalline order. The X-ray reflectivity (XRR) is one of the surface scattering techniques. It is used for studying the electron density profile of layered systems in the direction, perpendicular to the interface. (Pershan and Schlossman, 2012) Later SAXS has been enhanced and now also there is ultra small-angle X-ray scattering (USAXS) method which allows to reach length scales up to  $\mu\text{m}$  and above. (Ilavsky et al., 2018; Narayanan et al., 2017) USAXS is important for study long-range periodic order in soft matter systems and self-assembled nanomaterials. (Petukhov et al.,

2015) By X-ray scattering methods it is also possible to study time-dependent processes and transient dynamics in real-time. (Narayanan et al., 2017)

In the most of cases the best results of the structural characterization with X-ray methods can be achieved using synchrotron radiation, due to the high intensities and, therefore, high signal-to-noise ratio in rational time intervals of the data acquisition.

Coherent X-Ray diffraction imaging (CXDI or CDI) is a lensless imaging. It is the 2D speckle pattern obtained when a non-crystalline specimen is lightened by a coherent X-ray beam at different angles of the incident ray illumination. (Miao et al., 2015) After the application of suitable methods of tomographic reconstruction, 3D images of micron sized objects with a resolution of about tens of nanometers can be obtained. (Narayanan and Konovalov, 2020)

CXDI for the first time was applied in 1999 and has shown great promise for the study of various biological objects. (Miao et al., 1999) Thanks to this study, it is only necessary to measure the coherent diffraction pattern of the sample. Using this technique, it is possible to bypass the limitations imposed by an X-ray optical system and obtain high-resolution images. The idea of transforming the diffraction pattern belongs to the assumption of Sayre (Sayre, 1980; Sayre et al., 1998), and was applied in 1999 by Miao et al. (Miao et al., 1999)

Then Miao proved that the reconstruction of the diffraction patterns of the sample would allow obtaining full-fledged three-dimensional images in the future. (Miao et al., 1999; Shapiro et al., 2005) At first, the CXDI measurements were applied to metal test objects, what allowed to obtain two dimensional (Marchesini et al., 2003; Miao et al., 1999) and then

three dimensional images.(Miao et al., 2002) Later, images with stained biological specimens (Miao et al., 2003) and microcrystals (Williams et al., 2003) were reconstructed.

The method itself is relatively simple. However, it requires the source, providing coherent X-ray beam. Therefore, the method is possible to use only with synchrotron radiation. The sample is placed on a thin film. Next, a coherent beam of X-rays falls on it, and the far-field diffraction pattern is recorded by the camera of the charge-coupled device (CCD). The intensity measurements are converted to amplitudes and passed to the iterative algorithm (Fienup, 1978) to extract the phases. As CXDI is based on diffraction, the image is reconstructed by an inverse Fourier transformation. (Gallagher-Jones et al., 2014; Lima et al., 2009)

Iterative algorithms based on Fourier transformations was used for deriving the phases from the oversampled diffraction patterns. (Bauschke et al., 2003; Chen et al., 2007; Elser, 2003; Fienup, 1978, 1982; Luke, 2004; Marchesini, 2007) This process usually consists of 4 steps. (Miao et al., 2011)

1. A random phase set and the measured Fourier modulus are combined. The image is obtained by considering the inverse fast Fourier transform (FFT).
2. For the image a support is determined. The electron density beyond the support and the negative one within the support are approaching zero. As a result, a renewed image is gained.
3. The FFT is applied to the renewed image. The Fourier modulus and phases are calculated and then the new Fourier modulus is substituted for the measured one, whereas the new phases are remained constant.
4. The renewed image is obtained. For this the inverse (Fienup, 1978, 1982), error reduction (Fienup, 1978, 1982), differ-

ence map (Elser, 2003), guided hybrid input–output (Chen et al., 2007), shrink wrap (Marchesini, 2007), hybrid projection reflection (Bauschke et al., 2003), and relaxed averaged alternating reflectors. (Luke, 2004; Miao et al., 2011)

Even if the principle of the CDI method is rather clear and simple, the experimental part of it faces with some difficulties. Primarily, the diffraction patterns of a noncrystalline sample have a weaker intensity distribution in comparison with a crystal. Then, the incident beam must be coherent, and the necessary coherent length is conjugated to the oversampling ratio of the diffraction pattern. (Miao et al., 1998, 2002) Thirdly, in comparison with the images in the space, the diffraction intensity has a greater dynamic range. Because of this the data acquisition turns into a challenging task. In their fourth, for measuring diffraction patterns of a fine quality it is necessary that there are area detectors with both a high dynamic range and high quantum efficiency. Fifth, a beamstop should block the direct beam. This is necessary because the intensity of a direct beam is much higher than the diffracted one. The missing intensity in the center of the diffraction pattern because of the beamstop shows the low-frequency information. This is crucial to the phase-retrieval process. After all, the oversampling method with iterative algorithms is complicated to represent the experimental data because of the existence of a multiple kind of noise. But this method is good for simulated data. (Miao et al., 2011)

In 1999 Miao and his colleagues had resolved these difficulties. (Miao et al., 1999) All diffraction images were measured by a liquid nitrogen cooled charge-coupled device (CCD) camera that had high quantum efficiency and very low noise at used wavelengths. Then they had accumulated many patterns at the same specimen orientation and after that they had

summed up all acquired data. This was done to increase the dynamic range of the diffraction pattern. For dissolving the problem with a missing center, they had used data, obtained with a low-resolution tool such as an optical microscope image of a sample. Subsequently they had calculated the Fourier modulus received from the low-resolution image and after they had filled the missing intensity. Later the problem of a missing intensity in the center was resolved and it was not necessary to use low-resolution optical images. (Miao et al., 2005, 2011)

Lately CDI has developed into different methods.

1. Plane-wave CDI (Fig. 1.4(A)). In this method a sample is illuminated by a plane wave. As a result, the far-field diffraction image is measured. (Miao et al., 1999) The wavelength of the incident beam, the sample size, the detector pixel size and the distance between the sample and the detector are the factors that defines the oversampling ratio of the diffraction pattern. (Miao et al., 1998, 2003) For obtaining 3D images of an object, it is required to rotate around a tilt axis the sample during the experimental set. This is done for obtaining a set of 2D images of a diffraction patterns at different specimen orientation. In comparison with other methods, this one has some benefits, like:

- This method is insensitive to the vibration of a specimen during the time when it is in the zone of illumination.
- It is quite easy to obtain a 3D reconstruction of the sample structure.
- The diffraction intensity is not encumbered by Poisson noise in the direct beam and the diffraction intensity from upstream optics. (Xu et al., 2011)
- It can be used in a one-time experiment with intense coherent X-ray sources. That is why this method gave the

highest spatial resolution (up to 2 nm) and a possibility to construct 3D image. (Jiang et al., 2008, 2010; Miao et al., 2002, 2005, 2006; Nishino et al., 2009; Takahashi et al., 2009, 2010a,b)

The main disadvantage of this method is a requiring of a well-defined isolated objects. (Miao et al., 2011)

2. Bragg CDI (Fig. 1.4(B)). (Newton et al., 2010; Pfeifer et al., 2006; Robinson and Harder, 2009; Robinson et al., 2001; Williams et al., 2003) is mainly used for structure study of nanocrystals. The diffraction intensity distribution at each Bragg reflection is corresponded to the deformation inside the nanocrystal and to the shape function of it during the illumination of a nanocrystal by coherent X-ray wave. Nanocrystals' 3D shape function and the internal deformation field can be obtained in the case when numerous diffraction patterns around a Bragg reflection are acquired. If three or four Bragg peaks are measured, the full deformation tensor can be obtained. In comparison to other CXDI methods, only Bragg CDI allows to obtain the 3D deformation tensor and ion replacement inside nanocrystals at the nanometer scale resolution. (Miao et al., 2011)
3. Scanning or ptychographic CDI (Fig. 1.4(C)). (Dierolf et al., 2010; Giewekemeyer et al., 2010; Rodenburg et al., 2007; Thibault et al., 2008) In this method for assessing an illumination probe a circular aperture or focusing optics are used. During scanning of a sample through an illuminating probe, a sequence of two-dimensional diffraction patterns is obtained, each of which overlaps with neighboring ones. This redefinition can improve the convergence of the phase retrieval process. (Miao et al., 1998) The advantages of scanning CDI are in its applicability to extended objects, it

gives a reconstruction not only of the probe but also of the object simultaneously and with the fast convergence of the algorithm.

However, compared to plane wave CDI, scanning CDI has the following disadvantages:

- For obtaining each 3D image, 2D X-Ray probe scan is required. Moreover, any vibration of a sample can weaken the 3D resolution.
  - For weak diffusers (e.g., biological samples) Poisson noise in the illumination probe can destroy the high-resolution signal from the sample.
  - 3D reconstruction turns out more complicated during the interaction between the probe and the sample and the curvature of the Ewald sphere. This is especially noticeable at high resolution. (Miao et al., 2011)
4. Fresnel CDI (Fig. 1.4(D)). (Williams et al., 2006) In this type of CDI, a focusing optics (zone plate) is applied for creating a curved wave front to illuminate a sample. The illumination function of the probe should be obtained in advance in order to get the image of the sample. Usually, a detector measures two types of patterns of a prepared sample. At a higher scattering angles a diffraction pattern is measured. At a lower scattering angles a hologram or an inference patterns are obtained. The hologram is obtained by the interference of the scattered wave and the curved incident wave from the sample. Then these two patterns are merged into one. This is done for restoring the structure of the sample at high resolution.

The main advantages of Fresnel CDI are:

- It is possible to reconstruct an image of a sample subre-



gions from a single experimental data set.

- Rapid convergence of reconstructed images is due to the curvature of the incident wave.

On the contrary for Fresnel CDI, it is required that the sample is stable against the incident beam. Also, Fresnel CDI was applied to the scanning of a continuous sample. (Abbey et al., 2008a,b) In this case the technique is called keyhole diffractive imaging. This technique allows the option that visual field can be zoomed in or out by changing the position of the sample with the respect of beam focus. (Miao et al., 2011)

5. Reflection CDI (Fig. 1.4(E)). In this case we obtain 3D height maps of surface. The transverse resolution is a near-wavelength, vertical resolution is a sub-nm, phase and amplitude contrast is very high because of the short wavelength of the illumination light. (Robinson et al., 1999; Roy et al., 2011; Seaberg et al., 2014; Sun et al., 2012) A coherent X-ray beam lightens an object and as a result the diffracted light can be collected with very high numerical aperture. Then this method is blended with ptychographic imaging and only then images of an object are obtained. (Seaberg et al., 2014) This method is supplement to other imaging methods, such as scanning electron microscope (SEM) and atomic force microscopy (AFM) but this method gives less damage and higher contrast imaging in respect to other methods. (Miao et al., 2015)
6. Phase retrieval algorithms (Fig. 1.4(F)). There are iterating between real and reciprocal space. (Miao et al., 2015) Each iteration includes 4 steps:
  - At the beginning there is a random phase set. This set is combined with the measured Fourier magnitude. An

initial image is found by applying an inverse fast Fourier transform (FFT).

- It is possible to estimate a contribution of a support from the image. It depends on oversampling of the diffraction intensity. Outside the support the electron density is lowered, inside the support the negative electron density is changed.
- A new Fourier transform is formed by applying a FFT to the enhanced image.
- The magnitude is replaced by measured data. Then a more accurate assessment of the Fourier transform is obtained and is used for the further iteration.

These steps are repeated till the correct phase set is retrieved. (Miao et al., 2015)

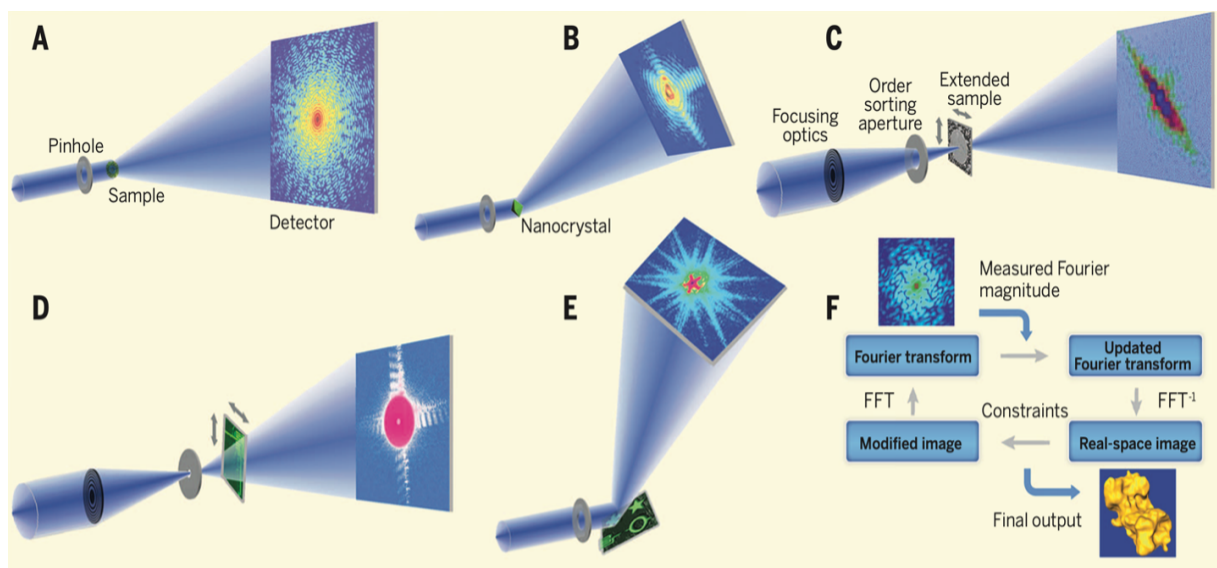


**Fig. 1.4** Schematic layout of five main CDI methods and iterative phase retrieval algorithms. (A) Plane-wave CDI. (B) Bragg CDI. (C) Ptychographic CDI. (D) Fresnel CDI. (E) Reflection CDI. (F) Phase retrieval algorithms. From (Miao et al., 2015).

The CXDI resolution, like in the case of crystallography, is restricted by the wavelength of the radiation and by the angle at which the scattered photons are counted. Despite the fact

that the diffraction imaging method dispenses with all the losses in the efficiency and contrast of the lenses, we expect that the radiation dose which is necessary to register a faint continuous pattern will also limit the resolution (Shapiro et al., 2005; Shen et al., 2004) However, at the beginning, the use of this method for biological objects was limited due to the fact that the induced radiation damage and the extended nature of biological samples can damage samples structure, the latter limits the use of most of the phasing algorithms. (Dixon et al., 2018)

In recent years, considerable progresses have been made in the visualization of a wide range of objects, including small particles and nanocrystals.(Chapman et al., 2006; Miao et al., 1999; Pfeifer et al., 2006; Williams et al., 2003; Zuo et al., 2003) However, most of the studied cases are related to non-biological systems, with some notable exceptions, such as *Escherichia coli* bacteria (Miao et al., 2003), freeze-dried yeast cells (Shapiro et al., 2005), mineral phase in bones (Jiang et al., 2008), unpainted viruses (Song et al., 2008b), and the human chromosome. (Nishino et al., 2009) There are serious limitations of the application of CXDI for studying biological samples: one of them is the radiation damage of the samples under the influence of the X-ray beam. However, this problem can be resolved by some specific approaches, such as cryocooling or recording a series of patterns from several identical samples. The latter one corresponds to an approach to solving the problem of visualizing a single molecule in future free electron lasers. However, some biological samples can withstand the minimum radiation dose required for their coherent imaging. (Dixon et al., 2018)

First CXDI experiments on biological samples had shown the capabilities of the visualization of cells or subcellular organelles with a resolution of 20-40 nm. (Miao et al., 2003; Nishino et al., 2009; Shapiro et al., 2005; Song et al., 2008b) These

experiments were carried out on dried samples. The most of biological samples are water-based and are very sensitive to radiation damage. To bring the conditions of the most natural state, the samples were frozen. (Glaeser and Taylor, 1978; Nermut, 1988; Schneider, 1998; Wang et al., 2000) The samples were prepared by rapid freezing in liquid ethane to minimize ice crystal formation. (Huang et al., 2009)

Summarizing, CXDI is perfect for quantitative 3D characterization of materials at the nanoscale. It is since X-rays have a larger penetration depth than electrons. Also, CDI can retrieve the mass density by quantifying the incident and diffracted X-ray flux. Hence, different phases in materials in 3D are recognized. (Jiang et al., 2013) Moreover, in case when the shell absorbs X-ray, the chemical contrast is provided. Magnetic contrast and molecular orientation are provided when their polarization can be used. So, CDI includes nanoscale chemical, elemental, and magnetic mapping of complex matter. (Shapiro et al., 2014; Song et al., 2008a; Tripathi et al., 2011) Finally, thanks to the high temporal resolution of the new coherent X-ray sources, it becomes possible to record the spin, fastest charge, and lattice motions in matter in different time scales and length. (Miao et al., 2015)

In this section we will consider the first application of CDI method for studying the structure of nanoengineered polymeric capsules, loaded with gold nanoparticles.

---

#### 1.4. **MAGNETIC NANOPARTICLES**

The discovery of new methods for the use of magnetic nanomaterials increases the relevance of their study. Due to the easy way of synthesis and cheapness of materials, the use of magnetic materials is very perspective. (Gilchrist et al., 1957; Moghimi

et al., 2001; Panyam and Labhasetwar, 2003; Wilkinson, 2003)

Quantum size effects and the large surface area of magnetic nanoparticles can vary some of the magnetic features. Since each particle can be seen as a single magnetic domain, quantum tunneling magnetization and superparamagnetic phenomena can be shown. (Goya et al., 2003) Superparamagnetic nanoparticles can be applied in a large field of biomedicine due to their chemical, physical, mechanical, and thermal features. (Arbab et al., 2003; Pankhurst et al., 2003; Reimer and Weissleder, 1996; Zborowski et al., 1997) For example: drug delivery, hyperthermia, magnetic resonance imaging (MRI), tissue repair, magnetofection, cellular therapy, such as cell labelling, targeting etc.

To use these particles in the field of biomedicine, they should include some features like biocompatibility, high magnetic saturation, and interactive functions at the surface. The surface of such particles can be modified by its functionalization. (Berry and Curtis, 2003) Modified magnetic nanoparticles have a great potential in the field of in vivo and in vitro applications. The efficiency of them depends on sizes of particles, high magnetic susceptibility, superparamagnetic behaviour etc. (Jordan et al., 2001; Tartaj et al., 2003)

Magnetic nanoparticles have proliferated in the drug delivery sphere (Lübbe et al., 2001; Rudge et al., 2000; Schütt et al., 1997), bioseparation (Neuberger et al., 2005), the immobilization of peptides, proteins, enzymes, biosensors etc. (Gupta and Gupta, 2005; Riggio et al., 2012; Rozhina et al., 2021) They have ideal size for these purposes: from submicrometer (up to several nanometers) to micrometer. In the last few years due to the prompt growth of nanotechnology and nanomaterials in medicine and biotechnology, nanoparticles have obtained signif-

icant focus. For example, they are very promising in the field for the delivery of anticancer drugs. One of the most used and easy made MNP is magnetite  $Fe_3O_4$ . This is because of its biocompatible, low toxicity, catalytic activity, and strong magnetic properties. Over last few years the usage of magnetite in the field of biotechnology and medicine was significantly increased. (Curtis and Wilkinson, 2001; Dresco et al., 1999; Fang et al., 2005; Huang et al., 2003)

It is quite important to prepare and store the colloidal solution of such particles. It is necessary to cover the nanoparticles with some kind of surface coating because without this protection the magnetic iron oxide particles form agglomerates and large clusters due to hydrophobic interactions between the particles. (Bailey, 1983; Charles and Popplewell, 1980; Hamley, 2003; Khalafalla and Reimers, 1980) As a result this clusters increase the actual particles size. Moreover, these clusters form a strong dipole-dipole interactions between them and show ferromagnetic behavior. (Hamley, 2003) Also, at the time when two different clusters getting closer, each of them comes into the magnetic field of the other one and gets further magnetized. (Tepper et al., 2003)

For effective stabilization of magnetic nanoparticles (MNPs), it is necessity to find a fairly dense chemical substance for covering them. In some cases, stabilizers are added during the synthesis of the particles. (Mendenhall et al., 1996) These coatings may be consisted of a few materials, e.g., inorganic compounds and organic polymers. (Daniel and Astruc, 2004; Merrill and Salzman, 1983; Yu et al., 2003)

---

#### 1.4.1. **Magnetic nanoparticles in drug delivery**

One of the most promising and perspective type of magnetite particles' application is in drug delivery field. In fact, they

could be used as a vehicle for a drug that could be transferred to a target zone and released there. In this case the charge, size and surface structure of magnetite are especially important. (Chouly et al., 1996) Moreover, magnetic properties of magnetite depend on their size. (Chatterjee et al., 2003) For example, particles with the size from 10 to 100 nm are optimal for human body, especially they are optimal for intravenous injection. This is related to the fact that they can be effectively distributed in certain tissues, can prevent penetration into small capillaries within the body tissues. In the case with particles' sizes are less than 10 nm, they are removed fast through extravasations and renal clearance. For the particles larger than 200 nm there are other problems. Most of them are insulated by the spleen because of mechanical filtration and then are eliminated by the cells of the phagocyte system. (Pratsinis and Vemury, 1996)

In 1970 Widder et al. had provided an idea of magnetic targeting. This concept includes the use of a magnetically susceptible material that is coated with a drug. Then this substance is injected into the body and an external magnet is used to direct the drug to the target area. For this, a sufficiently strong magnet must be used, since it is necessary to keep the particles in the field flow, for example, in the vascular network. (Rudge et al., 2000; Widder et al., 1978)

Magnetite particles were used for targeted delivery for the first time as it is described in (Rudge et al., 2000; Widder et al., 1983). They had been coated with crosslinked albumin. This system was used for encapsulation of doxorubicin. Yoshida sarcoma tumor was implanted in a rat tail and the complex of MNP and doxorubicin was used for its treatment. But this type of particles was not tested in humans' body because of scaling up and the problem of magnetic sensitivity. (Rudge et al., 2000;

Widder et al., 1983)

However, the possible negative consequences of the presence of inorganic particles in the body like magnetic nanoparticles should be taken into account. Experiments on the toxicity of magnetic nanoparticles were done *ex vivo*. The result of the experiments demonstrated that magnetite has rather low cytotoxicity and many side effects. (Bouhon et al., 1997; Gupta and Curtis, 2004) In any case to prevent capillary blockade the final size of a drug delivery system should not be larger than 5  $\mu\text{m}$ .

Gomez-Lopera et al. had described a method of synthesis of colloidal particles formed by the magnetite particles and a biodegradable polymer. (Gomez-Lopera et al., 2001) This experiment was done using a double emulsion technique in order to obtain polymeric spheres loaded with a drug. In this experiment it was important to find “ideal” colloidal particles that could be used in drug delivery sphere and magnetic field responsive. As a result, they found out that biodegradable polymers are perfect as drug carriers due to their minimum toxicity and immunological response. (Chilkoti et al., 2002; Najafi and Sarbolouki, 2003; Otsuka et al., 2003)

Incorporation of magnetic nanoparticles in the drug delivery system can be useful to reduce the dose of drugs and to reduce the side effects on healthy tissues. Moreover, it can reduce the price of a treatment.

---

#### 1.4.2. ***NP in layer-by-layer technique***

The usage of a complex of NP in LbL-technique allowed receiving of hybrid organic-inorganic multilayer composites. (Holland et al., 1998) By varying the NPs size and type of polymer in LbL complex, it is possible to achieve unique combinations of mechanical, magnetic, optical, and electrical properties. These



films showed promising characteristics in preparation of sensors, resists, light-emitting diodes, eclectically conductive films, non-linear optical devices, gas separation membranes. (Aliev et al., 1999; Mamedov et al., 2000)

The incorporation of  $Fe_3O_4$  particles in the *layer-by-layer* films is also possible. (Lu et al., 2003) The first films that had included magnetite were fabricated from cationic polydi-allyldimethylammonium (PDDA)-coated  $Fe_3O_4$  nanoparticles and anionic polyimides. These films were deposited on crystal silicon and quartz by LbL-technique. (Cao and Hu, 2006; Liu et al., 1997)

As a result, layered complex of magnetic nanoparticles can be synthesized on different substrates by the consecutive adsorption of polyelectrolytes. These films can be used for different applications. Moreover, the magnetic properties of  $Fe_3O_4$  nanoparticles in the film are saved.

---

## CHAPTER 2

---

# **MATERIALS AND METHODS**

---

## 2.1. Materials

Calcium chloride (anhydrous, granular), sodium carbonate (anhydrous), poly(4-styrenesulfonic acid) (PSS,  $M_w \sim 70000$ ), poly (allylamine hydrochloride) (PAH,  $M_w \sim 56000$ ), Polyethylenimine (PEI, 50% (w/v) in  $H_2O$ ), poly (diallyldimethylammonium chloride) (PDADMAC, 20 wt. % in  $H_2O$ ), chitosan (CHI,  $M_w \sim 50000-190000$ ), alginate (ALG,  $M_w \sim 120000-190000$ ), pectin (PE,  $M_w \sim 30000-100000$ ), Rhodamine B were purchased from Sigma-Aldrich Co.

Ethylenediaminetetraacetic acid (EDTA, 99%, pure), Iron(III) chloride hexahydrate (99+%, for analysis,  $FeCl_3 \cdot 6H_2O$ ), Iron(II) chloride tetrahydrate (99+%,  $FeCl_2 \cdot 4H_2O$ ), Sodium hydroxide (98%, pure, flakes,  $NaOH$ ) were purchased from Acros Organics.

Aquacobalamin (Vitamin B12) and demiglumine chlorin E6 were purchased from Alfa Aesar.

Fluorescein sodium salt was purchased from Carlo Erba.

Hydrochloric acid (1 mol/l (1 N), HCl), ammonia solution (25%,  $NH_4OH$ ) were purchased from VWR Chemicals.

Gold NPs were synthesized previously in our scientific group. (Berzina et al., 2011) In this work the already prepared particles were used. The capsules were loaded according this protocol (Erokhina et al., 2013).

HEK293FT (ATCC CRL-11268) cell lines were used in the work as templates. The cell lines were given by the lab "Gene and Cellular Biomedical Technologies" (Kazan Federal University). (Gomzikova et al., 2018, 2019)

Water, used in the experiments for the solutions preparation and washing, was purified by Milli-Q system and had the

resistance of 18.2 MΩ cm.

---

## 2.2. Methods

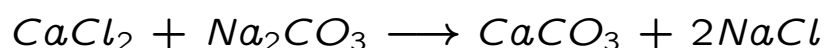
---

### 2.2.1. Fabrication of capsules by layer-by-layer technique

---

#### 2.2.1.1. Synthesis of templates

Templates were prepared according to the protocol that is described in literature (Volodkin et al., 2004a). In the beaker 1ml of 0.33M sodium carbonate  $Na_2CO_3$  was added to 1 ml of 0.33M calcium chloride  $CaCl_2$  (the volume ration is 1:1) and actively mixed on a magnetic stirrer for 20 sec. Immediately after adding sodium carbonate, the solution turned white due to the formation of a suspension of calcium carbonate  $CaCO_3$  microparticles. The microparticles were placed into Eppendorf tubes, centrifuged at 1410 rpm for 1 min and washed three times with water. It was done to prevent the crystallization of  $CaCO_3$  microparticles. Moreover, it is necessary to cover the  $CaCO_3$  microparticles with a polymer immediately after they are produced. This step allows to avoid the process of forming agglomerates and particles clumping. The synthesis temperature and the centrifugation temperature is 24°C. The reaction of the formation of microparticles is following:



#### 2.2.1.2. Shell formation

The protocol of the NPCs fabrication is described in literature (Donath et al., 1998). We have followed it. The basic steps of depositing layers to spherical objects using LbL technique are shown in the Fig. 2.1.

After the third washing of templates ( $CaCO_3$  particles that were synthesized on previous step), we have replaced water with

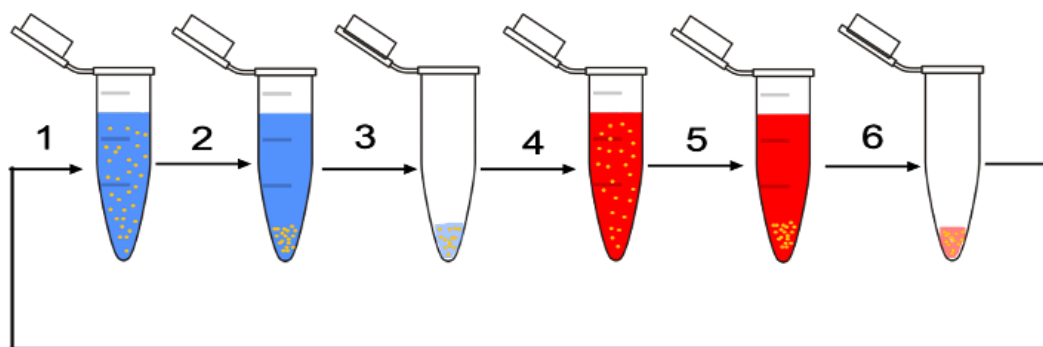


**Fig. 2.1** Scheme of shell formation. 1) Polyanion solution was added to the templates. 2) Centrifugation. 3) Supernatant is removed. Washed at least 3 times. 4) Adding of polycation solution. 5) Centrifugation. 6) Supernatant is removed. Washed at least 3 times. These steps are repeated till the required number of layers are received.

polyelectrolyte, specifically, with a polyanion. As a polyanion have been used:

- PSS;
- ALG;
- PE.

The suspension of templates with a polyanion was stirred for 10 min. Then the polyelectrolyte solution was replaced with water. The sample was washed three times to clean from the unadsorbed polyelectrolyte. After each adding of polyelectrolyte and washing, the sample was centrifuged at 4240 rpm for 1 min, the centrifugation temperature is 24°C. One layer is ready. When the sample is washed three times, 1 ml of the polycation was inserted. As a polyanion have been used:

- PAH;
- PDADMAC;
- CHI;
- PEI.

The same procedure as for polyanion was done. The pro-

cedure was repeated as many times as it was necessary for the experiment, till reaching the desired number of layers in the shell.

The concentration of all polyelectrolytes was 2 mg/ml except CHI. The concentration for CHI was 0.5 mg/ml. Also, some amount yellow (0.25 - 0.5 ml) of 1N HCl was added to CHI solution before the salt is dissolved. The centrifugation temperature is 24°C.

---

### 2.2.1.3. ***The dissolution of a core***

As soon as the required number of layers is formed, the core should be dissolved to fabricate hollow capsules. Hollow capsules can be used then for encapsulation. For dissolving, 1N HCl or 0.2M EDTA (pH 5-7) can be used. There are some specific features of using them. The Hydrochloric acid dissolves the core faster, the reaction is visible due to the formation of carbon dioxide. Unfortunately, it is more reactive and can destroy the capsule completely or the upper polymer layers. This behaviour can be explained due to the low pH that is required for dissolution of the core. Vice versa, EDTA solution is a more "sparing" acid and dissolute the core a little bit longer. In some cases, several portions of EDTA are required for dissolving the core. (Antipov et al., 2003a; Pastorino et al., 2015)

In case of EDTA, the 1 ml of 0.2 M solution was added to the sample (Fig. 2.2).

It was incubated for 30 minutes, washed with a distilled water 3 times. The procedure can be repeated for the second time if it is necessary. The pH of EDTA should be 5-6. After adding of EDTA/water, the sample was centrifuged at 5650 rpm for 5 minutes.

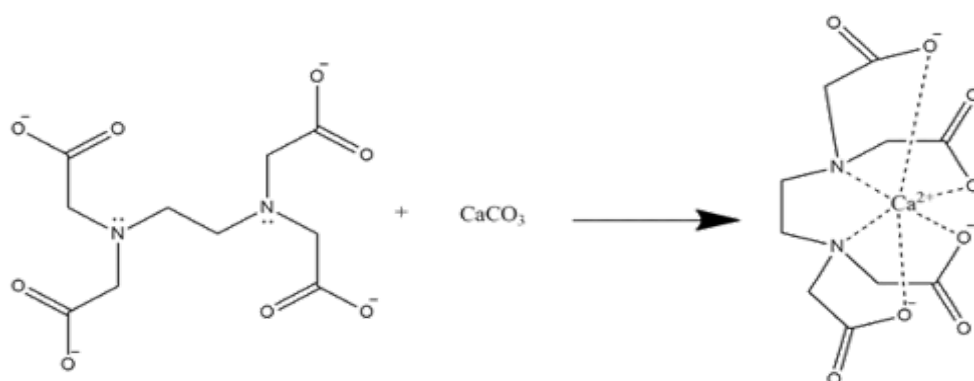


**Fig. 2.2** The formation of a Ca-EDTA complex

Similarly, 1N HCl can be used. In this case, it was added to the sample dropwise till the formation of  $CO_2$  bubbles.



After the dissolution of the core, the solution turns from white to transparent.

### 2.2.2. *Sample preparation for CXDI*

The capsules were prepared according to the protocol described above (2.2.1.2.). There were 2 types of capsules: one with 6 layers of polymers in the shell and the other – with 12 layers. CXDI measurements were carried out at ID10 station of European Synchrotron Radiation Facilities (ESRF), 8.1 keV radiation was used. The sample detector distance was 5280 mm. (Narayanan and Konovalov, 2020; Stadler et al., 2008)

Hollow polyelectrolyte capsules were fabricated in 0.15M NaCl solution by alternating adsorption of PSS/PAH layers on  $CaCO_3$  microparticles. The template was dissolved at pH 4 with 1 ml of EDTA (0.2 M), centrifuged at 24°C and washed 3 times. 1 ml of  $CdCl_2$  (0.125M) was added to each type of specimens and stored overnight at 4°C. This was done to increase the contrast of the objects. Then, microcapsules were centrifuged at 24°C, washed ( $n = 3$ ) and stored at 4°C.

Fabricated hollow capsules were divided and loaded with 5

nm and 50 nm gold nanoparticles, respectively. When pH was 4, the NPCs were open and loaded with gold nanoparticles, at pH 9 – they were closed.

For CXDI measurements, silicon nitride windows with the following parameters were used: frame:10.0×10.0 mm, 200  $\mu\text{m}$  thick; membrane: 3.0×2.0 mm, 100 nm thick, product code: SiRN-10.0-200-3.0-100 (Silson, UK). In the case of dry samples, the drop of solution is poured and dried directly on the membrane. For the measurements in liquid, a frame was built with the 3D printer, in which the two membranes formed the “chamber” to contain the drop. To prevent the evaporation of the liquid, the whole perimeter of the double membrane system was covered by the “vacuum grease”. The sample was fixed in a special frame with the window size, corresponding to the external sizes of the membrane frame (Fig. 2.3). (Erokhina et al., 2017, 2021)

The scheme of the experiment is shown in Fig. 2.3. Samples were rotated with respect to the incident X-ray beam in the range of

- $-70^{\circ}$ – $70^{\circ}$ . Diffraction patterns were acquired after each  $0.2^{\circ}$ . Data acquisition at each point was 1 s.
- $-64^{\circ}$ – $64^{\circ}$ . Diffraction patterns were acquired after each  $0.25^{\circ}$ . Data acquisition at each point was 2 s.
- $-72^{\circ}$ – $68^{\circ}$ . Diffraction patterns were acquired after each  $0.25^{\circ}$ . Data acquisition at each point was 2 s.
- $-68^{\circ}$ – $70^{\circ}$ . Diffraction patterns were acquired after each  $0.25^{\circ}$ . Data acquisition at each point was 2 s.
- $-66^{\circ}$ – $70^{\circ}$ . Diffraction patterns were acquired after each  $0.2^{\circ}$ . Data acquisition at each point was 1 s.
- $-68^{\circ}$ – $68^{\circ}$ . Diffraction patterns were acquired after each  $0.2^{\circ}$ .



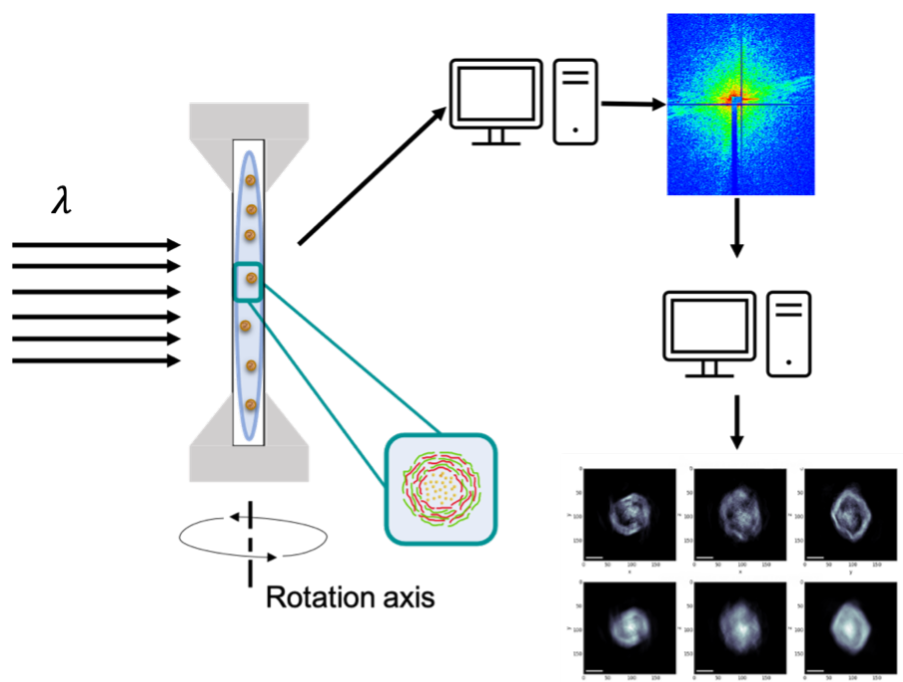


**Fig. 2.3** Scheme of the experiment: NPC solution is placed between 100-nm-thick silicon nitrate membranes, during the acquisition it is rotated around the vertical axis and shifted along the height for the position adjustment, when necessary. Diffraction patterns were acquired at each rotation angle. Reconstruction of the capsules structure was done according to the protocol on ID-10 beamline (ESRF).

Data acquisition at each point was 1 s.

Then the resulting diffraction patterns were processed according to the computer protocol of the ID10 line. As a result, the reconstructed images were obtained.

Some points of the calculations, that are included in the protocol, is described below. Firstly, it is necessary to remove the background scattering. The diffraction patterns were acquired for each tilt angle by changing the position of the frame. For acquiring correct intensities, the background pattern was deducted from the diffraction pattern. Some parts of the low-resolution zone of the acquired diffraction pattern were blocked by a beam stop. (Fig. 2.4)

Pixels with missing values were left as unknown, others were extracted according to the symmetry. All received pro-

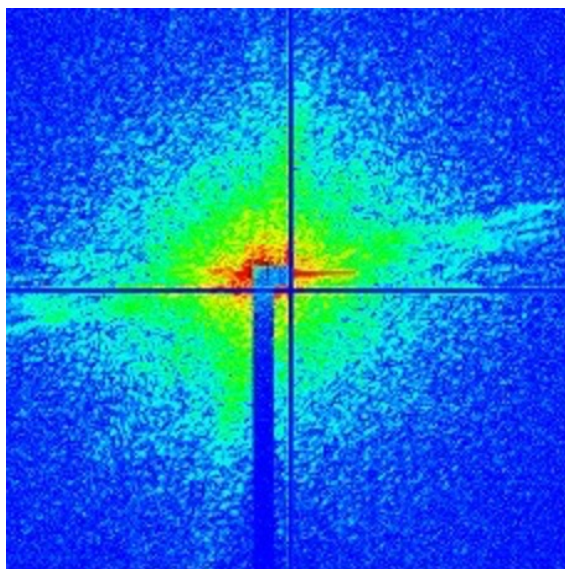
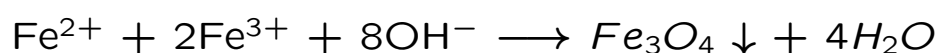


**Fig. 2.4** The typical representation of the diffraction pattern acquired from a sample. The two-dimensional projection.

jections were studied in this way using a data analysis done in Matlab. (Rodriguez et al., 2015; Xu et al., 2011)

### 2.2.3. *Synthesis of magnetite*

The magnetic nanoparticles were prepared according to the protocol described in the literature (Lu et al., 2006; Shchukin et al., 2003). The MNPs stabilized with polyelectrolyte were prepared. Initially, unstabilized magnetic particles were synthesized following the protocol described by Lu et al. in 2006 (Lu et al., 2006) with minor alterations. Namely, 2 ml of 1M  $FeCl_3 \cdot 6H_2O$  and 0.5 ml of 2M  $FeCl_2 \cdot 4H_2O$  were mixed, stirred vigorously and heated up to 80°C. A volume ratio of two salts is 4:1. Then dropwise (1 drop/sec) was added 25 ml of 0.5M NaOH or 1M  $NH_3 \cdot H_2O$  during stirring of the mixture. While the alkaline solution was added, a dark magnetic suspension appeared immediately. The reaction of the process is following:



After adding of alkaline solution, the mixture was heated up to 95°C with vigorously stirring for 30 minutes. Then the mixture was cooled to room temperature, the precipitate was

collected by an external magnet, and the supernatant was replaced with water. The mixture was washed with water until the pH was approximately 7.0.

Then 1 ml of the synthesized NP was placed into the solution of polycationate (PDADMAC, PAH, PEI) with its concentration of 10 mg/ml. The mixture was sonicated for 20 minutes. Then this sample was washed with a water 5 times. After it was passed with a syringe through the 0.45  $\mu\text{m}$  filter. The particles are ready to use.

---

#### **2.2.4. *Fabrication of capsules with MNP***

The procedure of synthesis capsules with magnetic nanoparticles in the shell is the same but there is the only difference. It is necessary to use a solution with stabilized by a polymer magnetic nanoparticles as one of the last layers. Then, as usual, the sample was centrifugated and washed 3 times. After it, the oppositely charged polyelectrolyte was added.

---

#### **2.2.5. *Transmission and fluorescent optical microscopy***

Images were taken by Fluorescence Optical Microscope Nikon Ni-E with Camera Type: Nikon DS-Qi2 in transmission geometry. Exposure time was 300 ms. All images were acquired and elaborated according to NIS Elements Imaging software. Samples were placed on glass supports. It was possible to study objects in transmission mode of a microscope.

---

#### **2.2.6. *Scanning Electron Microscopy (SEM)***

SEM measurements were carried out by Zeiss Supra microscope with accelerating voltage of 1 kV. This low voltage was used for investigation of thin dielectric samples without sputtering a conductive layer on them. Samples were dried on silicon supports. The surface of supports were treated by depositing of

$PEI - (PSS - PEI)_2$  layers for better adhesion of capsules and particles. Silicon supports are quite good conductive materials with a smooth surface.

---

### 2.2.7. *Transmission electron microscopy (TEM)*

TEM analysis was performed by a TEM JEOL JEM-2200FS with Schottky field emission gun at 80 kV. For TEM observations the samples were prepared depositing a drop of the suspension containing the magnetite nanoparticles on a commercial TEM grid covered with a thin carbon film. The grid was kept in air at room temperature until complete solvent evaporation.

---

### 2.2.8. *Atomic force microscopy (AFM)*

AFM images were obtained using a Dimension Icon microscope (Bruker, USA), operating in Peak Force Tapping mode, using a Scan Asyst-Air probe (Bruker) (nominal length 115 $\mu$ m, tip radius 2nm, spring constant 0.4N/m, 1–2 nN scanning force at a scanning rate in the 0.8–0.9 Hz range). Scanning was carried out in air at room temperature. The sample was prepared on silicon supports. The core was dissolved, and the measurements were done on dried samples.

---

### 2.2.9. *Spectrophotometric experiments*

Spectrophotometric experiments were performed with a UV/Vis double-beam spectrophotometer (V730, Jasco, Tokyo, Japan) , by using 1 cm pathlength quartz cuvette.

---

### 2.2.10. *Red Green Blue (RGB) color model*

For characterization the color inside and outside the capsules, we have used the RGB color model. It is an additive color model. The red, green, and blue are primary colors of light. They are mixed in different options for representing a wide se-

lection of colors. (Hirsch, 2004) The RGB color model gives the response of a point to the individual red, green, and blue levels. The color is represented as values triplet of red, green, and blue. Each value varies from zero to a defined maximum. In the case when all the components are zero, it means the black color. The red, green and blue use 8 bits each, which have integer values from 0 to 255. In this case there are  $256 \times 256 \times 256 = 16777216$  possible colors. This system is widely used in computer graphic.

In any graphic editor, it is required to use such tool as a pipette. By placing this tool at the desired point, we get the RGB triplet for this point. That is, we get three numbers, namely, the number of bits corresponding to red, green, and blue shades, that are used for obtaining the original color.

---

## CHAPTER 3

---

# **RESULTS and DISCUSSION**

### 3.1. Synthesis of microcapsules by LbL technique

The capsules that can be used as a container for delivery of chemical substances were synthesized according to the scheme described previously (Fig. 2.1).

As the first step of these process, calcium carbonate ( $\text{CaCO}_3$ ) particles for their successive utilization as templates were fabricated according to 2.2.1.1. Their shape and size were analyzed by optical microscope (Fig. 3.1). The particles size varies in range from 3.64  $\mu\text{m}$  to 6.03  $\mu\text{m}$ . The shape of capsules is mostly spherical, but in some cases deviations are observed and the capsules are more faceted. The size distribution of  $\text{CaCO}_3$  particles, obtained after analysis of 10 acquired images, is in Fig. 3.2.

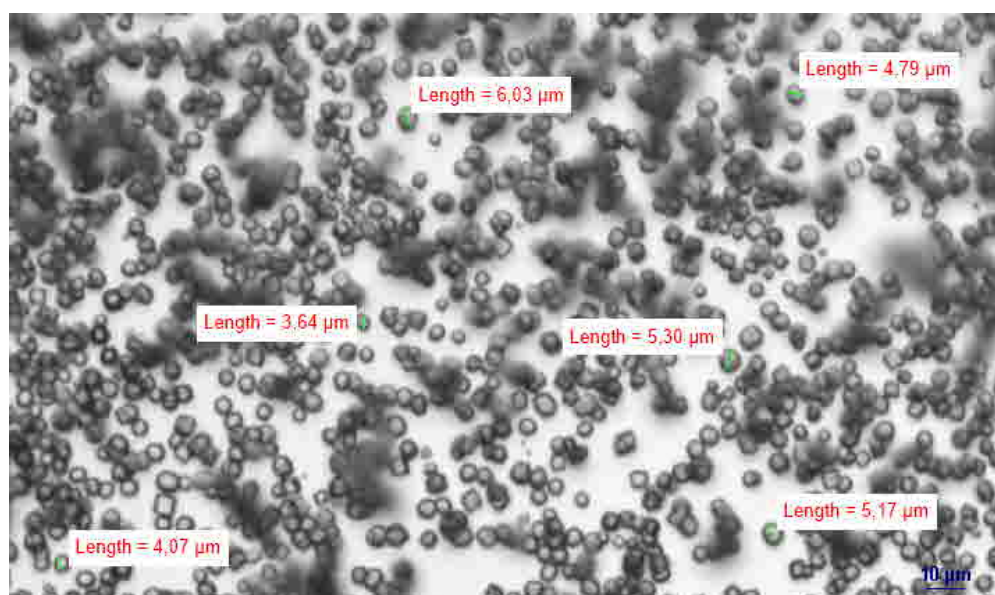


**Fig. 3.1**  $\text{CaCO}_3$  particles. Images captured by optical microscope.

As a next step, these particles were covered by polymers. The minimum required number of layers in the shell was 6, as it was shown that after this thickness the shell is continuous and stable. For one type of NPCs PSS solution and PAH solution were used, for the other – PSS solution and PDADMAC

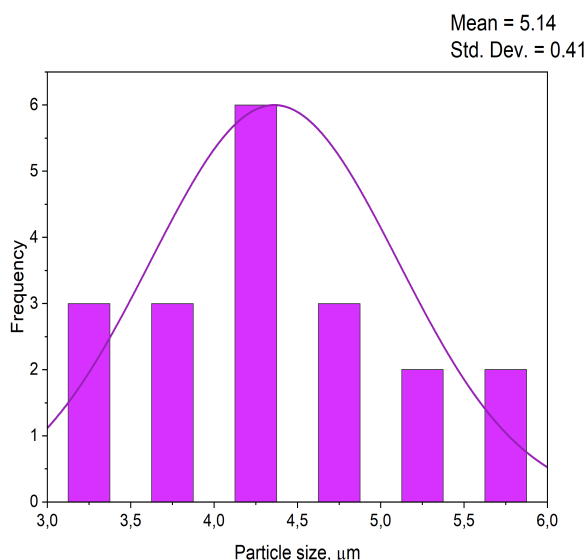


**Fig. 3.2** Size distribution of  $\text{CaCO}_3$  particles in  $\mu\text{m}$

solution. The formation of these shells was verified by scanning electron microscope (SEM) and optical microscope. The results are reported in Fig. 3.3-3.6. The size distribution of  $\text{CaCO}_3 - (\text{PSS} - \text{PAH})_3$  particles vary in range from  $2.537 \mu\text{m}$  to  $6.016 \mu\text{m}$ . The size distribution of  $\text{CaCO}_3 - (\text{PSS} - \text{PDADMAC})_3$  particles vary in range from  $9.956 \mu\text{m}$  to  $13.823 \mu\text{m}$ . As it is reported in literature ((Gong et al., 2005; Guzmán et al., 2009) the thickness of  $(\text{PSS} - \text{PAH})_3$  is in range from 8 nm to 8.8 nm, the thickness of  $(\text{PSS} - \text{PDADMAC})_3$  is in range from 9.2 nm to 12.1 nm. In this regard, there are differences in the size of capsules in Fig. 3.3 and 3.5. Also, the structure of PAH and PDADMAC molecules (table 1.2) is different. PAH is more linear compared to PDADMAC. Therefore, there is a difference in the external appearance and thickness of the capsules in Fig. 3.3 and 3.5.

Then the templates were dissolved by EDTA solution.



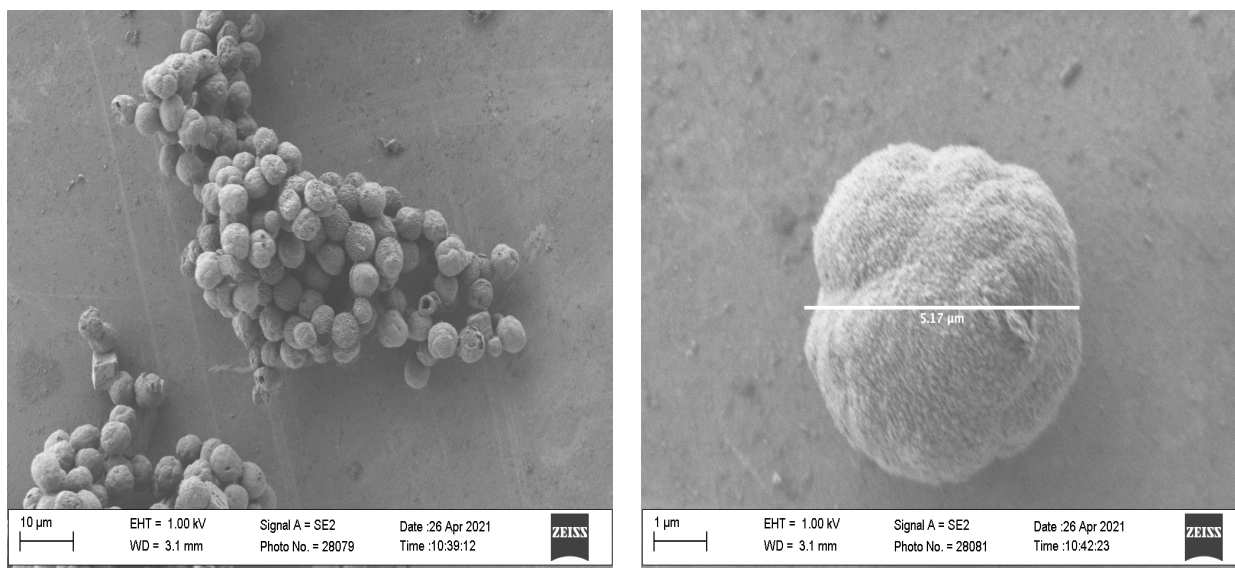


Fig. 3.3 SEM images of  $CaCO_3-(PSS - PAH)_3$  surface.

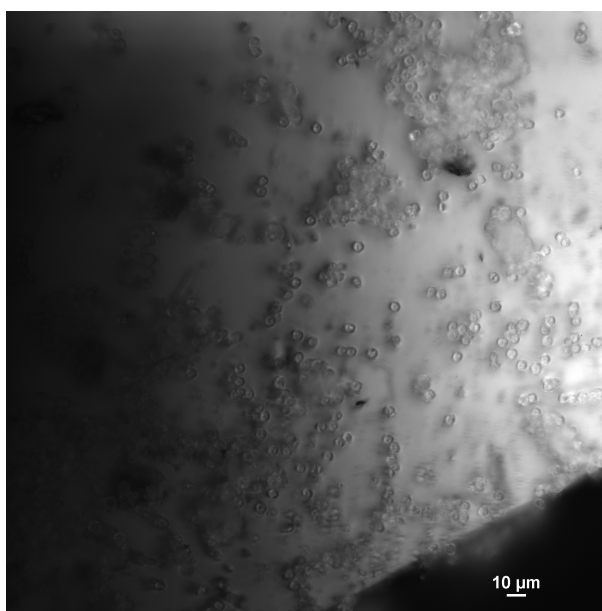


Fig. 3.4 Images of  $CaCO_3-(PSS - PAH)_3$  from optical microscope.

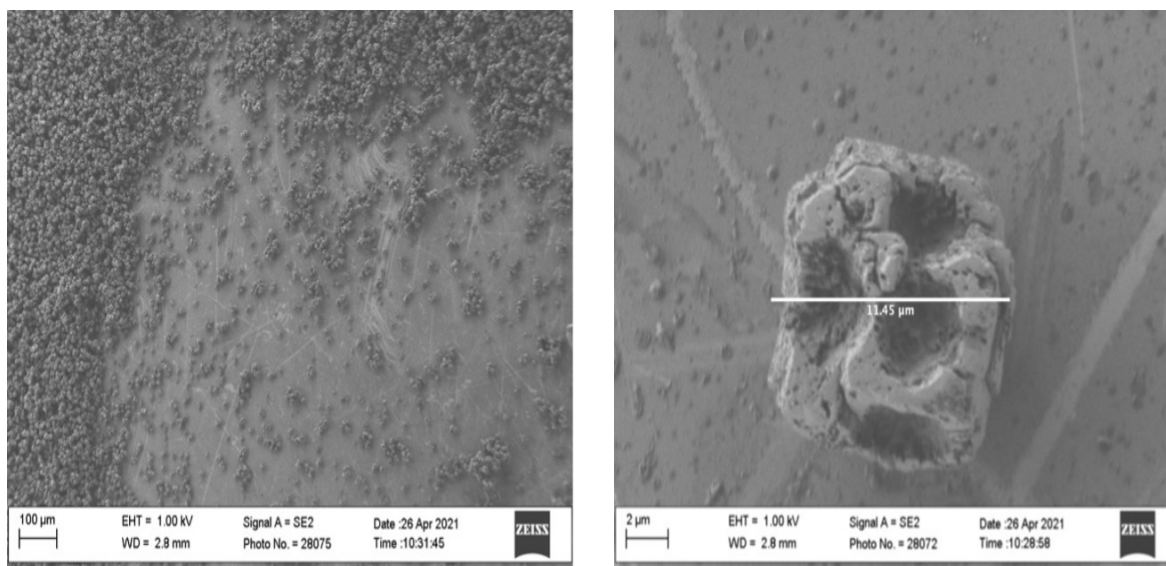


Fig. 3.5 SEM images of  $\text{CaCO}_3\text{-(PSS - PDADMAC)}_3$  particles.

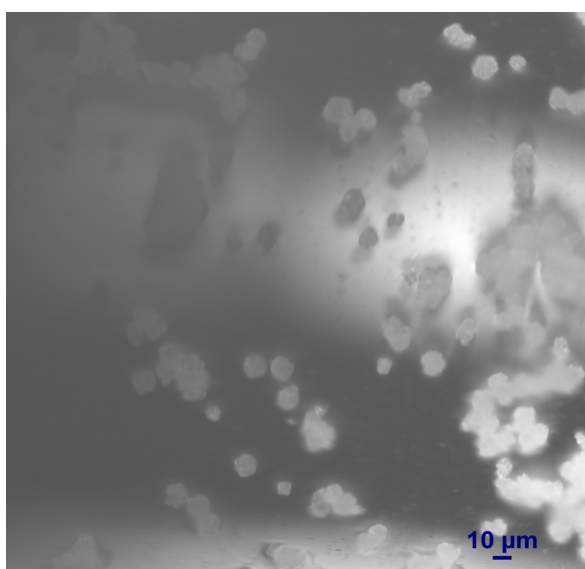
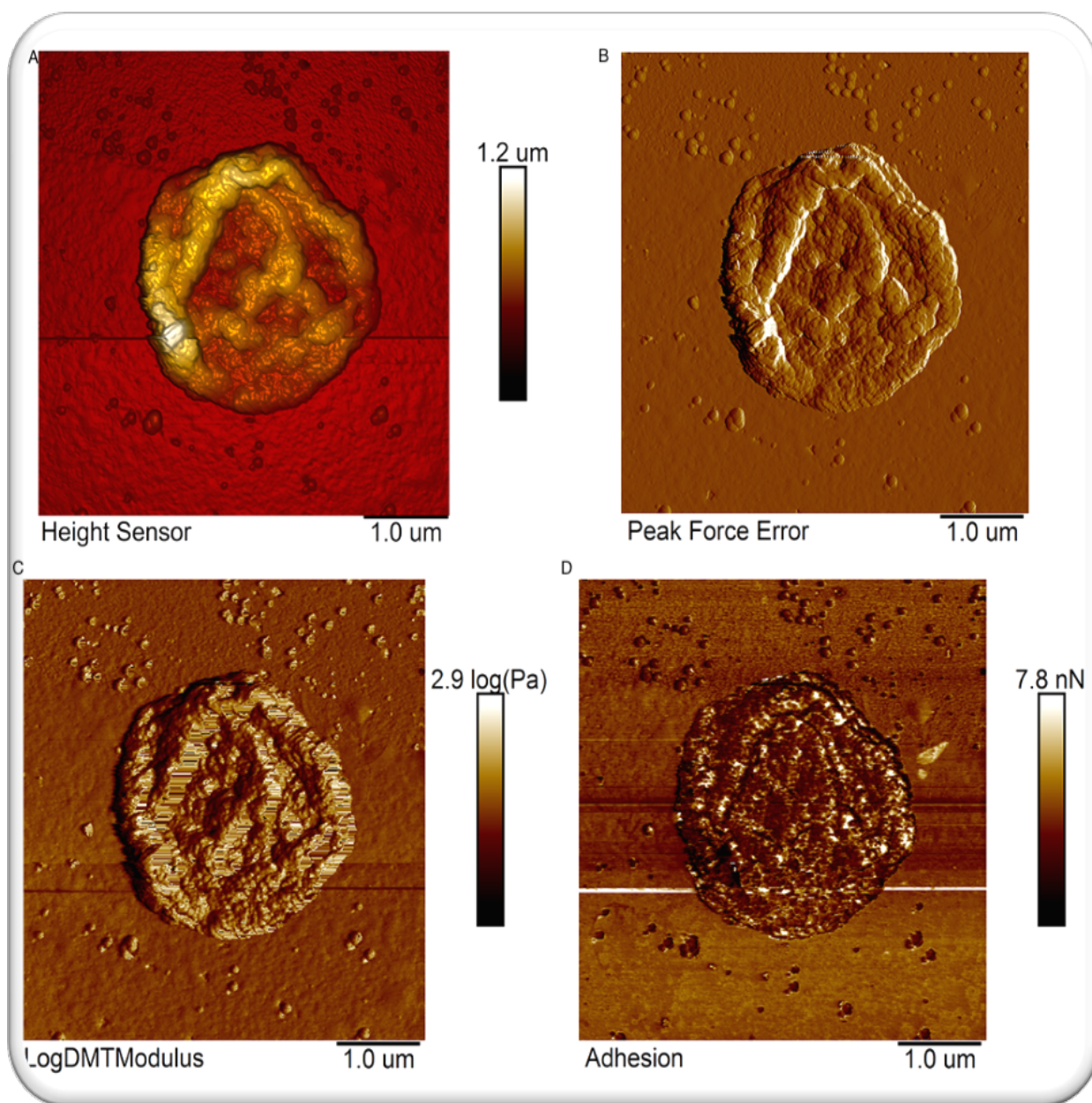


Fig. 3.6 Images of  $\text{CaCO}_3\text{-(PSS - PDADMAC)}_3$  from optical microscope.

NPCs were studied by atomic force microscopy (AFM). Fig. 3.7 (A) reports the surface topography of the sample. It can be seen that the height of a dried capsule is  $1.2 \mu\text{m}$ . These data were obtained through contact or tapping mode. By comparison, with the peak force error technique it is possible to obtain information about mechanical deformation and energy dissipation, as well as data about surface morphology. Thus, the peak force error mode is much more efficient than the tapping or the contact mode. Peak force error images are the characteristic feature of

PeakForce Tapping AFM mode, where the maximum value of the tip-surface interaction force is used as a constant set point for each pixel of the scanned area. Due to the surface topography inhomogeneity, a non-zero difference between the real peak force value and the set point exists. Therefore, peak force error imaging is sensitive to topography deviations and demonstrates the best lateral resolution, yielding in most spectacular images during lateral scanning, as seen in Fig. 3.7 (B) During the scanning of capsules, a force curve is recorded at each scan point, which describes the dependence of the interaction force between the AFM probe and the sample on the distance between them. The software processing of the force curves and their analysis are carried out directly during the scanning process, which makes it possible to simultaneously obtain information about the surface relief of the sample and its mechanical parameters, including the force of adhesion between the probe and the sample. (Fakhrullina et al., 2017; Xu et al., 2018) Fig. 3.7 (C) shows the Young's modulus distribution of the sample. Young's modulus characterises the material's stiffness in Pascals. Fig. 3.7 (D) shows the adhesion force distribution of the material.

The height of the capsule was about 860 nm, and the diameter was about 3  $\mu\text{m}$ . The results are reported in Fig. 3.8.



**Fig. 3.7** Atomic force microscopy (Peak Force Tapping mode) of  $(PSS - PAH)_3$  capsules. (A) Sensor height (topography); (B) Peak Force Error map; (C) the logarithm of the elastic modulus based on the Young's Modulus; (D) adhesion.

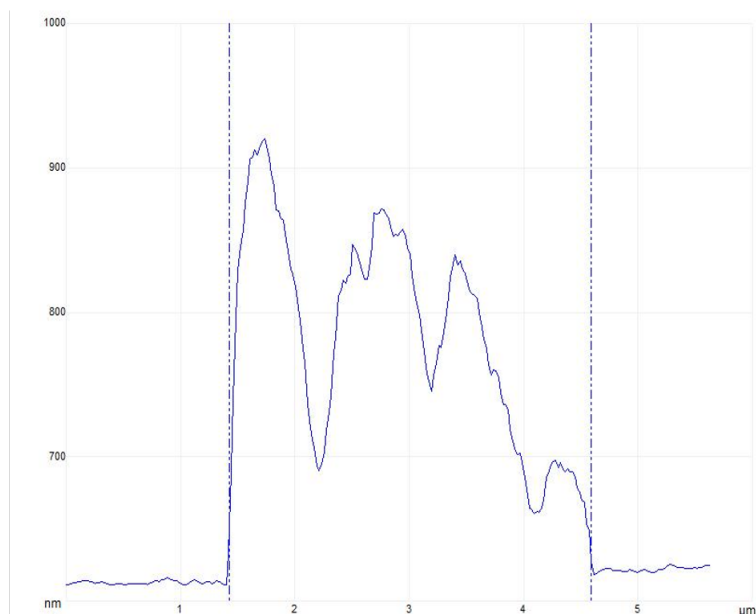


**Fig. 3.8** Height profile of a single capsule obtained using atomic force microscopy.

Also, we tried to use as a template HEK-cells instead of calcium carbonate. The structure was studied by SEM. Fig. 3.9 shows these HEK cells covered with polymers.

In this case we have obtained the final structure *HEK* –  $(CHI - ALG)_3$ .

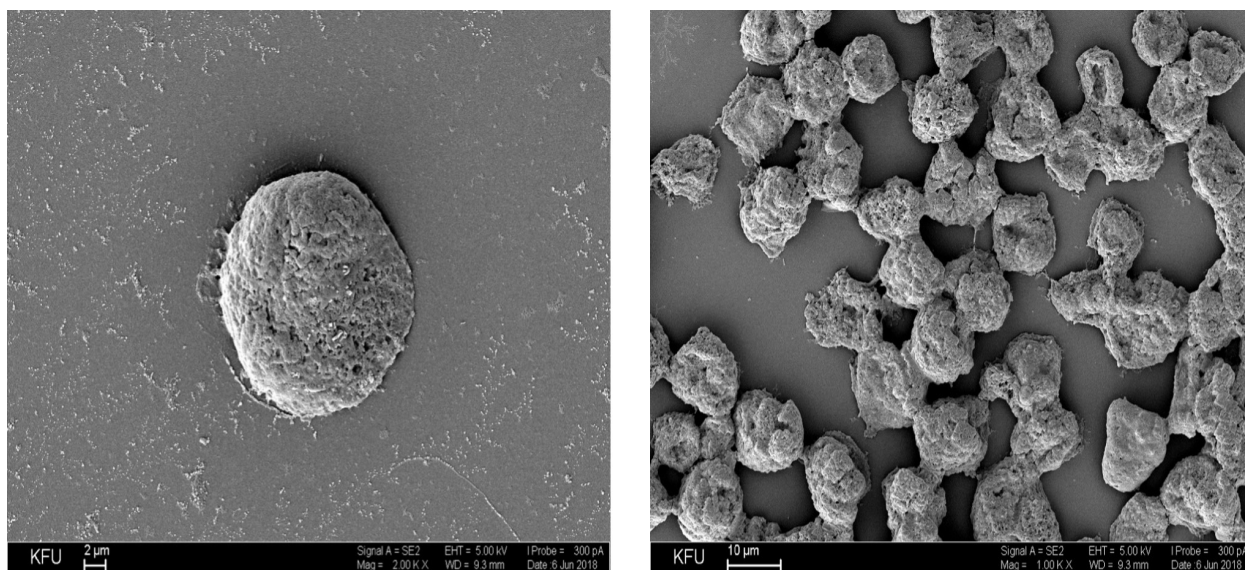


**Fig. 3.9** SEM images of NPCs where HEK cells are used as templates. Left - the single particle. Right - the complex of particles

---

### 3.2. Coherent X-Ray diffraction Imaging

Images of the polymeric capsule under dry conditions are shown in Fig. 3.10 in three projections and appropriate cross sections: a) and d) are top views; b) and e) are front views; c) and f) are side views for the cross section (a, b, c) and the plane projection (d, e, f). The same analogy is for subsequent images.<sup>1</sup>

It can be mentioned that the images are similar to those that were received previously using SEM. The measurements were carried out for dried samples, while their natural environment is liquid. Due to the drying of the sample on solid supports, there is a deformation of their shape and size. It is impossible to build a reliable 3D model of the sample in natural conditions. All these issues were later eliminated by measuring in a liquid medium.

Reconstructed images of NPCs in liquid medium are shown in Fig. 3.11 in three projections and appropriate cross sections. As is clear from the figure, the shape in this case is practically ideal sphere slightly disturbed due to the presence of gold nanoparticles in the core. The presence of these particles is visible in images of the cross sections.

For the first time CXDI technique was applied for studying NPCs. The structure of these kind of objects is quite different under dry and liquid conditions. Therefore, it can be considered

---

<sup>1</sup>The results of this chapter were partially reported in these journal articles:

- Erokhina, S., L. Pastorino, D. Di Lisa, A. G. Kiiamov, D. A. Tayurskii, S. Iannotta, V. Erokhin, and A. R. Faizullina. "3D structure reconstruction of nanoengineered polymeric capsules using Coherent X-Ray diffraction imaging." *MethodsX* 8 (2021): 101230.
- Erokhina, S., L. Pastorino, D. Di Lisa, Airat Gazinurovich Kiiamov, A. R. Faizullina, Dmitrii Al'bertovich Tayurskii, S. Iannotta, and V. Erokhin. "Coherent X-ray diffraction imaging of nanoengineered polymeric capsules." *JETP Letters* 106, no. 8 (2017): 540-543.

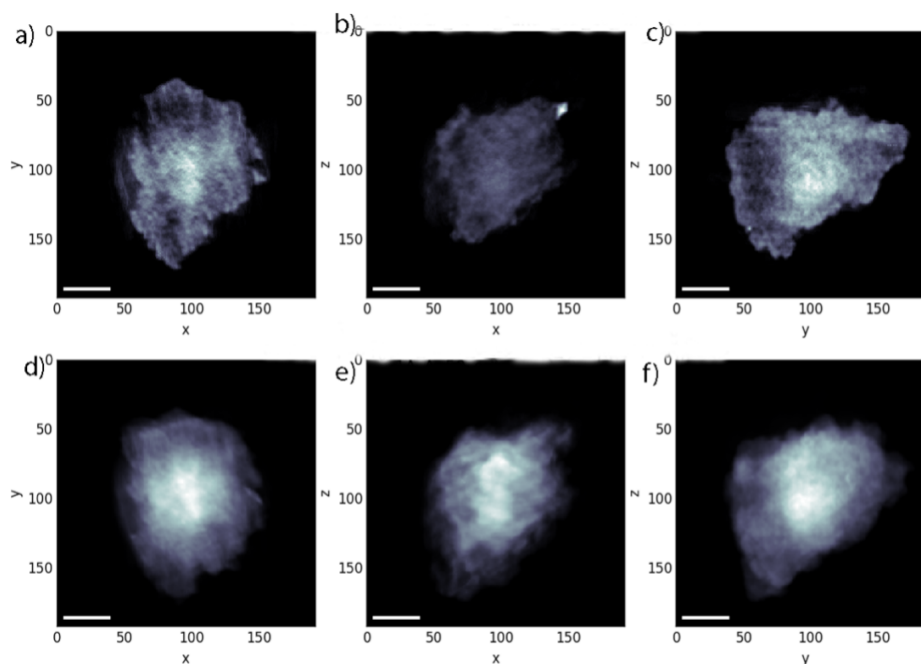


**Fig. 3.10** Reconstructed images of 5- $\mu\text{m}$  NPC loaded by 50-nm gold nanoparticles under dry conditions. . a, b, c – are the cross sections, d, e, f – are the plane projections. a, d are top views; b, e are front views; c, f are side views. The same analogy is for subsequent images.

as direct evidence that CXDI is a powerful tool for characterizing objects in liquid medium, that is natural for them. Moreover, it can visualize not only the shape of the objects but also the structure of their inner part. As it is obvious from two images, presented above, there is a significant difference of a dried sample from its liquid one in shape, sizes etc.

Moreover, NPCs at different pH were studied. In other words, NPCs were considered in detail at pH 4.0, pH 6.5, and pH 8.5.

As it was shown earlier, depending on the pH of the medium, this object can be in different states. Namely, at pH 4.0 the capsules are open, at pH 6.5 they are in intermediate state, and at pH 9.0 they are closed. This related to a permeability of the shell. Analyzing the X-ray coherent diffraction imaging data,

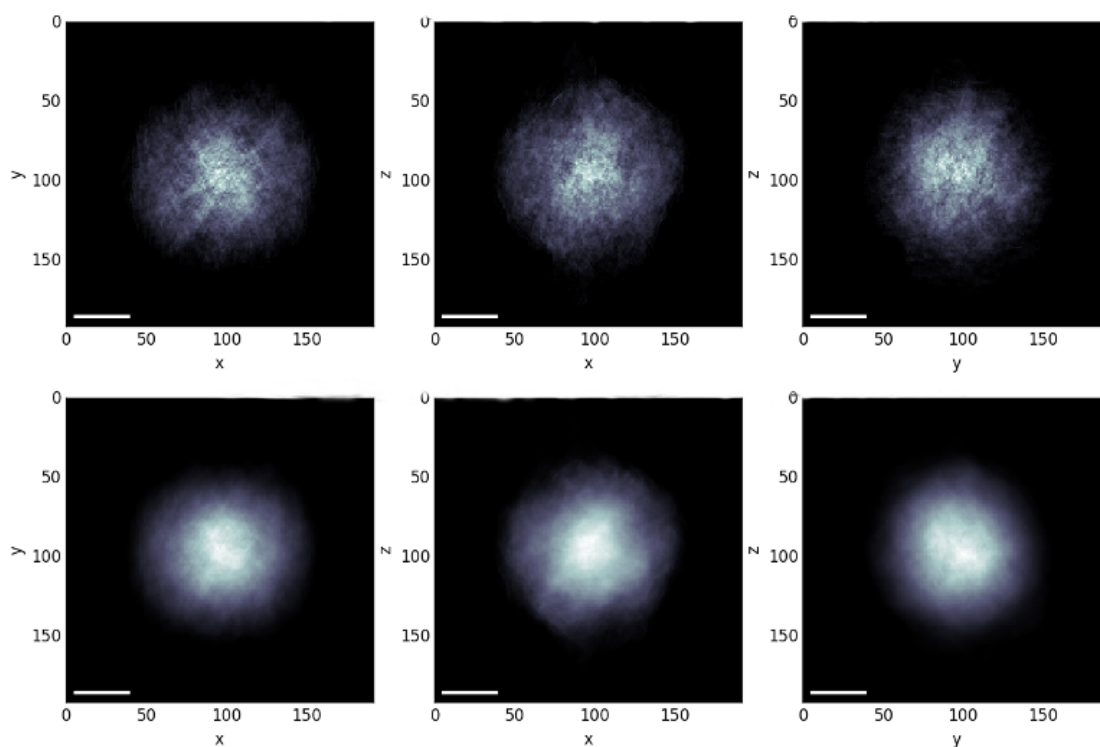


**Fig. 3.11** Reconstructed images of 5- $\mu\text{m}$  NPC loaded by 50-nm gold nanoparticles in liquid medium.

this dependence can also be visualized.

The permeability properties of not decorated polyelectrolyte capsules have been investigated as a function of pH by means of CXDI.

Fig. 3.12 shows reconstructed images of NPC loaded by 5-nm gold nanoparticles at pH 6.5. Gold nanoparticles are present both in the shell and in the core of capsules. It is noticeable that the capsules shells are closed, preventing gold nanoparticles release from them.

In contrast, for the same type of NPCs at pH 4.0, the reconstructed image, shown in Fig. 3.13, demonstrates that gold nanoparticles are distributed throughout the capsule volume. There is no clear border of the capsule. Very likely, some of them were released to the surrounding liquid medium. In addition, the shape of the capsule is significantly disturbed, what indicates also the formation of pores in their shells.



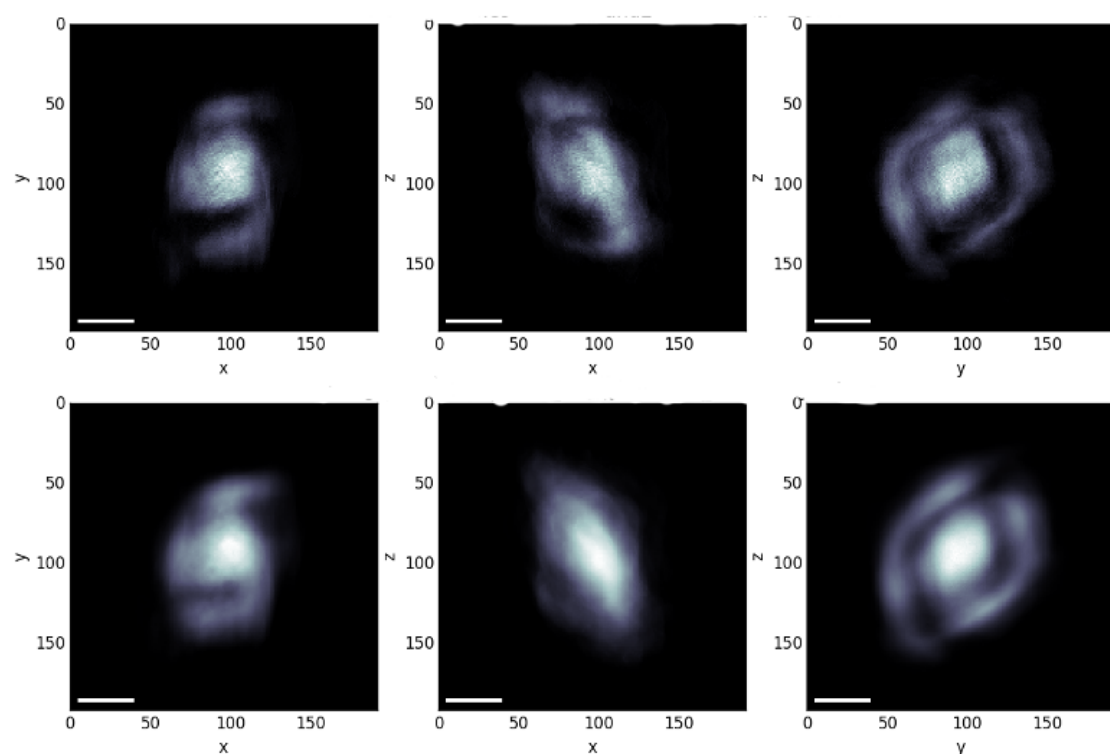


**Fig. 3.12** Reconstructed images of 6 PSS/PAH layers NPC loaded by 5-nm gold nanoparticles at pH 6.5 in liquid medium.

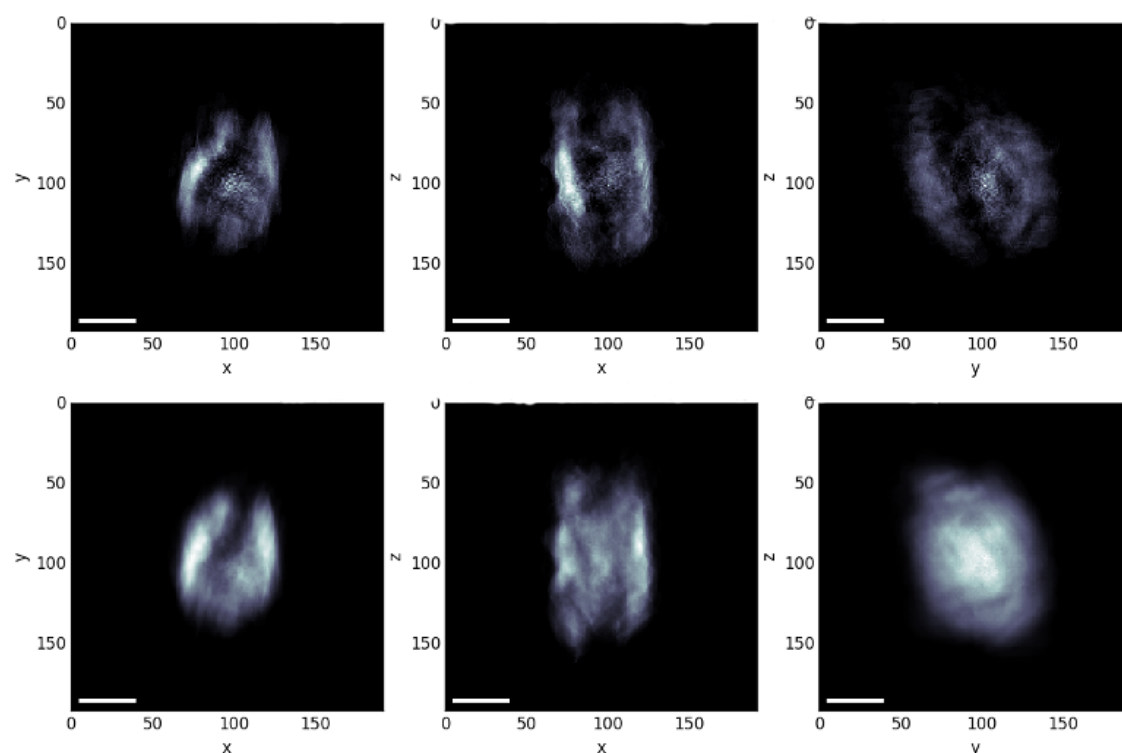


**Fig. 3.13** Reconstructed images of 6 PSS/PAH layers NPC loaded by 5-nm gold nanoparticles at pH 4 in liquid medium.

The same analogy can be done for the capsules, loaded with 50 nm gold nanoparticles. Under acidic conditions, it is

possible to observe the distribution of gold nanoparticles over the entire volume and there is no define shape of the capsules (Fig. 3.14), at pH 6.5 (neutral medium) (Fig.3.15) the shape of capsules approaching to spheric one, the gold nanoparticles are going to the center of the core, and then at pH 8.5, which corresponds to alkaline conditions, the gold nanoparticles are concentrated in the core, the shape is spheric (Fig. 3.16).

In these experiments two sizes of gold nanoparticles were used. Some capsules were loaded with 5 nm gold nanoparticles, one with 50 nm. This was done in order to control the kinetics of capsule pore opening but due to some technical problems during the experiment and lack of the time (allocated time was 5 days only) , we were not able to study these kinetic dependences.

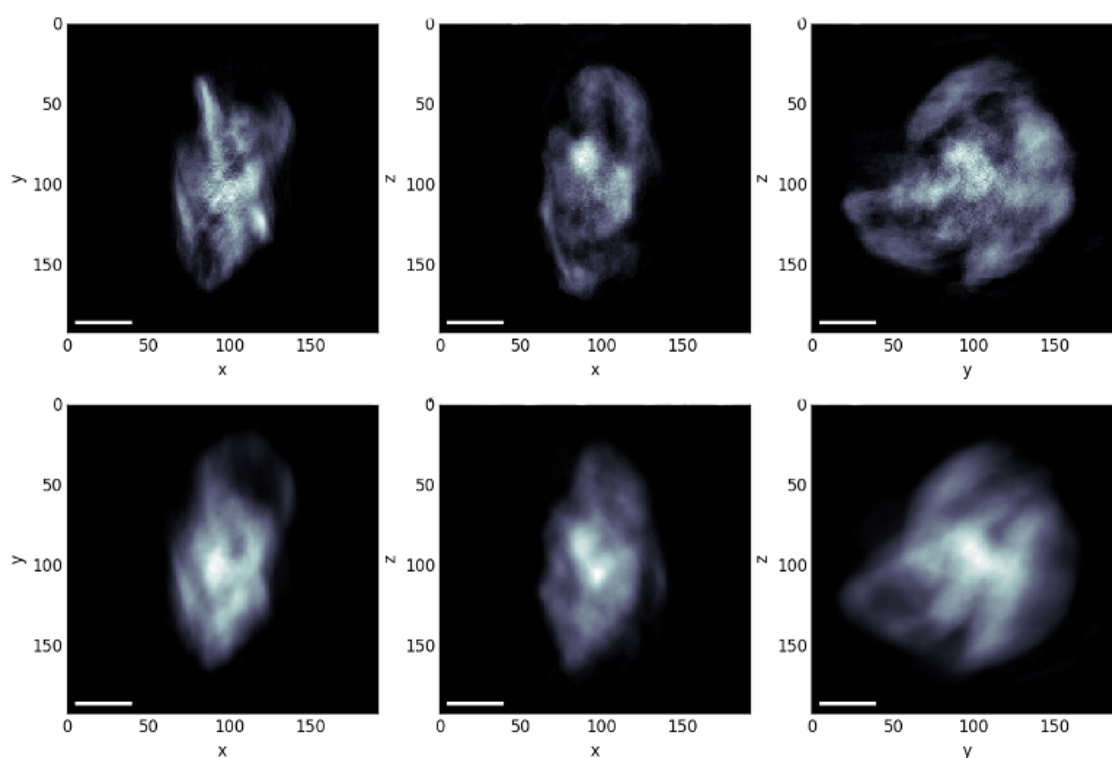


**Fig. 3.14** Reconstructed images of 12 PSS/PAH layers NPC loaded by 50 nm gold nanoparticles at pH 4 in liquid medium.

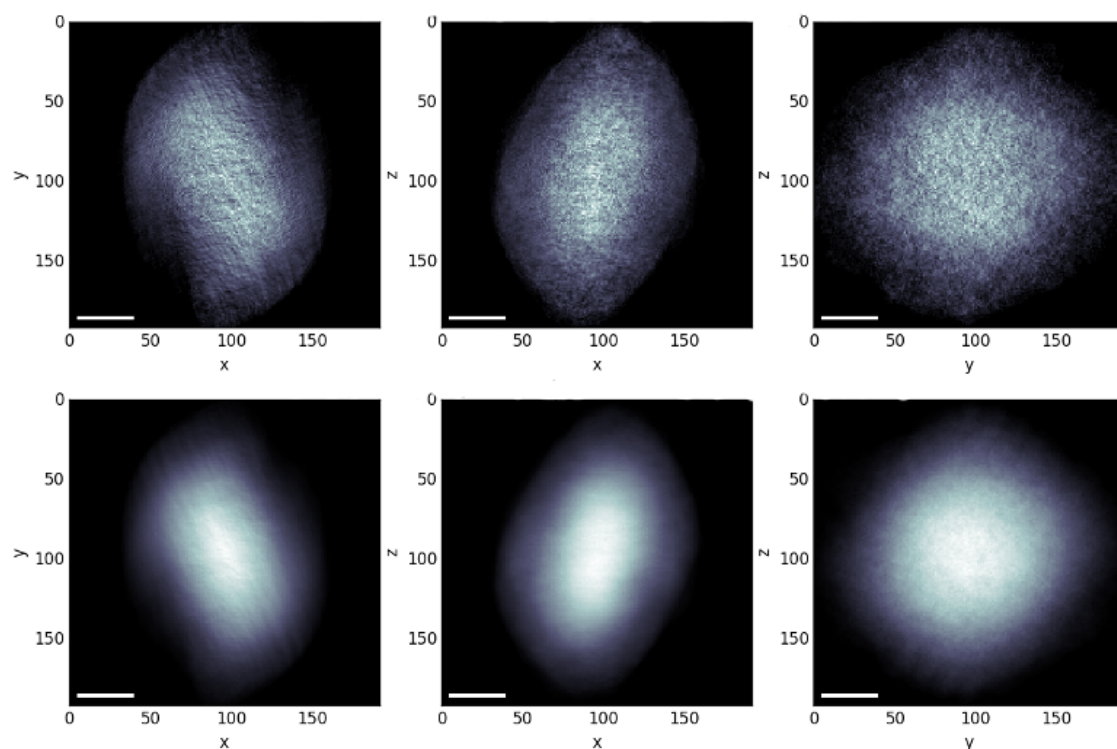


**Fig. 3.15** Reconstructed images of 12 PSS/PAH layers NPC loaded by 50-nm gold nanoparticles at pH 6.5 in liquid medium.

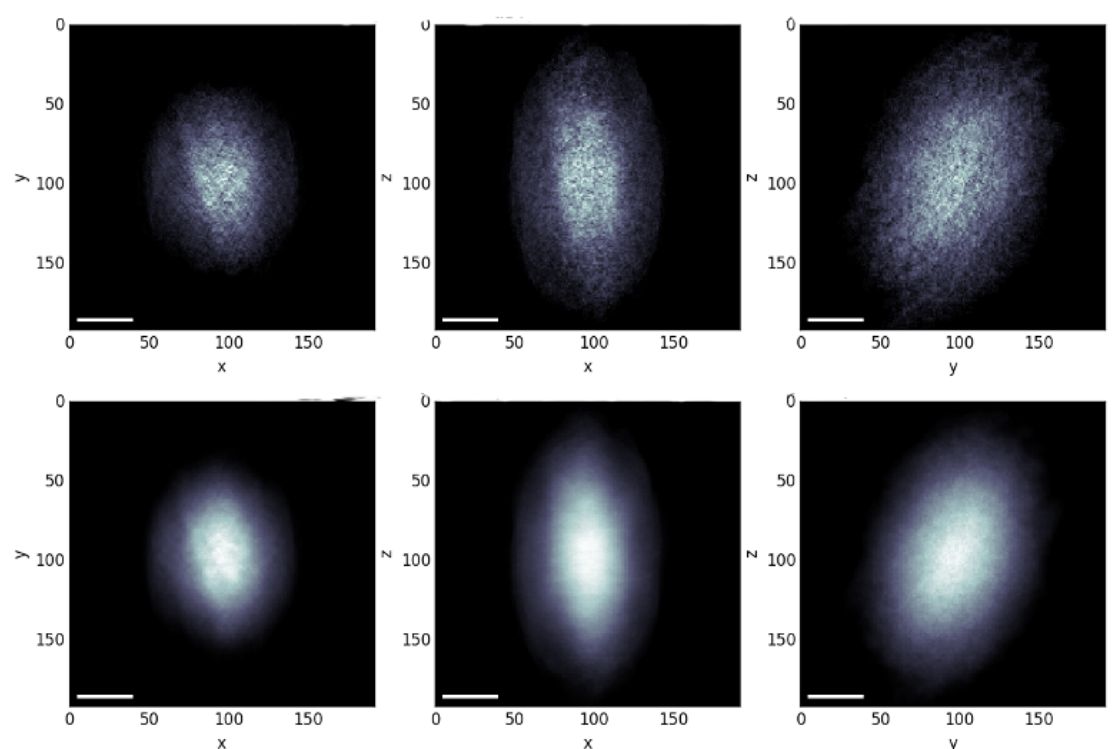


**Fig. 3.16** Reconstructed images of 12 PSS/PAH layers NPC loaded by 50-nm gold nanoparticles at pH 8.5 in liquid medium.

In an alkaline environment, the capsule shell is completely

closed. This is noticeable considering that gold particles are concentrated exclusively in the core of capsules.

Therefore, under acidic conditions, it is clearly shown that the gold nanoparticles are randomly distributed throughout the entire volume, there is no clearly defined shape of the capsule, and there is not a sharp boundary between capsule and surrounding liquid. We can conclude that the shell is open and partial release of gold nanoparticles occurs. At pH 6.5 which corresponds to neutral medium, as it is seen on Fig. 3.12, the shell pores of NPCs are closed, AuNPs are in both states: they are present both in the center of the core and close to the shell. It may be due to the beginning of the pores opening and starting of the release of encapsulated particles. In this case, the spherical shape of the capsules is more clearly visible. At pH 8.5 the pores are closed, the AuNPs are in the entire inner volume of capsules, the particle distribution is chaotic, but we can see that they are more concentrated in the center of the core.

Hence, according to this dependence, the shell permeability is well described as a function of pH.

Thereby, we can conclude that CXDI can be used for studying the objects in liquid media. Moreover, it is also possible to study their properties by changing environmental conditions, such as pH (what was done in this work), composition, ionic strength, temperature, etc. (Erokhina et al., 2021, 2017)

---

### 3.3. ***Magnetite nanoparticles characterization***

The magnetic nanoparticles were prepared according to 2.2.4. After stabilization of FeNPs with a polycationate, the sample was washed 5 times with water. The solution contains visible aggregates of iron particles (Fig. 3.17).

Firstly, SEM measurements were done. As it is clear from

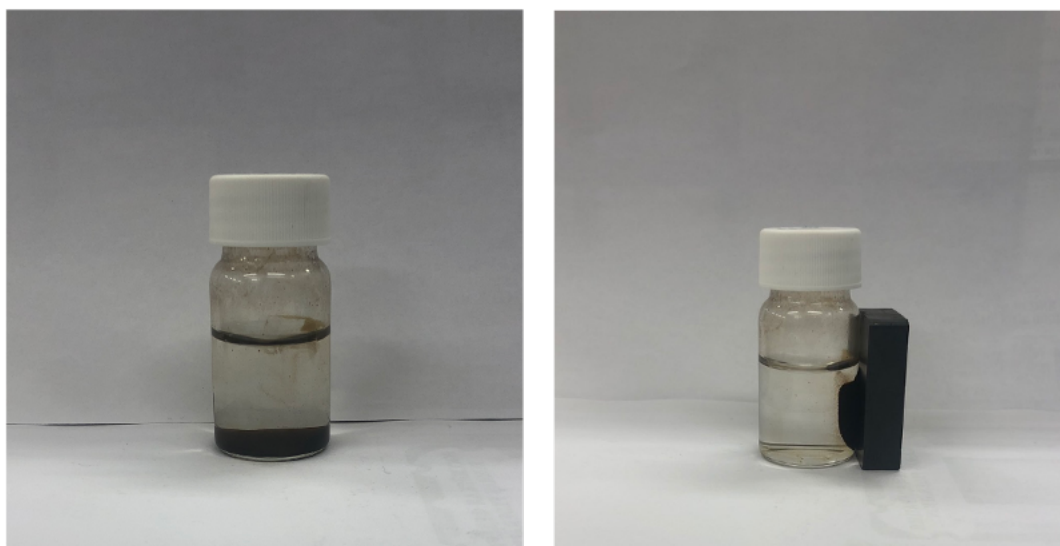


**Fig. 3.17** Magnetic separation of the prepared black product suspended in water without (left) and with (right) a magnetic field.

Fig. 3.18, the sample is quite aggregated.

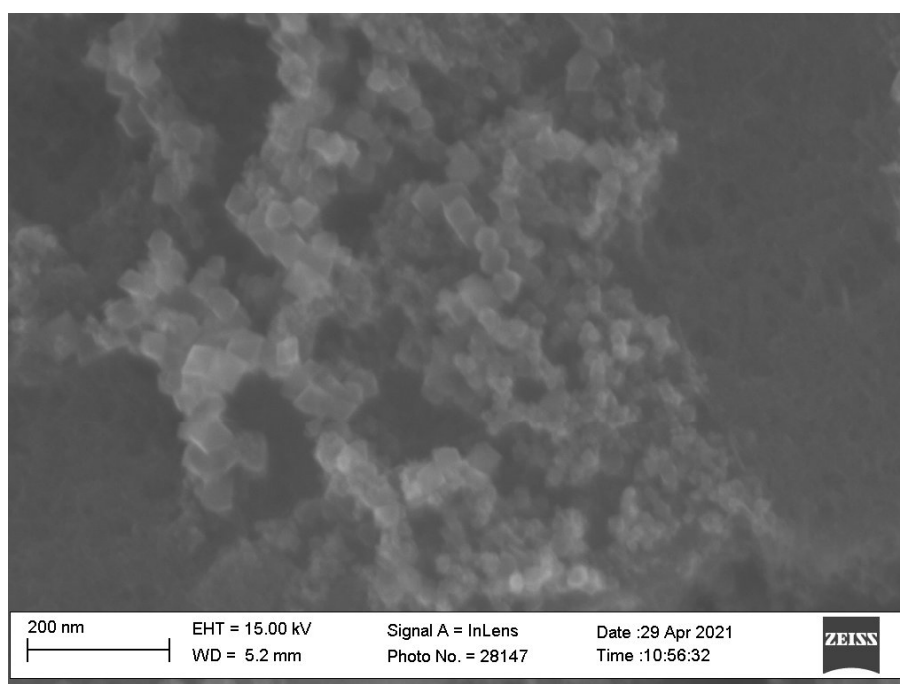


**Fig. 3.18** SEM images of MNP's.

Then, after washing, the solution was passed with a syringe through the  $0.45 \mu\text{m}$  filter to obtain a more homogeneous solution of magnetic particles. After the filtration, the solution was less concentrated, the particles were distributed in the whole volume, the solution was brown but through it the light could be passed (before filtration it was brownish black, it was

impossible to pass light through it). No big aggregates have been observed, the shape of particles was more defined. The size distribution was within 27-50 nm range (Fig. 3.19). As it is described in (García-Alonso et al., 2010) and in (Lu et al., 2006), the size of obtained MNPs, that they have obtained, are  $15 \pm 2$  nm and  $40 \pm 3$  nm respectively. For the characterization of these MNPs in this papers TEM imaging was used.

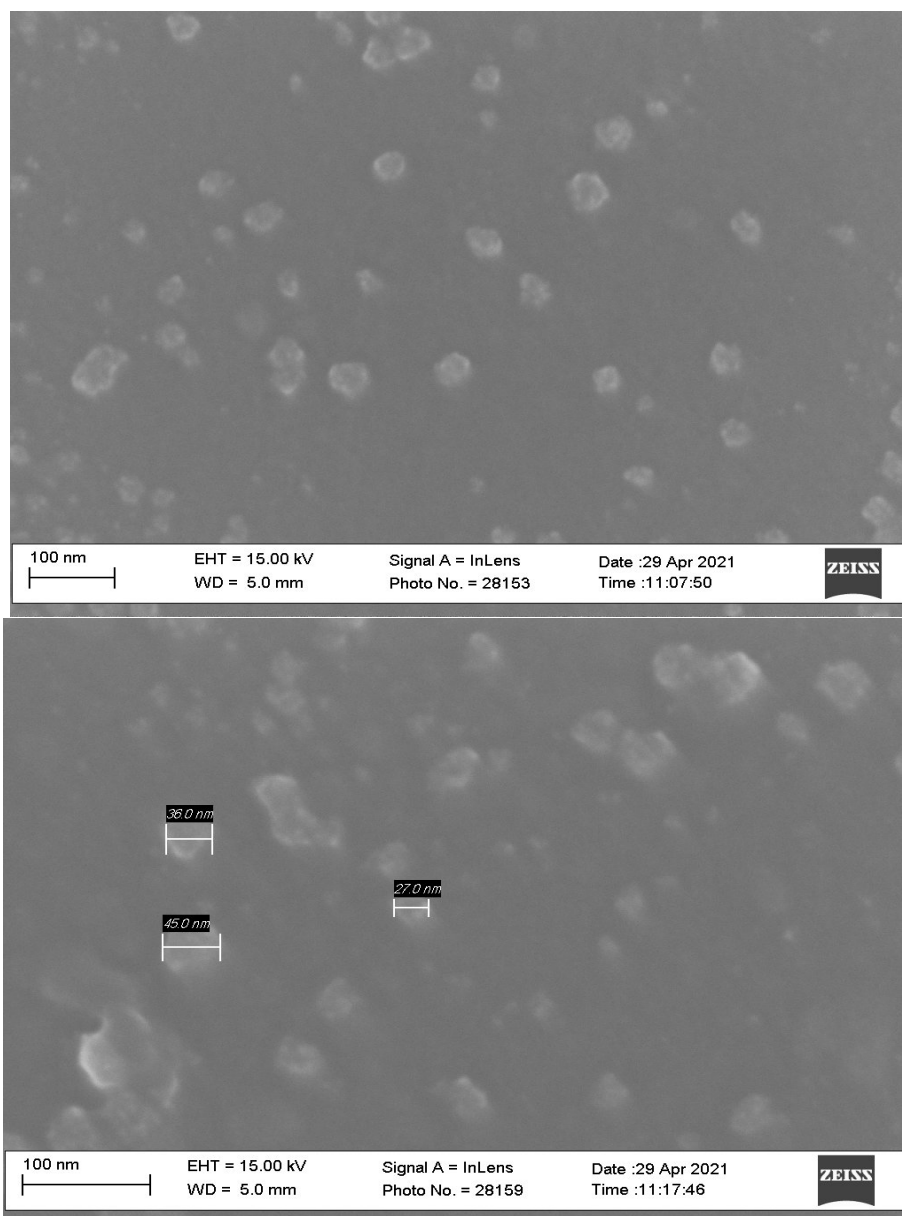


**Fig. 3.19** SEM images of MNP's after filtration. Top – overall picture. Bottom – overall picture with signed particles' dimensions.

For more precise visualization and characterization, TEM

measurements have been carried out. (Fig. 3.20)

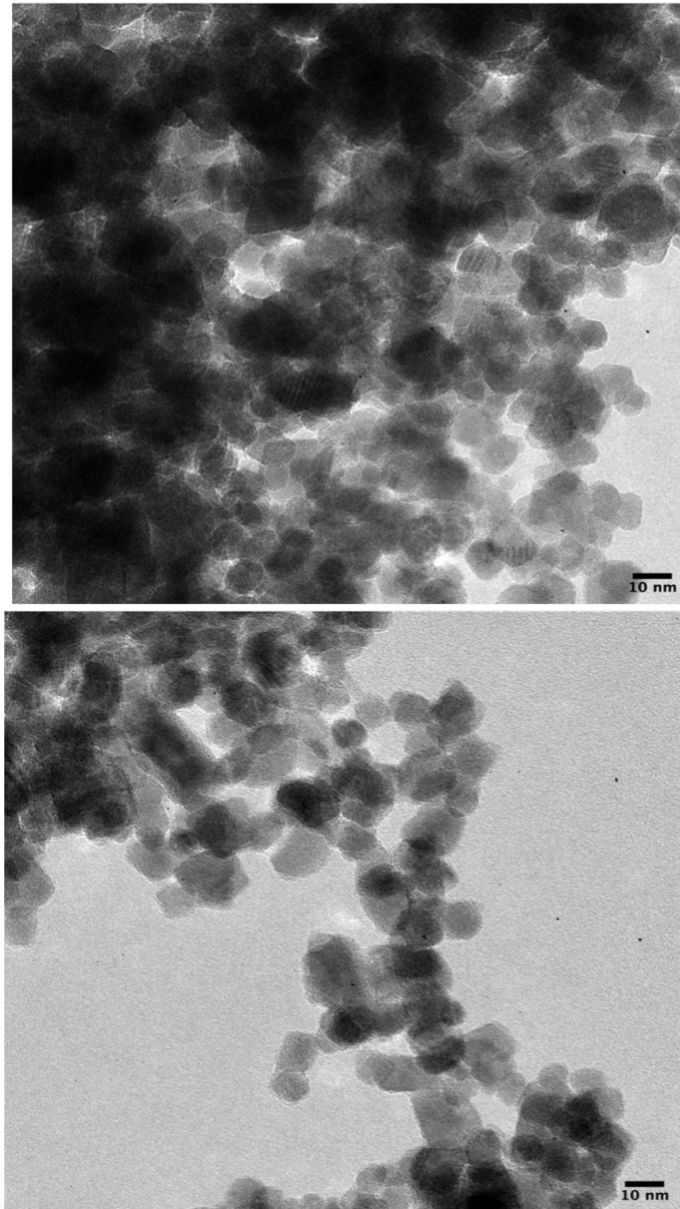


**Fig. 3.20** TEM images of MNP's. Left – more concentrated zone, right – less concentrated zone.

The size distribution of FeNPs (Fig. 3.21) was found to be within 10-40 nm range, what is comparable with values, estimated from SEM images. As it is clear from the images, magnetite nanoparticles form agglomerates with each other. The shape of FeNPs is mainly spherical.

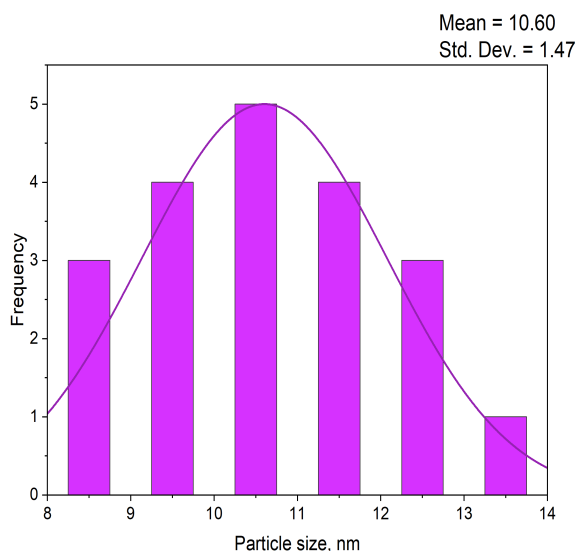


Fig. 3.21 Size distribution of FeNPs in nm.

SEM images of NPCs with MNPs in the shell is presented in Fig. 3.22.

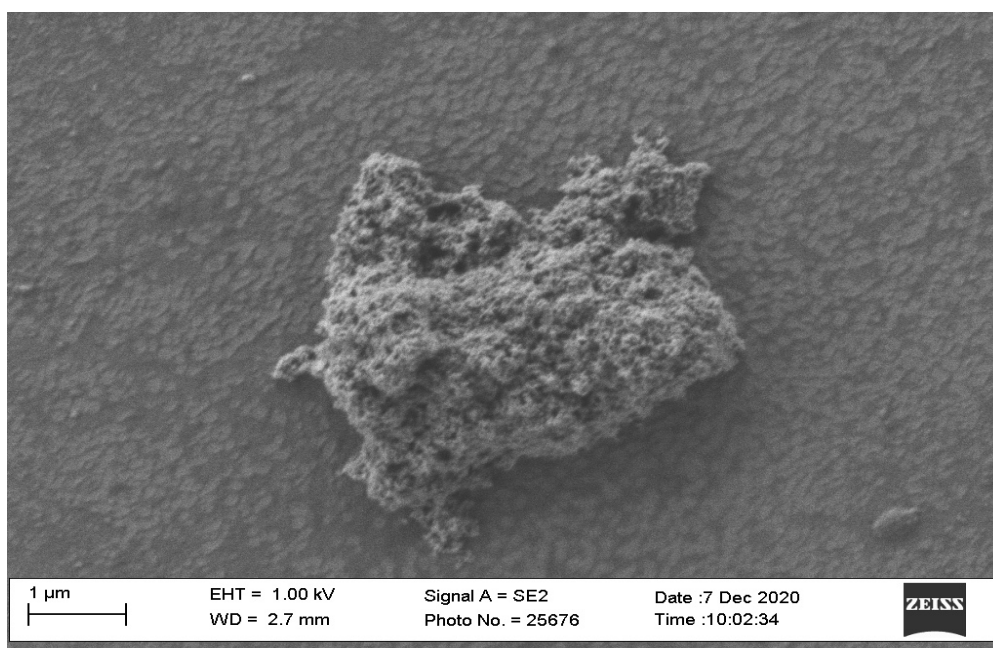
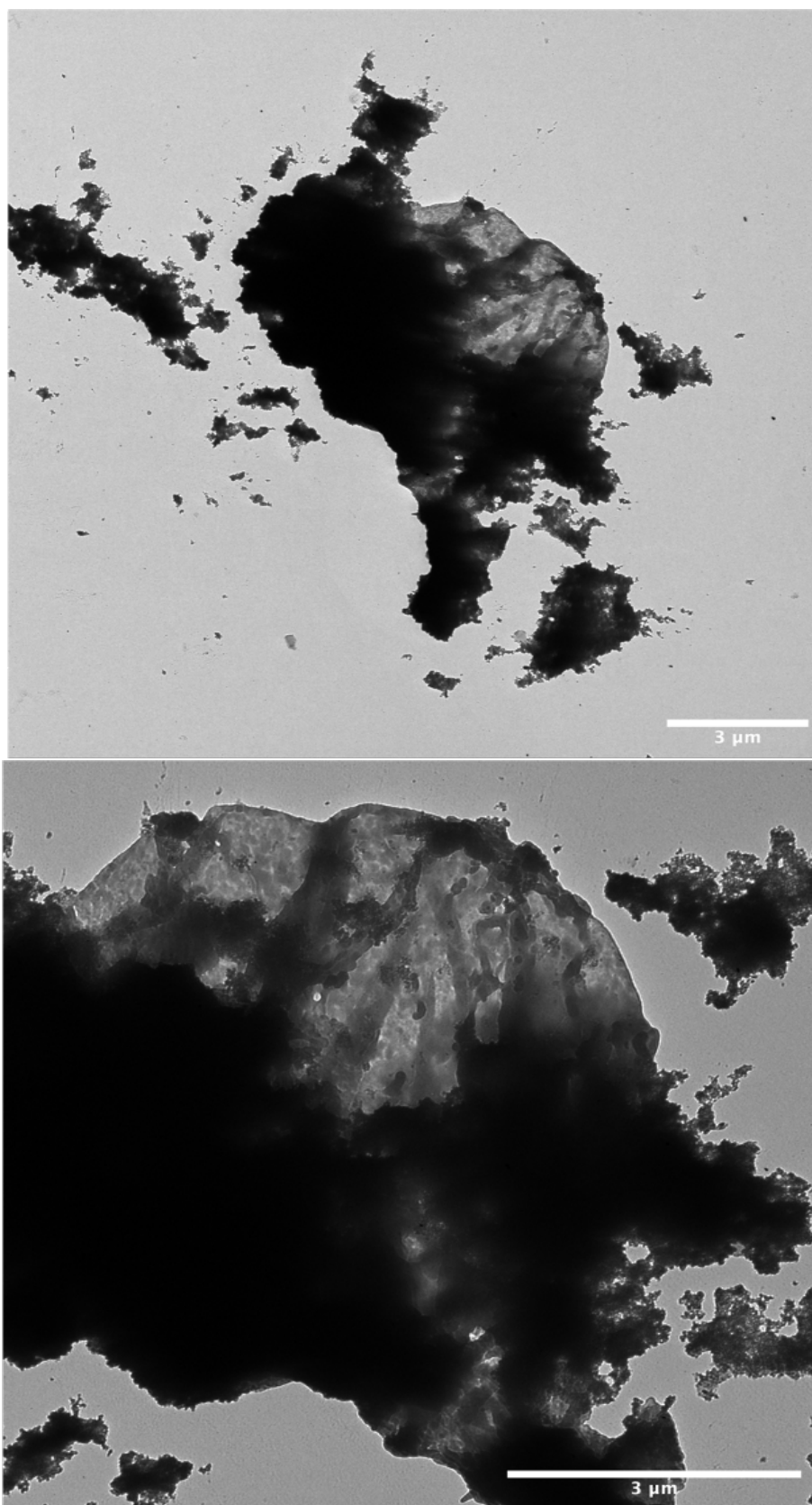


Fig. 3.22 SEM images of  $CaCO_3-(PSS - PAH)_2-(PSS - MNP/PAH) - PSS$  particles.

TEM image of the capsules with FeNP is shown in Fig. 3.23. In the complex of FeNPs and capsules, we can see that magnetite nanoparticles are in the shell. Analyzing this image it is possible to claim that some part of the core was not dissolved (black zone on the left).





**Fig. 3.23** TEM images of MNP's after filtration. Top – overall picture. Bottom – overall picture with signed particles' dimensions.

### 3.4. Energy-dispersive X-ray analysis

For the elemental analysis of the complexes composition energy-dispersive X-ray analysis (EDX) experiments have been applied. Analysis of the acquired spectra allowed to identify elements that presented in the sample.

Top images of the Fig. 3.24 represent  $CaCO_3-(PSS - PAH)_2-(PSS - MNP/PAH) - PSS$  complex (left) and  $(PSS - PAH)_2-(PSS - MNP/PAH) - PSS$  complex, where the core was dissolved with a 1N HCl (right). EDX spectra of appropriate samples are shown in the bottom images. Analysing these data it is possible to see that on Fig. 3.24 left there are traces of calcium that arrives from the core, silicon that arrives from a support, sulfur comes from PSS, iron from magnetite, carbon and oxygen are in both polymers. On the contrary, in Fig 3.24 right, where the core was dissolved, we don't have the traces of calcium, but chlorine arrives from hydrochloric acid. Sulfur signal lost due to the low concentration and its damping due to the vicinity of chlorine peak. The estimated percentage of each element's concentration within the sample for the Fig. 3.24 left is presented in table 3.1, and for Fig. 3.24 right is table 3.2.

**Table 3.1** Quantitative distribution of elements for  $CaCO_3-(PSS - PAH)_2-(PSS - MNP/PAH) - PSS$ .

Element	Weight %	Atomic %
C	15.71	29.21
O	17.8	24.84
Si	48.62	38.65
Ca	0.17	0.09
Fe	17.26	6.9
<b>Total</b>	100	

Table 3.2 Quantitative distribution of elements for  $(PSS - PAH)_2-(PSS - MNP/PAH) - PSS$ .

Element	Weight %	Atomic %
C	9.08	17.77
O	20.23	29.72
Si	53.5	44.78
Cl	1.98	1.31
Fe	15.21	6.4
Total	100	

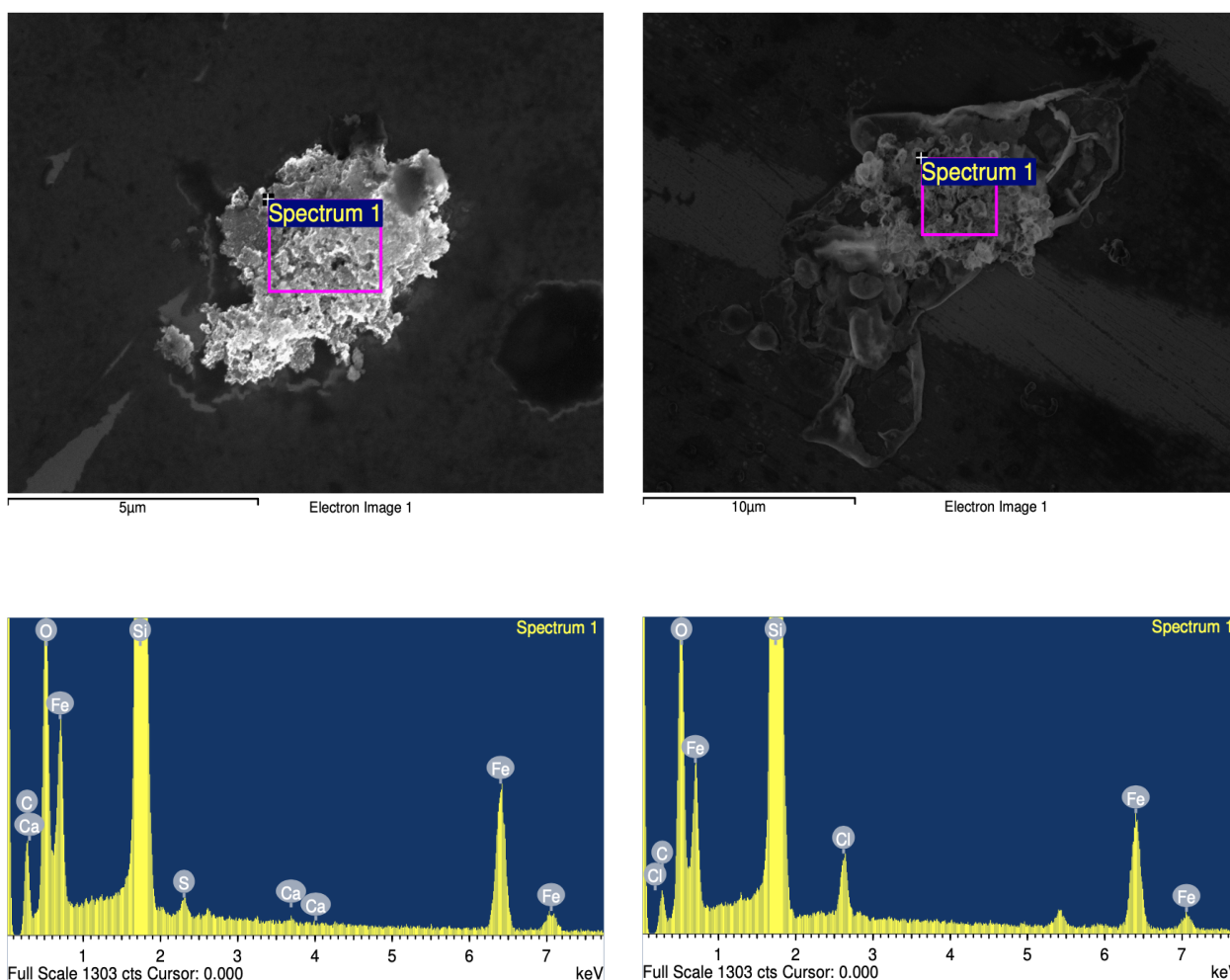


Fig. 3.24 SEM images (upper panels) and EDX spectra (bottom panels) of  $CaCO_3-(PSS - PAH)_2-(PSS-MNP/PAH)-PSS$  (left) and  $(PSS - PAH)_2-(PSS-MNP/PAH)-PSS$  (right).

### 3.5. Ultraviolet–visible spectroscopy (UV-VIS)

UV-VIS measurements were carried out to find out the characteristic wavelength of FeNPs, to find out is there any influence of the polymer that is used for stabilisation of MNPs and to

see any influence of the concentration.

Fig. 3.25 presents the UV-VIS spectra of the synthesized MNP. The absorbance of the particles was measured in the range of 200 – 1000 nm. In the literature the absorption peak for this type of particles is in range 220 - 350 nm. (Aguilar-Méndez et al., 2020; Chaki et al., 2015; Razack et al., 2020) The absorption peak that was measured for our sample is at 294 nm that corresponds to the results obtained in literature. The broad distribution of peaks values depends on the particle size. With decreasing particle size, the maximum absorbance is found at shorter wavelength. (Vollath, 2013)

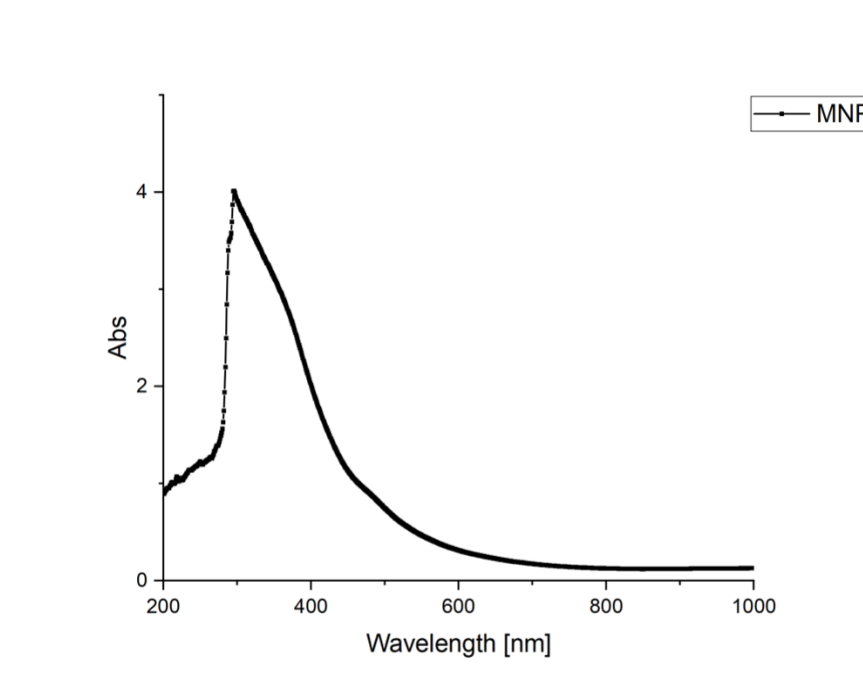


**Fig. 3.25** UV-VIS spectra of the magnetite nanoparticles.

In the work of Villegas et al. (Villegas et al., 2020) there was a comparison of UV–Vis spectra of magnetic nanoparticles dispersed in different mediums. That is why we have compared the absorption peak of MNPs stabilized with different polymers. We compared the MNPs dispersed in PEI solution and in water. As it is clear from Fig. 3.26, the absorbance peak in the UV region at the wavelength of 294 nm is present for both speci-

mens. However, in the case of nanoparticles, stabilized with a polymer MNPs, the absorbance peak is more flat, compared to pure particles. Also the peak height is less than in case of water solution. Thus, we can conclude that polymer stabilization makes influences on the type of the peak, but does not affect the absorption wavelength.

In (Villegas et al., 2020), the authors have mentioned, that depending from the medium the type of the peak can change.

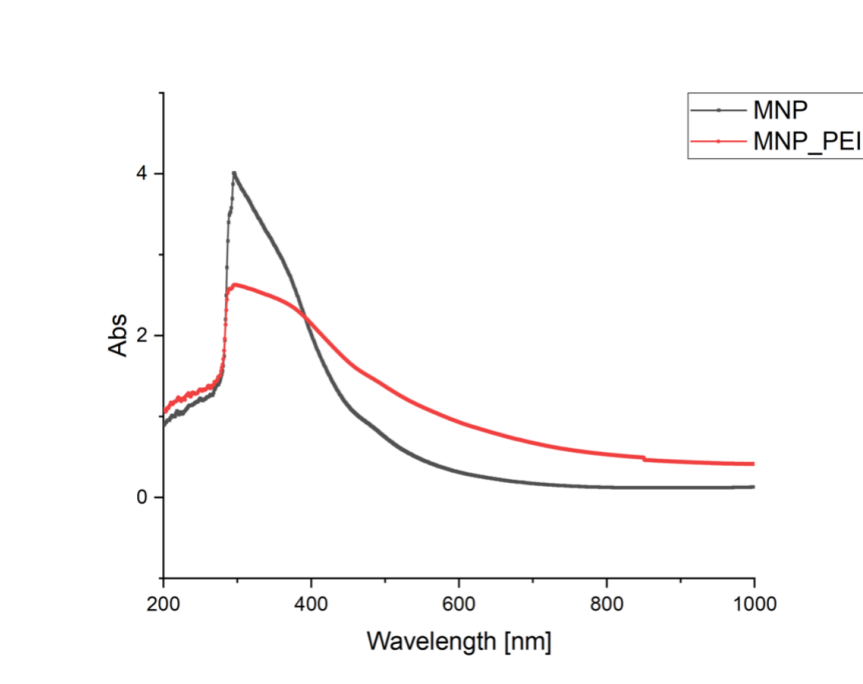


**Fig. 3.26** UV-VIS spectra of the utilized reagents: black – pure MNPs, red – MNPs stabilized with PEI.

Likewise, it was interesting to see any dependence of the solution concentration on the wavelength. For this case we started our measurements with a concentrated solution of MNPs dispersed in PAH. In the Fig. 3.27 the green line corresponds to the concentrated solution. As in the case of PEI, the absorbance peak is flat. The violet line corresponds to dilution 1 to 2. The solution was diluted gradually. But in any case the characteristic wavelength was the same. The gradual dilution does not affect the absorption wavelength, the peak shape does not change.

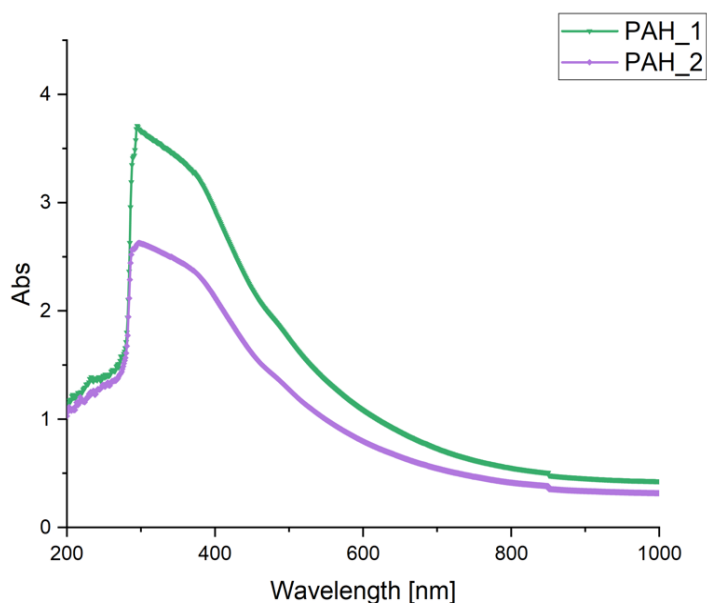


**Fig. 3.27** UV-VIS spectra of the MNPs stabilized with a PAH: the green is diluted solution 1 to 1, the violet is 1 to 2.

---

### **3.6. Loading and delivery of capsules. Release of inner substance**

For this experiment  $CaCO_3$  particles were soaked in the solutions with the fluorescent dyes. The prepared  $CaCO_3$  particles were placed in the Rhodamine B solution and in the Fluorescein sodium salt solution. The concentration of the fluorescent dyes solutions was 2 mg/ml. The particles were left in the solution for 24h. This was done for allowing dyes to enter inside the pores of  $CaCO_3$  particles.

First of all, we have checked that both types of dyes have entered inside the pores of  $CaCO_3$  particles. This fact is clearly confirmed by Fig. 3.28 for fluorescein sodium salt. The similar picture was confirmed for Rhodamine B. This image was acquired by the fluorescence optical microscope using FITC filter. The presence of the green background indicates that some of dye molecules are still in the solution.

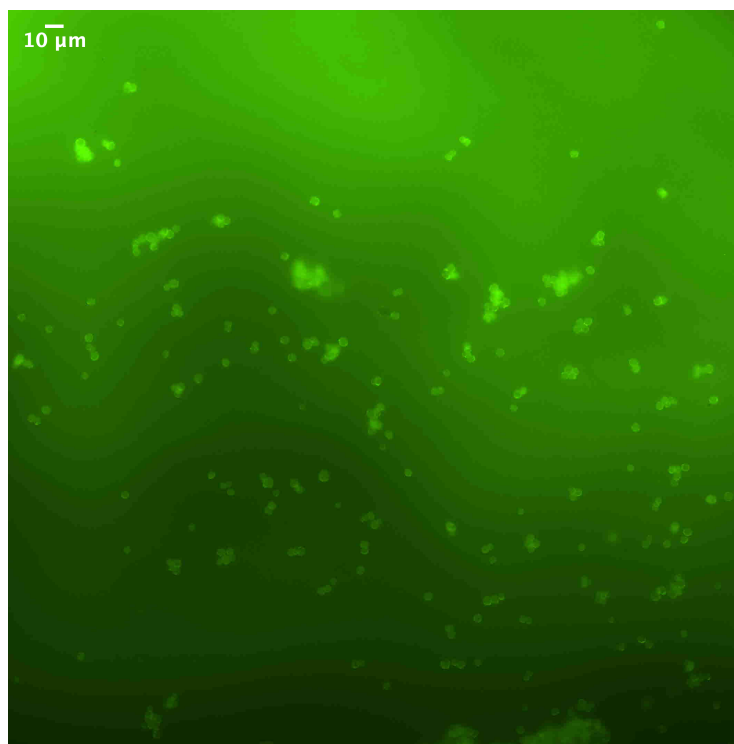


**Fig. 3.28** Optical fluorescent microscope image of  $\text{CaCO}_3$  particles with associated fluorescein sodium salt using FITC filter.

Images were acquired by Fluorescence Optical Microscope Nikon Ni-E with Camera Type: Nikon DS-Qi2 in transmission geometry. Exposure time was 300 ms. Samples were placed as a liquid drop on a glass substrate. Then, directly on the glass supports, the templates were dissolved by adding EDTA solution (0.2 M). The general scheme of the experiment is represented in Fig. 3.29.

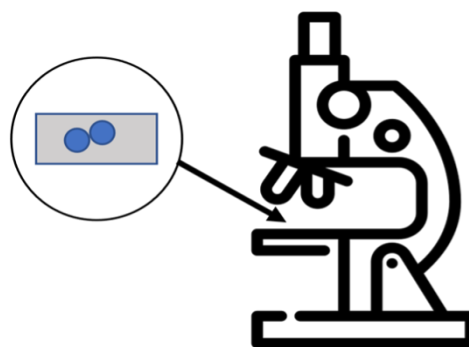


**Fig. 3.29** General scheme of the experiment.

After soaking the particles for 24h, the supernatant was replaced with a polymer solution. As a first layer PSS was

### 3.6. **LOADING AND DELIVERY OF CAPSULES. RELEASE OF INNER SU**

used. The final structures were:

- $CaCO_3$ /Fluorescein sodium salt  $-(PSS - PDADMAC)_2 - (PSS - MNP/PDADMAC)$ ;
- $CaCO_3$ / Rhodamin B  $-(PSS - PDADMAC)_2 - (PSS - MNP/PDADMAC)$ .

Two types of samples, loaded with different fluorescent dyes, were fabricated. Images of these samples were acquired by the fluorescence optical microscope, using a FITC filter for samples with fluorescein sodium salt dyes and TRITC filter for samples with rhodamine B dyes. The images are shown in Fig. 3.30 and Fig. 3.31 respectively.

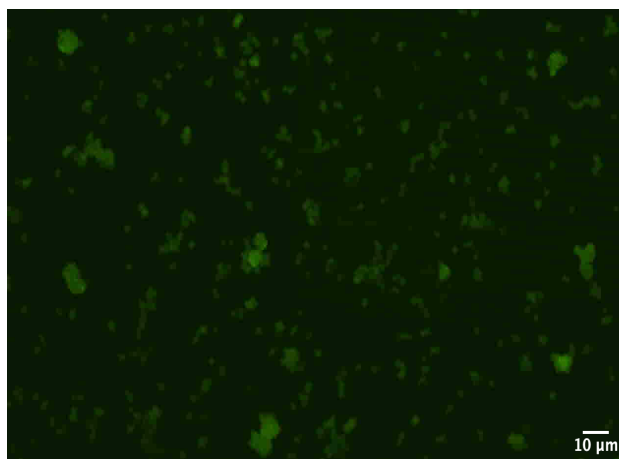


**Fig. 3.30** Optical fluorescent microscope image of  $CaCO_3$ / Fluorescein sodium salt  $-(PSS - PDADMAC)_2 - (PSS - MNP/PDADMAC)$  using FITC filter.

As it is clear from Fig. 3.30 and Fig. 3.31, dye molecules are mainly present in the core of fabricated objects.

During the shell fabrication, magnetite nanoparticles were incorporated to the last layer. Two drops of capsule solutions were placed onto the glass support for the microscope, as it is schematically shown in the Fig. 3.32. These solutions contained  $CaCO_3$ / Fluorescein sodium salt  $-(PSS - PDADMAC)_2 - (PSS - MNP/PDADMAC)$ , and  $CaCO_3$ / Rhodamin B  $-(PSS -$



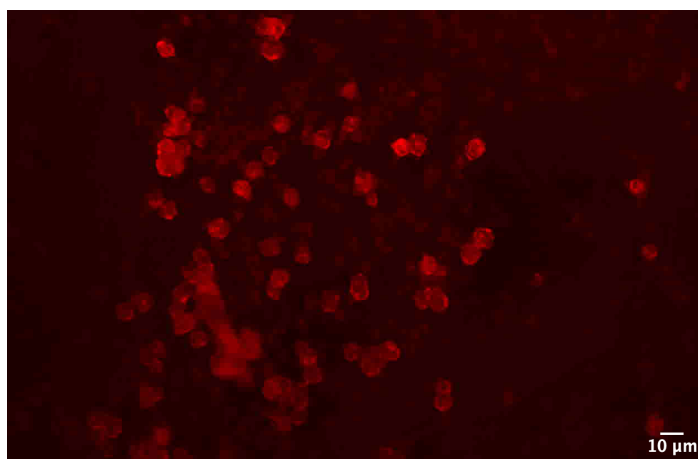


**Fig. 3.31** Optical fluorescent microscope image of  $\text{CaCO}_3$ / Rhodamin B - $(\text{PSS} - \text{PDADMAC})_2 - (\text{PSS} - \text{MNP}/ \text{PDADMAC})$  using TRITC filter.

$\text{PDADMAC})_2 - (\text{PSS} - \text{MNP}/ \text{PDADMAC})$ , respectively. After placing, the capsules in both solutions were moved by the external magnet to a desirable area under the microscope focus.

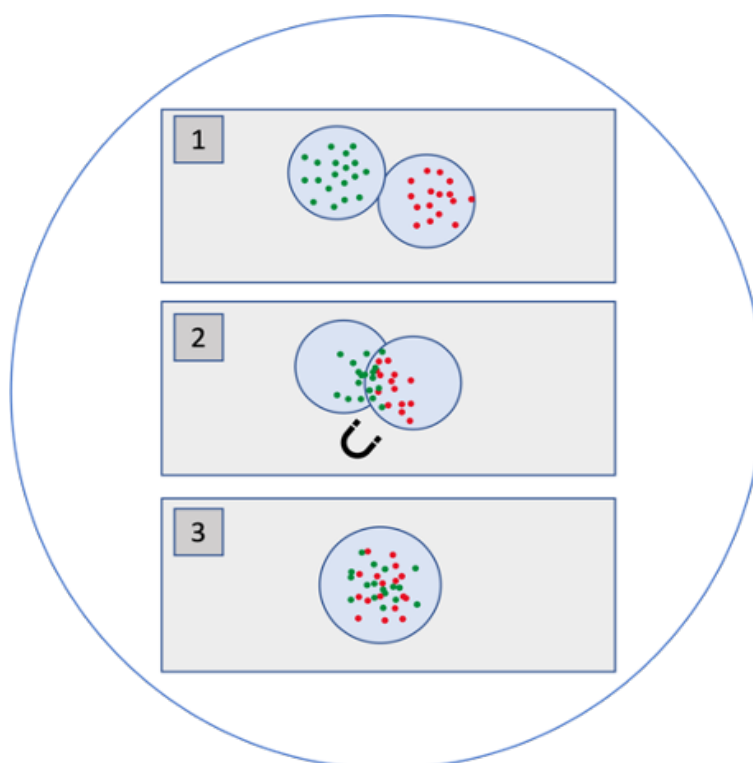


**Fig. 3.32** Schematic view of the experiment. 1) Two different drops with loaded dyes in the core of containers are placed on the glass. The drops are placed near each other. 2) With an external magnet the particles are moved to one point. 3) Two types of containers are mixed between each other.

### 3.6. **LOADING AND DELIVERY OF CAPSULES. RELEASE OF INNER SU**

It was difficult to capture this process of movement by the fluorescence optical microscope. So there is only the picture of mixture of two drops (Fig. 3.33).

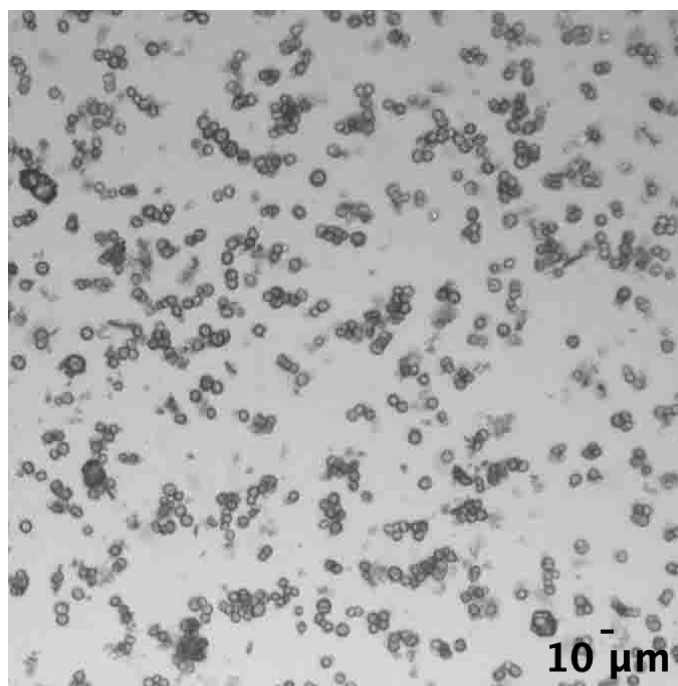


**Fig. 3.33** Mixture of  $\text{CaCO}_3$ /Fluorescein sodium salt  $-(\text{PSS} - \text{PDADMAC})_2 - (\text{PSS} - \text{MNP}/\text{PDADMAC})$  and  $\text{CaCO}_3$ / Rhodamin B  $-(\text{PSS} - \text{PDADMAC})_2 - (\text{PSS} - \text{MNP}/\text{PDADMAC})$ , delivered to the focus area by external magnet

Imaging in a normal (not fluorescent) mode (Fig. 3.33) did not represent any difference among capsules after their displacement and delivery to the defined area. It was possible to see the difference of objects distribution only in the fluorescence mode, using different filters. TRITC filter was used for imaging objects with Rhodamine B dyes inside it, while FITC filter was used for imaging containers with fluorescein sodium salt. Of course, it was impossible to visualize both types of containers simultaneously, because dyes have different fluorescent spectra what required the change of filters.

Images were acquired in the same point, using different filters, where two different types of containers were delivered (Fig. 3.34).

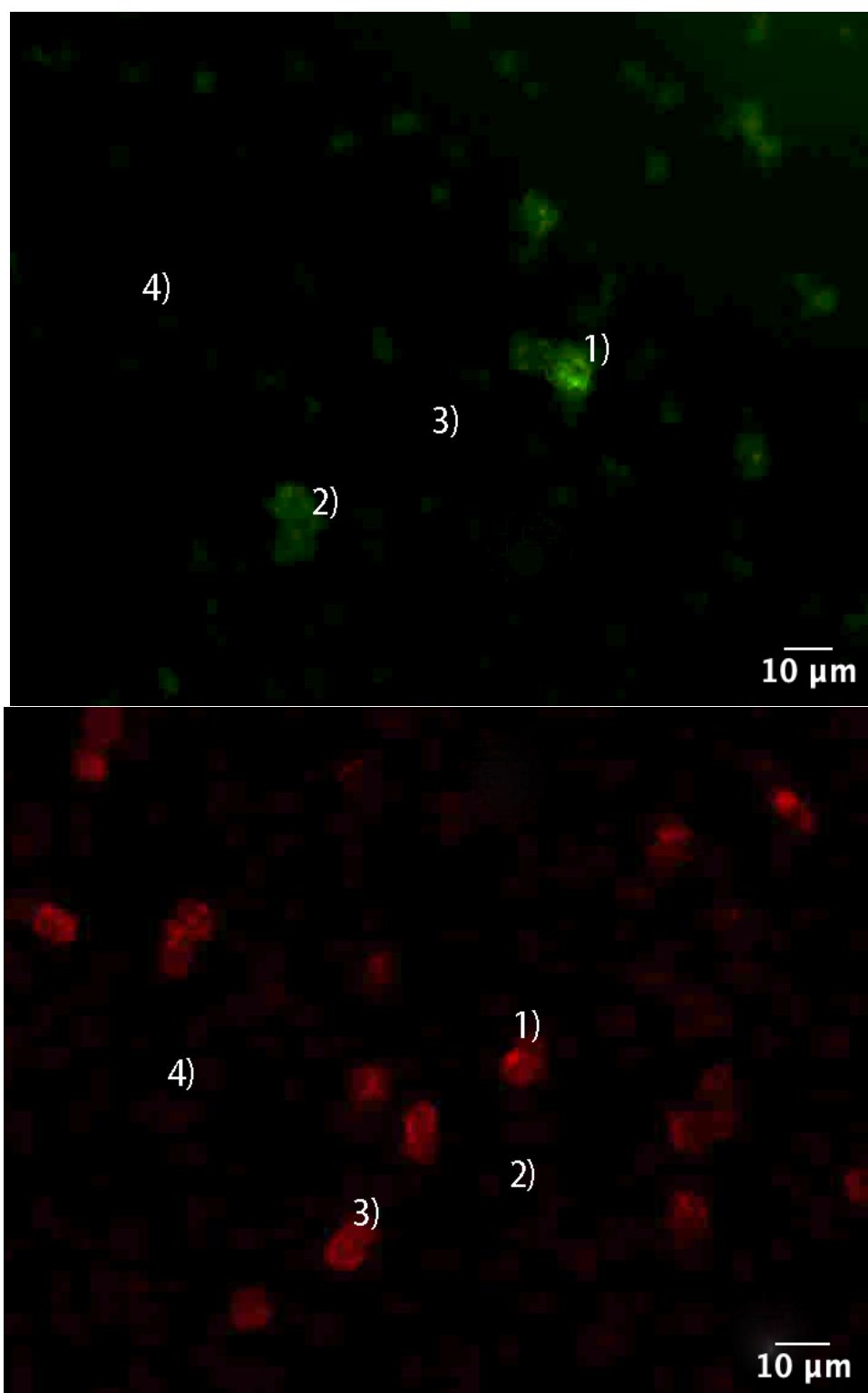


**Fig. 3.34** Optical fluorescent microscope images of mixture of  $\text{CaCO}_3$ /Fluorescein sodium salt - $(\text{PSS} - \text{PDADMAC})_2 - (\text{PSS} - \text{MNP}/\text{PDADMAC})$  and  $\text{CaCO}_3$ / Rhodamin B - $(\text{PSS} - \text{PDADMAC})_2 - (\text{PSS} - \text{MNP}/\text{PDADMAC})$ . Top- using FITC filter. Bottom - using TRITC filter.

As it is clear from Fig. 3.34, both types of capsules were effectively delivered to the same area. In order to show the effi-

### 3.6. **LOADING AND DELIVERY OF CAPSULES. RELEASE OF INNER SUBSTANCE**

ciency of the encapsulation, we compared RGB values of inner zones of capsules and of a medium surrounding it. Analysing images, we have found out the RGB values of different points, marked in Fig. 3.34 as 1 - 4. The values of the intensities in different points are presented in Table 3.3, allowing to make conclusions about the efficiency of the encapsulation of dyes.

**Table 3.3** The distribution of dyes in the core and in the solution by comparison RGB values.

No. in the Fig.3.34	Fluorescein sodium salt (Red Green Blue)	Rhodamin B (Red Green Blue)
<b>1</b>	39 <b>138</b> 0	<b>144</b> 1 0
<b>2</b>	0 <b>51</b> 0	0 0 0
<b>3</b>	0 0 0	<b>98</b> 1 0
<b>4</b>	0 0 0	0 0 0

Analyzing these data, we can conclude that dyes are mainly concentrated inside the core of the fabricated objects. For the characterization of an inner substance the bold value is more interesting. Fluorescein sodium salt gives green color, Rhodamine B – red one. In the RGB triplet, Green characterizes fluorescein sodium salt, red – Rhodamine B. As we can see the value of these numbers is the maximum for corresponding color. RGB values of the surrounding solution is aspires to zero which corresponds to the black color.

As the next step, we have dissolve the  $CaCO_3$  cores by adding EDTA solution (pH=6-7). Optical transmission image of the resultant solution is shown in Fig. 3.35.

Similarly, to the previous case, no special features can be seen in the transmission mode: therefore, we have changed the mode to a fluorescent one using two types of filters. The acquired images are shown in Fig. 3.36. It is to note that there are spheric particles which has colored shell due to the incorporation of dyes. The presence of colored background indicates that

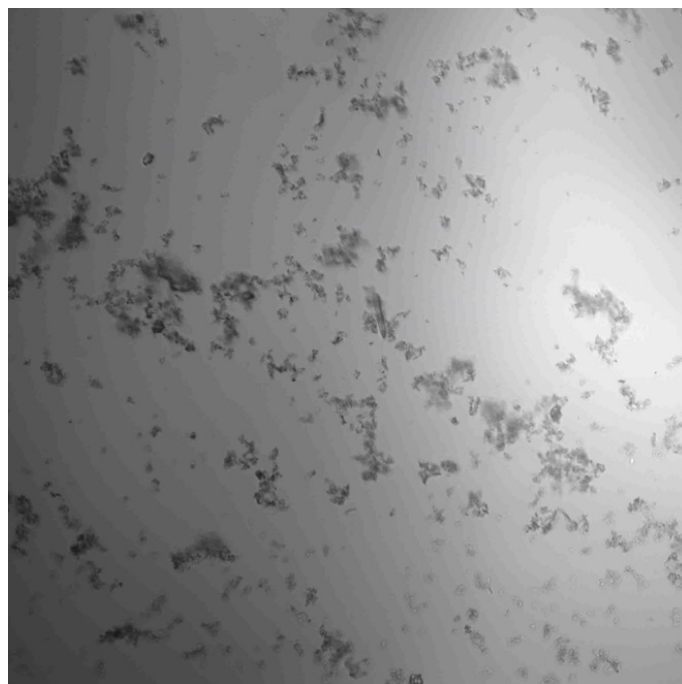


**Fig. 3.35** Optical image of the sample after the core dissolution by adding EDTA solution.

a part of dye molecules has left the core, that can be connected to the fact that dyes have rather small sizes (around 1 nm). In any case in this colored medium, we can explicitly distinguish capsules (Fig. 3.36, points 1) and 3)).

As it is clear from Fig. 3.36, there is an intermediate state. Some dyes are inside the capsules, some of them are out. To show the release of dyes, again we compared RGB values in chosen points (Fig. 3.36 1)-4)). The comparison of these values allow to see the efficiency of the release (table 3.4).

**Table 3.4** The distribution of dyes in the core and in the solution by comparison RGB values after dissolving the core with EDTA

No. in the Fig.3.36	Fluorescein sodium salt (Red Green Blue)	Rhodamin B (Red Green Blue)
<b>1</b>	19 <b>53</b> 6	<b>67</b> 0 0
<b>2</b>	8 <b>31</b> 0	<b>45</b> 0 0
<b>3</b>	45 <b>82</b> 17	<b>96</b> 0 0
<b>4</b>	8 <b>31</b> 0	<b>45</b> 0 0

Analyzing these data (the bold ones), we can conclude that

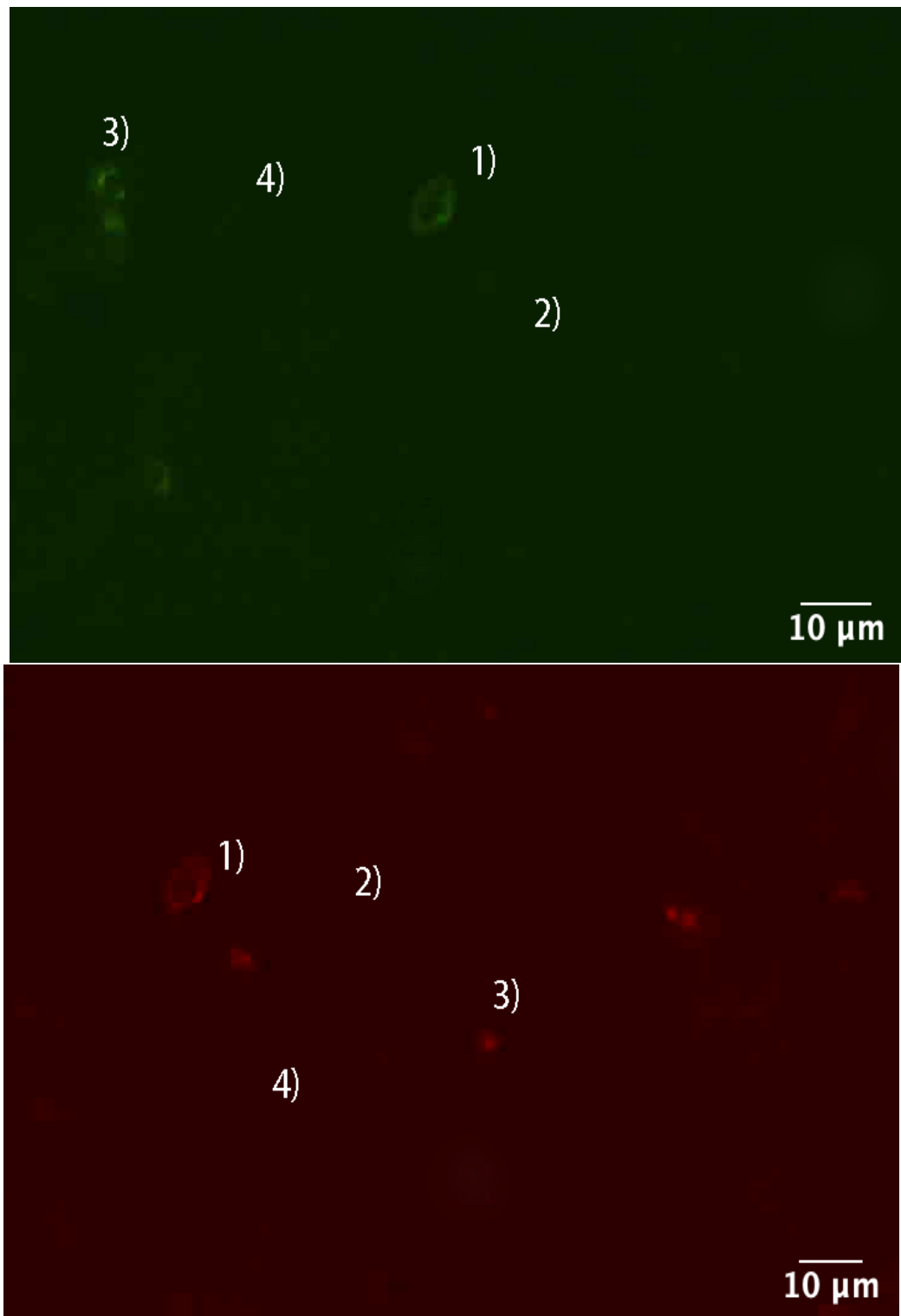


**Fig. 3.36** Optical fluorescent microscope images of the mixture of two types of capsules loaded with different dyes after core dissolution. Top – FITC filter, bottom – TRITC filter.

inside the core the concentration of dyes is higher than in the solution. Moreover, it shows that a significant amount of dyes was released in the solution.

### 3.6. **LOADING AND DELIVERY OF CAPSULES. RELEASE OF INNER SU**

After that, hydrochloride acid was added to this mixture for opening pores in the capsules with dissolved templates, what must result in the fact that the dyes are completely in the solution. Taking into account that the material of the template is still present in the solution, we can expect the formation of a crystal of  $\text{CaCl}_2 \cdot 2\text{H}_2\text{O}$ . during drying of the solution under the illumination. 10 minutes of the sample illumination has resulted into the crystal formation, as it is shown in Fig. 3.37.

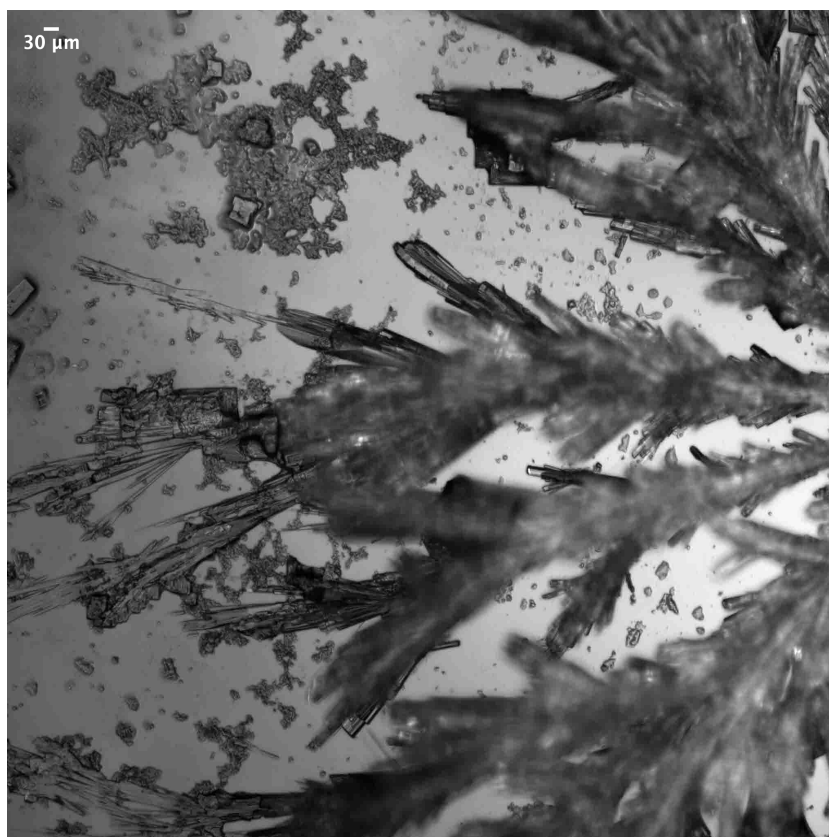


**Fig. 3.37**  $\text{CaCl}_2 \cdot 2\text{H}_2\text{O}$  crystal formed after drying of the surrounding water.

If the release of dyes from capsules was successful, they will remain in the solution and will settle down on the formed crystal. In Fig. 3.38 we see how the dyes were distributed on the formed crystal.

Comparison of images, shown in In Fig. 3.38, demonstrates that these two different dyes were adsorbed on the formed  $\text{CaCl}_2 \cdot 2\text{H}_2\text{O}$  crystal in different ways, very likely due to the

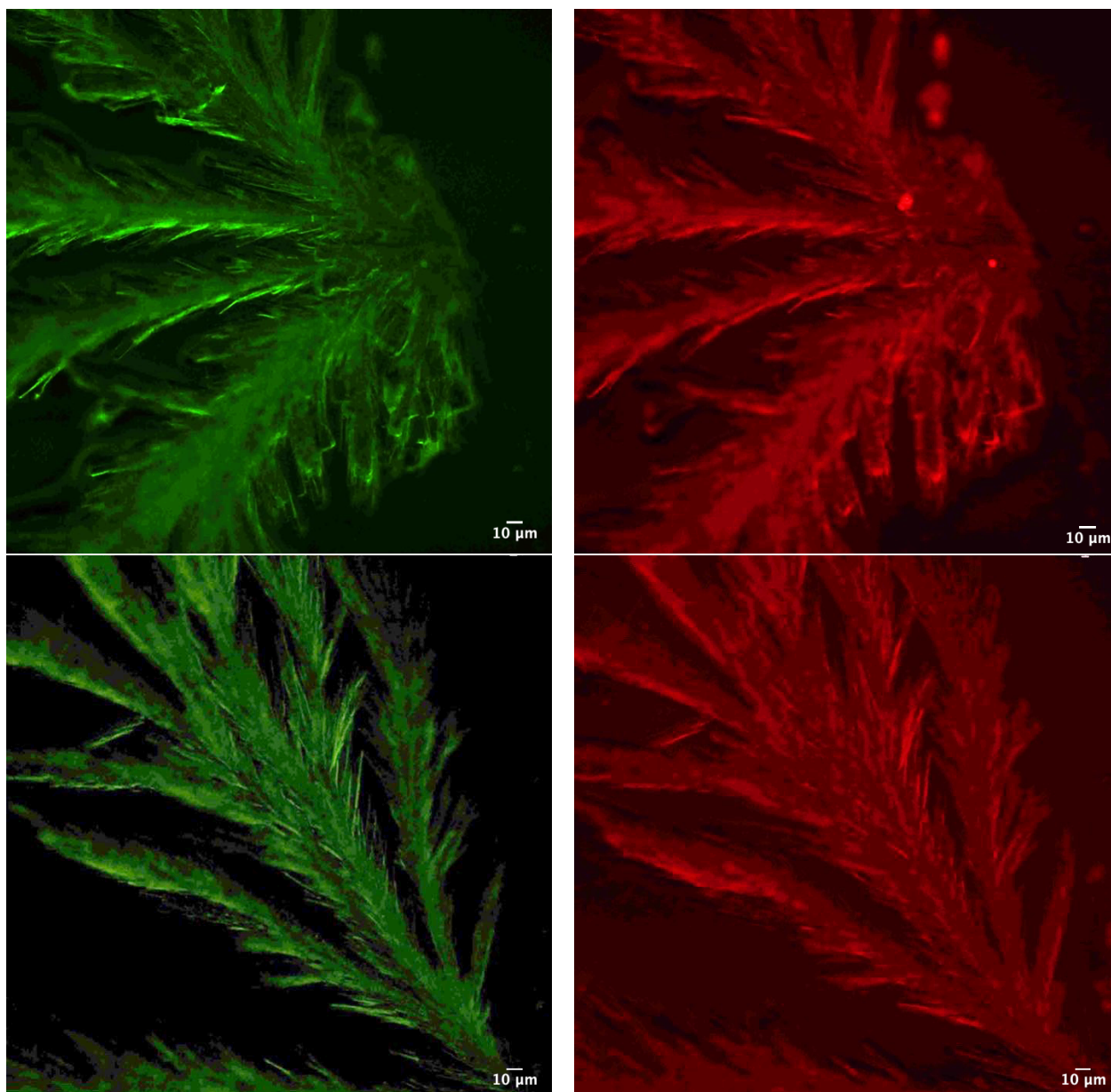


**Fig. 3.38**  $CaCl_2 \cdot 2H_2O$  crystal. Left – FITC filter, right – TRITC filter.

difference in the initial encapsulation efficiency (as the result, difference in the concentration in the solution before drying). However, these images demonstrate the fact that the release was done and all dyes molecules were released into surrounding solution and adsorbed on the  $CaCl_2 \cdot 2H_2O$  crystals. It is to note that no spherical objects with sizes, corresponding to that of templates were observed in these images.



#### 3.7. Loading of capsules with aquacobalamin (vitamin B12) and dimeglumine chlorin E6 inside capsules

For the encapsulation of aquacobalamin and dimeglumine chlorin E6, hollow capsules with magnetite nanoparticles in the shell were prepared. The polymers that were used in layer-by-layer technique were biodegradable and biocompatible. In this case chitosan and alginate were taken. The shell is composed by 3 bilayers of CHI-ALG, penultimate layer included magnetite nanoparticles. The final structure of the shell is  $(ALG - CHI)_2 - (ALG - MNP/CHI) - ALG$ . Also, there were capsules without magnetite in the shell and in this case the final structure of the shell was  $(ALG - CHI)_3$ . As a core  $CaCO_3$  particles were used as a core, then the core was dissolved by EDTA solution as it was described above. Loading was performed by leaving the formed hollow microcapsules in aquacobalamin solution (3 mg/ml) for 24 h with continuous shaking. Afterward, the capsules were precipitated, and the water was replaced by a buffer at pH = 9.6. For the characterization, capsules were dried on silica slide whose surface was previously charged by deposition of  $PEI - (PSS - PEI)_2$  layers.

Vitamins are one of the most important classes of micronutrients that are essential for human life. Each vitamin needs a different number of genes, proteins, enzymes. Vitamin  $B_{12}$  mainly performs its role in bone marrow, liver, intestinal epithelium, and neurocytes. In medicine it is quite important to use it for painful syndrome treatment, for myelin restoring and for anemia prevention. It is important for folate metabolism and homocysteine neutralization, DNA methylation, nucleotide biosynthesis, and anemia prevention. (Gromova et al., 2021; Maiorova et al., 2019)

Derivatives of chlorine E6 are used as a basis for the syn-

### 3.7. **LOADING OF CAPSULES WITH AQUACOBALAMIN (VITAMIN B12)**

thesis of cationic photosensitizers. These photosensitizers are usually applied for photochemical destruction of pathogenic microorganisms. This reaction is the basis of photodynamic therapy. The objects of this therapy are viruses, bacteria, fungi, and protozoa. (Carpenter et al., 2012; Plaetzer et al., 2009)

As a result of encapsulation, loaded capsules were fabricated. This demonstrates the effectiveness of encapsulation process and demonstrates the first steps in the field of targeted delivery. The incorporation of magnetite nanoparticles in the shell allows to use external magnetic field for their delivery in the body. Opening of the pores in the targeted zone can be achieved by changing pH, temperature, laser etc.

SEM images of capsules  $(ALG-CHI)_2-(ALG-MNP/CHI)-ALG$  and  $(ALG-CHI)_3$  loaded with aquacobalamin (vitamin  $B_{12}$ ) are shown in Fig. 3.39.

SEM images of capsules  $(ALG-CHI)_2-(ALG-MNP/CHI)-ALG$  and  $(ALG-CHI)_3$  loaded with dimeglumine chlorin E6 are shown in Fig. 3.40.

As it is clear from these figures, capsules have spherical shape that indicates that there are some inner substances inside them. As it is well shown in literature (Erokhina et al., 2009, 2013), drying of hollow capsules results in the smooth objects on the support. Therefore, spherical form of dried sample of these objects indicates that some substance was really encapsulated into them. There are two other arguments that prove that inner substance had entered inside the capsules. First, the capsules in eppendorf were colored in rose and green, which corresponds to the color of Vitamin  $B_{12}$  and chlorin E6, respectively. Second, during the measurements on optical microscope it was seen, that the inner substance of capsules were colored.

In the case of capsules with magnetite nanoparticles in the

### 3.7. LOADING OF CAPSULES WITH AQUACOBALAMIN (VITAMIN B12)

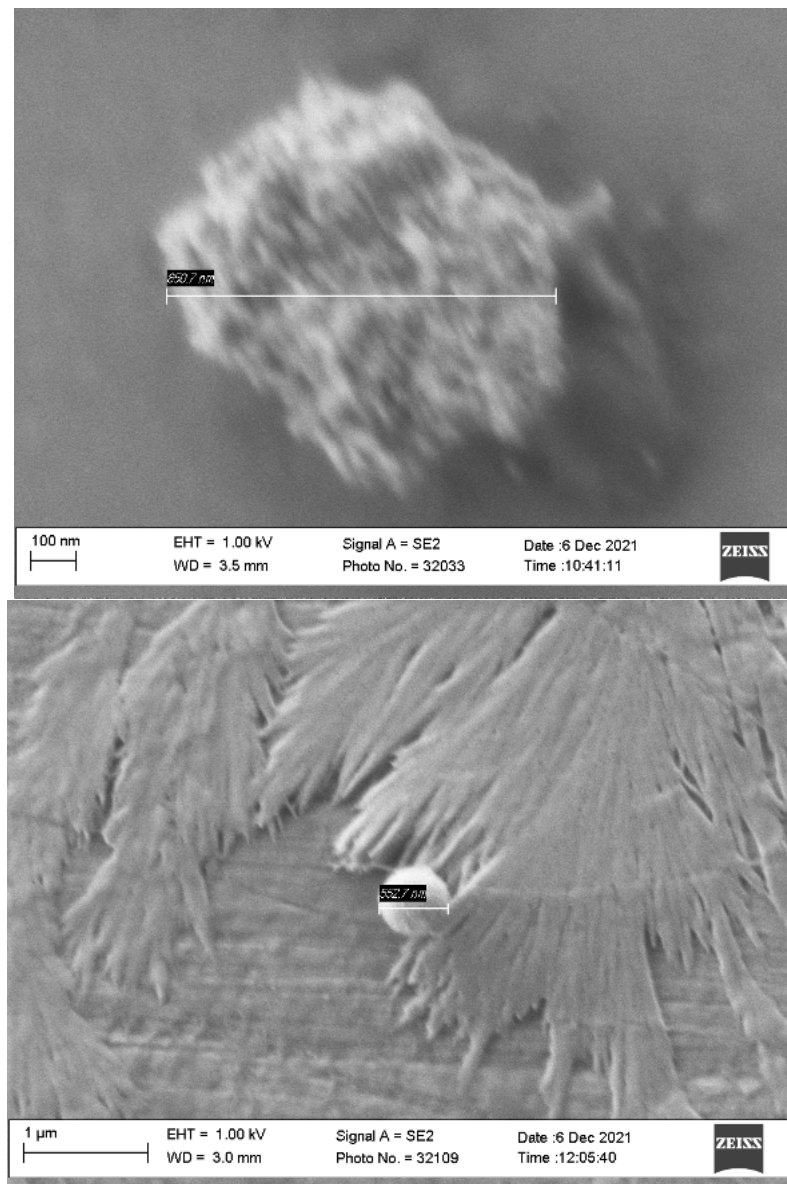


**Fig. 3.39** SEM images of: top –  $(ALG - CHI)_2 - (ALG - MNP/CHI) - ALG - B_{12}$ ; bottom –  $(ALG - CHI)_3 - B_{12}$ .

shell, we see inhomogeneity of the surface due their presence. The prepared and loaded capsules are ready for further use.

### 3.7. LOADING OF CAPSULES WITH AQUACOBALAMIN (VITAMIN B12)

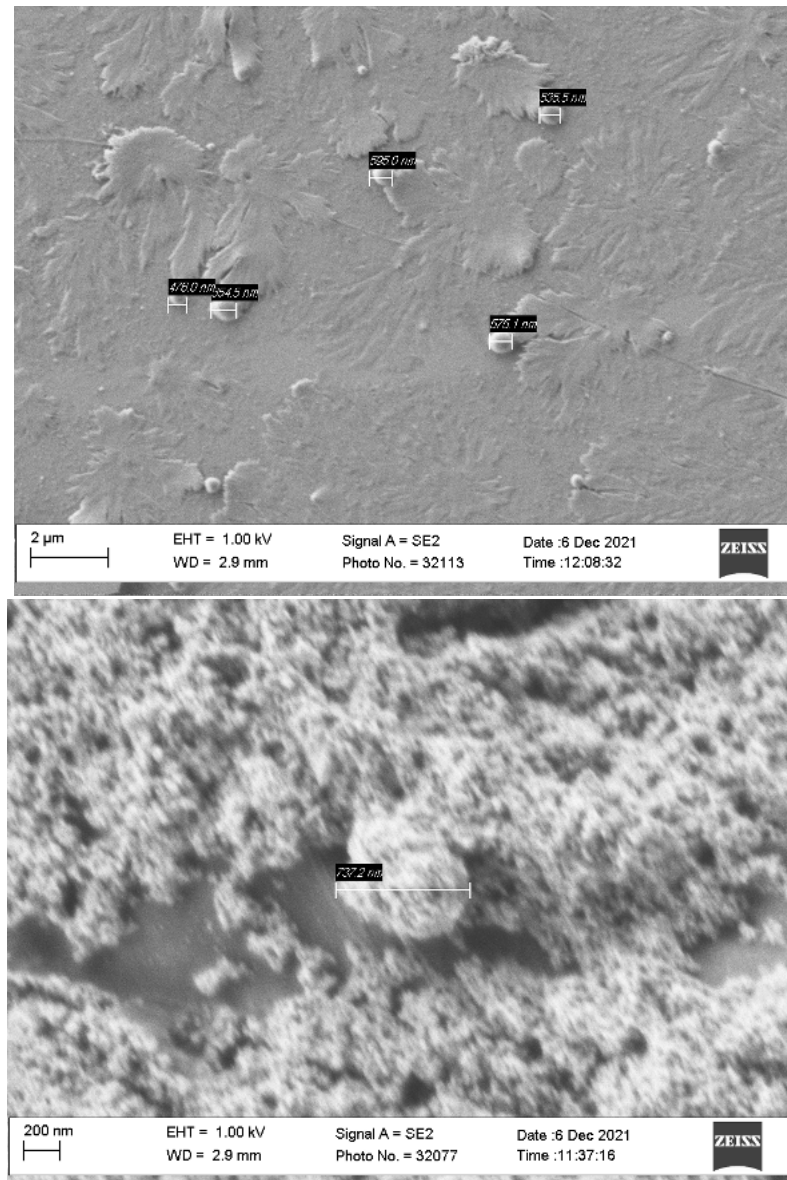


**Fig. 3.40** SEM images of: top –  $(\text{ALG} - \text{CHI})_2 - (\text{ALG} - \text{MNP}/\text{CHI}) - \text{ALG} - E_6$ ; bottom -  $(\text{ALG} - \text{CHI})_3 - E_6$ .

---

## CHAPTER 4

---

# **GENERAL CONCLUSIONS**

The LbL technique was used for synthesizing of a hollow capsules that can be used for drug delivery. In order to fabricate them different polymers, including biodegradable ones, were used. During this work these capsules were studied by different methods. This allowed to obtain new information about them. Moreover, the complicated and powerful method, such as coherent X-Ray diffraction imaging, was applied for studying. In the present work this method was applied for the first time for the investigation of polymeric capsules. Reconstructed images have revealed a significant difference with images, obtained in dried conditions using SEM: the shape of capsules was found to be practically a spherical one. Moreover, CXDI allowed to study the variation of the shell permeability as a function of the pH of a medium, revealing redistribution of the encapsulated gold nanoparticles.

The internal part of capsules can be used for encapsulation of active compounds, such as pharmaceutical preparations. The architecture of the shell, instead, can provide functional properties to these objects, allowing their targeted delivery and induced release of encapsulated substances. For example, the shell can be functionalized by the incorporation of magnetite nanoparticles. This option allows to use an external magnetic field for the delivery of capsules in a defined area in the body. For some specific industrial or therapeutic applications, it is necessary to deliver two or more different compounds to the fixed point and provide their simultaneous release. If it happens before the target point, the compounds can react with surrounding medium products and, therefore, they will not be able to perform the required action in the desirable zone. Therefore, in the framework of this thesis work we have fabricated two types of capsules with magnetic nanoparticles in the shell, loaded by different dye molecules. These two types of capsules were deliv-

ered to a defined zone by the application of external magnetic field. The release of the encapsulated dyes was done by the variation of pH of the liquid medium, what was revealed using fluorescent microscopy. This experiments have demonstrated the possibility of using different types of capsules, bringing them to a desirable zone and releasing of encapsulated substances in the desirable point. The release of several different compounds has resulted in a reaction between them, what can be used in industry and/or pharmaceuticals, when two or more compounds must be safely delivered to a defined zone and make a reaction only in this restricted area.

Obviously, the main aim of the capsules using is delivery and release of encapsulated substances, that has a practical importance. For these reasons, two essential bio-active substances were selected. Aquacobalamin (Vitamin B12) and dimeglumine chlorin E6 are two promising and important compounds. Aquacobalamin (Vitamin B12) is quite essential in a human body and dimeglumine chlorin E6 is used as a catalysator in photodynamic therapy. They were successfully loaded in capsules, the shell of which was fabricated using also biocompatible polymers. Moreover, the shell of these capsules was functionalized by magnetite nanoparticles incorporation. As a result, encapsulated samples functionalized by magnetite were synthesized and are ready to use in biomedical sphere.

Summarizing, the following results were obtained in this thesis work:

1. Hollow capsules of micron and submicron sizes were fabricated, using also biocompatible polymers for the shell formation.
2. The capsules were loaded with different substances, such as gold nanoparticles, dyes, and Vitamin B12 and dimeglumine

chlorin E6 for the first time.

3. The shell of the capsules was functionalized by magnetic nanoparticles and the possibility of targeted delivery using external magnetic field has been demonstrated.
4. The capsules were characterized at each stage of their formation.
5. For the first time the coherent X-Ray diffraction imaging technique was applied for studying these objects.
6. It has been demonstrated a significant difference in the structure of capsules in dry and wet conditions.
7. It has been directly demonstrated the variation of shells permeability (redistribution of encapsulated gold nanoparticles) in natural liquid conditions.
8. It has been demonstrated the possibility of the delivery of two different types of capsules, loaded by different dyes, to a desirable area with their successive simultaneous release, induced by the pH variation.



---

## REFERENCES

- Abbey, B., Nugent, K. A., Williams, G. J., Clark, J. N., Peele, A. G., Pfeifer, M. A., De Jonge, M., and McNulty, I. (2008a). Keyhole coherent diffractive imaging. *Nature Physics*, 4(5):394–398.
- Abbey, B., Williams, G. J., Pfeifer, M. A., Clark, J. N., Putkunz, C. T., Torrance, A., McNulty, I., Levin, T., Peele, A. G., and Nugent, K. A. (2008b). Quantitative coherent diffractive imaging of an integrated circuit at a spatial resolution of 20 nm. *Applied Physics Letters*, 93(21):214101.
- Adalsteinsson, T., Dong, W.-F., and Schönhoff, M. (2004). Diffusion of 77 000 g/mol dextran in submicron polyelectrolyte capsule dispersions measured using pfg-nmr. *The Journal of Physical Chemistry B*, 108(52):20056–20063.
- Aguilar-Méndez, M. Á., Espinosa-Solares, T., de María Guerrero-Toledo, F., Canseco-González, D., Velázquez-Hernández, A., Aguilar-Moreno, G. S., and Navarro-Cerón, E. (2020). Synthesis and characterisation of magnetite nanoparticles using gelatin and starch as capping agents. *IET Nanobiotechnol*, 14(1):94–97.
- Aliev, F. G., Correa-Duarte, M. A., Mamedov, A., Ostrander, J. W., Giersig, M., Liz-Marzán, L. M., and Kotov, N. A. (1999). Layer-by-layer assembly of core-shell magnetite nanoparticles: Effect of silica coating on interparticle interactions and magnetic properties. *Advanced materials*, 11(12):1006–1010.

- Allen, T. M. and Cullis, P. R. (2013). Liposomal drug delivery systems: from concept to clinical applications. *Advanced drug delivery reviews*, 65(1):36–48.
- An, Z., Tao, C., Lu, G., Möhwald, H., Zheng, S., Cui, Y., and Li, J. (2005). Fabrication and characterization of human serum albumin and L- $\alpha$ -dimyristoylphosphatidic acid microcapsules based on template technique. *Chemistry of materials*, 17(10):2514–2519.
- Andres, C. M. and Kotov, N. A. (2010). Inkjet deposition of layer-by-layer assembled films. *Journal of the American Chemical Society*, 132(41):14496–14502.
- Antipov, A. A., Shchukin, D., Fedutik, Y., Petrov, A. I., Sukhorukov, G. B., and Möhwald, H. (2003a). Carbonate microparticles for hollow polyelectrolyte capsules fabrication. *Colloids and surfaces A: physicochemical and engineering aspects*, 224(1-3):175–183.
- Antipov, A. A., Sukhorukov, G. B., and Möhwald, H. (2003b). Influence of the ionic strength on the polyelectrolyte multilayers' permeability. *Langmuir*, 19(6):2444–2448.
- Anwunobi, A. and Emeje, M. (2011). Recent applications of natural polymers in nanodrug delivery. *J Nanomedic Nanotechnol S*, 4(002).
- Arbab, A. S., Bashaw, L. A., Miller, B. R., Jordan, E. K., Lewis, B. K., Kalish, H., and Frank, J. A. (2003). Characterization of biophysical and metabolic properties of cells labeled with superparamagnetic iron oxide nanoparticles and transfection agent for cellular mr imaging. *Radiology*, 229(3):838–846.
- Ariga, K., Lvov, Y., Ichinose, I., and Kunitake, T. (1999). Ultra-thin films of inorganic materials (sio<sub>2</sub> nanoparticle, montmorillonite microplate, and molybdenum oxide) prepared by alternate

layer-by-layer assembly with organic polyions. *Applied clay science*, 15(1-2):137–152.

Ariga, K., Lvov, Y., and Kunitake, T. (1997). Assembling alternate dye- polyion molecular films by electrostatic layer-by-layer adsorption. *Journal of the American Chemical Society*, 119(9):2224–2231.

Ariga, K., Lvov, Y. M., Kawakami, K., Ji, Q., and Hill, J. P. (2011). Layer-by-layer self-assembled shells for drug delivery. *Advanced drug delivery reviews*, 63(9):762–771.

Bailey, R. (1983). Lesser known applications of ferrofluids. *Journal of magnetism and magnetic materials*, 39(1-2):178–182.

Bauschke, H. H., Combettes, P. L., and Luke, D. R. (2003). Hybrid projection–reflection method for phase retrieval. *JOSA A*, 20(6):1025–1034.

Bédard, M. F., Braun, D., Sukhorukov, G. B., and Skirtach, A. G. (2008). Toward self-assembly of nanoparticles on polymeric microshells: near-ir release and permeability. *Acs Nano*, 2(9):1807–1816.

Bédard, M. F., Munoz-Javier, A., Mueller, R., Del Pino, P., Fery, A., Parak, W. J., Skirtach, A. G., and Sukhorukov, G. B. (2009). On the mechanical stability of polymeric microcontainers functionalized with nanoparticles. *Soft Matter*, 5(1):148–155.

Berry, C. C. and Curtis, A. S. (2003). Functionalisation of magnetic nanoparticles for applications in biomedicine. *Journal of physics D: Applied physics*, 36(13):R198.

Berth, G., Voigt, A., Dautzenberg, H., Donath, E., and Möhwald, H. (2002). Polyelectrolyte complexes and layer-by-layer capsules from chitosan/chitosan sulfate. *Biomacromolecules*, 3(3):579–590.

Berzina, T., Pucci, A., Ruggeri, G., Erokhin, V., and Fontana,

- M. P. (2011). Gold nanoparticles–polyaniline composite material: Synthesis, structure and electrical properties. *Synthetic metals*, 161(13-14):1408–1413.
- Bouhon, I. A., Shinkai, M., Honda, H., and Kobayashi, T. (1997). Enhancement of cytokine expression in transiently transfected cells by magnetoliposome mediated hyperthermia. *Cytotechnology*, 25(1):231–234.
- Burke, S. E. and Barrett, C. J. (2003). pH-responsive properties of multilayered poly (L-lysine)/hyaluronic acid surfaces. *Biomacromolecules*, 4(6):1773–1783.
- Büscher, K., Graf, K., Ahrens, H., and Helm, C. A. (2002). Influence of adsorption conditions on the structure of polyelectrolyte multilayers. *Langmuir*, 18(9):3585–3591.
- Cao, D. and Hu, N. (2006). Direct electron transfer between hemoglobin and pyrolytic graphite electrodes enhanced by Fe<sub>3</sub>O<sub>4</sub> nanoparticles in their layer-by-layer self-assembly films. *Biophysical chemistry*, 121(3):209–217.
- Cao, G. and Wang, Y. (2011). Nanostructures and nanomaterials—synthesis, properties and applications, 357 world scientific publishing co pte. *Ltd., Singapore*, 358.
- Carpenter, B. L., Feese, E., Sadeghifar, H., Argyropoulos, D. S., and Ghiladi, R. A. (2012). Porphyrin-cellulose nanocrystals: a photobactericidal material that exhibits broad spectrum antimicrobial activity. *Photochemistry and photobiology*, 88(3):527–536.
- Caruso, F., Caruso, R. A., and Möhwald, H. (1998a). Nano-engineering of inorganic and hybrid hollow spheres by colloidal templating. *Science*, 282(5391):1111–1114.
- Caruso, F., Furlong, D. N., Ariga, K., Ichinose, I., and Kunitake, T. (1998b). Characterization of polyelectrolyte–protein

multilayer films by atomic force microscopy, scanning electron microscopy, and fourier transform infrared reflection- absorption spectroscopy. *Langmuir*, 14(16):4559–4565.

Caruso, F., Lichtenfeld, H., Giersig, M., and Mohwald, H. (1998c). Electrostatic self-assembly of silica nanoparticle-polyelectrolyte multilayers on polystyrene latex particles. *Journal of the American Chemical Society*, 120(33):8523–8524.

Caruso, F. and Möhwald, H. (1999). Protein multilayer formation on colloids through a stepwise self-assembly technique. *Journal of the American Chemical Society*, 121(25):6039–6046.

Caruso, M. M., Schelkopf, S. R., Jackson, A. C., Landry, A. M., Braun, P. V., and Moore, J. S. (2009). Microcapsules containing suspensions of carbon nanotubes. *Journal of Materials Chemistry*, 19(34):6093–6096.

Chaki, S., Malek, T. J., Chaudhary, M., Tailor, J., and Deshpande, M. (2015). Magnetite  $Fe_3O_4$  nanoparticles synthesis by wet chemical reduction and their characterization. *Advances in Natural Sciences: Nanoscience and Nanotechnology*, 6(3):035009.

Chapman, H. N., Barty, A., Bogan, M. J., Boutet, S., Frank, M., Hau-Riege, S. P., Marchesini, S., Woods, B. W., Bajt, S., Benner, W. H., et al. (2006). Femtosecond diffractive imaging with a soft-x-ray free-electron laser. *Nature Physics*, 2(12):839–843.

Charles, S. and Popplewell, J. (1980). Progress in the development of ferromagnetic liquids. *IEEE transactions on magnetics*, 16(2):172–177.

Chatterjee, J., Haik, Y., and Chen, C.-J. (2003). Size dependent magnetic properties of iron oxide nanoparticles. *Journal of Magnetism and Magnetic Materials*, 257(1):113–118.

- Chen, C.-C., Miao, J., Wang, C., and Lee, T. (2007). Application of optimization technique to noncrystalline x-ray diffraction microscopy: Guided hybrid input-output method. *Physical Review B*, 76(6):064113.
- Chen, J., Huang, L., Ying, L., Luo, G., Zhao, X., and xiao Cao, W. (1999). Self-assembly ultrathin films based on diazoresins. *Langmuir*, 15:7208–7212.
- Chilkoti, A., Dreher, M. R., and Meyer, D. E. (2002). Design of thermally responsive, recombinant polypeptide carriers for targeted drug delivery. *Advanced drug delivery reviews*, 54(8):1093–1111.
- Chouly, C., Pouliquen, D., Lucet, I., Jeune, J., and Jallet, P. (1996). Development of superparamagnetic nanoparticles for mri: effect of particle size, charge and surface nature on biodistribution. *Journal of microencapsulation*, 13(3):245–255.
- Cortez, C., Tomaskovic-Crook, E., Johnston, A. P., Scott, A. M., Nice, E. C., Heath, J. K., and Caruso, F. (2007). Influence of size, surface, cell line, and kinetic properties on the specific binding of a33 antigen-targeted multilayered particles and capsules to colorectal cancer cells. *Acs Nano*, 1(2):93–102.
- Curtis, A. and Wilkinson, C. (2001). Nantotechniques and approaches in biotechnology. *TRENDS in Biotechnology*, 19(3):97–101.
- Dai, Z., Voigt, A., Leporatti, S., Donath, E., Dähne, L., and Möhwald, H. (2001). Layer-by-layer self-assembly of polyelectrolyte and low molecular weight species into capsules. *Advanced Materials*, 13(17):1339–1342.
- Daniel, M.-C. and Astruc, D. (2004). Gold nanoparticles: assembly, supramolecular chemistry, quantum-size-related proper-

ties, and applications toward biology, catalysis, and nanotechnology. *Chemical reviews*, 104(1):293–346.

Danton, G. H. and Dietrich, W. D. (2005). Neuroprotection: Where are we going? In *From Neuroscience To Neurology*, pages 237–265. Elsevier.

De Cock, L. J., De Koker, S., De Geest, B. G., Grooten, J., Vervaet, C., Remon, J. P., Sukhorukov, G. B., and Antipina, M. N. (2010). Polymeric multilayer capsules in drug delivery. *Angewandte Chemie International Edition*, 49(39):6954–6973.

De Geest, B. G., Sanders, N. N., Sukhorukov, G. B., Demeester, J., and De Smedt, S. C. (2007). Release mechanisms for polyelectrolyte capsules. *Chemical Society Reviews*, 36(4):636–649.

Decher, G. (1997). Fuzzy nanoassemblies: toward layered polymeric multicomposites. *science*, 277(5330):1232–1237.

Decher, G. and Hong, J.-D. (1991). Buildup of ultrathin multilayer films by a self-assembly process, 1 consecutive adsorption of anionic and cationic bipolar amphiphiles on charged surfaces. In *Makromolekulare Chemie. Macromolecular Symposia*, volume 46, pages 321–327. Wiley Online Library.

Decher, G., Hong, J. D., and Schmitt, J. (1992). Buildup of ultrathin multilayer films by a self-assembly process: Iii. consecutively alternating adsorption of anionic and cationic polyelectrolytes on charged surfaces. *Thin solid films*, 210:831–835.

Déjugnat, C., Koehler, K., Dubois, M., Sukhorukov, G. B., Moehwald, H., Zemb, T., and Guttman, P. (2007). Membrane densification of heated polyelectrolyte multilayer capsules characterized by soft x-ray microscopy. *Advanced Materials*, 19(10):1331–1336.

Déjugnat, C. and Sukhorukov, G. B. (2004). ph-responsive prop-

erties of hollow polyelectrolyte microcapsules templated on various cores. *Langmuir*, 20(17):7265–7269.

Delcea, M., Möhwald, H., and Skirtach, A. G. (2011). Stimuli-responsive lbl capsules and nanoshells for drug delivery. *Advanced drug delivery reviews*, 63(9):730–747.

Dierolf, M., Menzel, A., Thibault, P., Schneider, P., Kewish, C. M., Wepf, R., Bunk, O., and Pfeiffer, F. (2010). Ptychographic x-ray computed tomography at the nanoscale. *Nature*, 467(7314):436–439.

Dixon, M. L., De La Vega, A., Mills, C., Andrews-Hanna, J., Spreng, R. N., Cole, M. W., and Christoff, K. (2018). Heterogeneity within the frontoparietal control network and its relationship to the default and dorsal attention networks. *Proceedings of the National Academy of Sciences*, 115(7):E1598–E1607.

Donath, E., Sukhorukov, G. B., Caruso, F., Davis, S. A., and Möhwald, H. (1998). Novel hollow polymer shells by colloid-templated assembly of polyelectrolytes. *Angewandte Chemie International Edition*, 37(16):2201–2205.

Dresco, P. A., Zaitsev, V. S., Gambino, R. J., and Chu, B. (1999). Preparation and properties of magnetite and polymer magnetite nanoparticles. *Langmuir*, 15(6):1945–1951.

Dubreuil, F., Elsner, N., and Fery, A. (2003). Elastic properties of polyelectrolyte capsules studied by atomic-force microscopy and ricm. *The European Physical Journal E*, 12(2):215–221.

Dyab, A. K., Ozmen, M., Ersoz, M., and Paunov, V. N. (2009). Fabrication of novel anisotropic magnetic microparticles. *Journal of Materials Chemistry*, 19(21):3475–3481.

Elser, V. (2003). Solution of the crystallographic phase prob-



lem by iterated projections. *Acta Crystallographica Section A: Foundations of Crystallography*, 59(3):201–209.

Elsner, N., Dubreuil, F., and Fery, A. (2004). Tuning of microcapsule adhesion by varying the capsule-wall thickness. *Physical Review E*, 69(3):031802.

Erokhina, S., Benassi, L., Bianchini, P., Diaspro, A., Erokhin, V., and Fontana, M. (2009). Light-driven release from polymeric microcapsules functionalized with bacteriorhodopsin. *Journal of the American Chemical Society*, 131(28):9800–9804.

Erokhina, S., Konovalov, O., Bianchini, P., Diaspro, A., Ruggiero, C., Erokhin, V., and Pastorino, L. (2013). Release kinetics of gold nanoparticles from collagen microcapsules by total reflection x-ray fluorescence. *Colloids and Surfaces A: Physicochemical and Engineering Aspects*, 417:83–88.

Erokhina, S., Pastorino, L., Di Lisa, D., Kiiamov, A., Tayurskii, D., Iannotta, S., Erokhin, V., and Faizullina, A. (2021). 3d structure reconstruction of nanoengineered polymeric capsules using coherent x-ray diffraction imaging. *MethodsX*, 8:101230.

Erokhina, S., Pastorino, L., Di Lisa, D., Kiiamov, A. G., Faizullina, A., Tayurskii, D. A., Iannotta, S., and Erokhin, V. (2017). Coherent x-ray diffraction imaging of nanoengineered polymeric capsules. *JETP Letters*, 106(8):540–543.

Fakhrullina, G., Akhatova, F., Kibardina, M., Fokin, D., and Fakhrullin, R. (2017). Nanoscale imaging and characterization of *Caenorhabditis elegans* epicuticle using atomic force microscopy. *Nanomedicine: Nanotechnology, Biology and Medicine*, 13(2):483–491.

Fang, B., Wang, G., Zhang, W., Li, M., and Kan, X. (2005). Fabrication of Fe<sub>3</sub>O<sub>4</sub> nanoparticles modified electrode and its application for voltammetric sensing of dopamine. *Electroanalysis*:

*An International Journal Devoted to Fundamental and Practical Aspects of Electroanalysis*, 17(9):744–748.

Fery, A. and Weinkamer, R. (2007). Mechanical properties of micro-and nanocapsules: Single-capsule measurements. *Polymer*, 48(25):7221–7235.

Fienup, J. R. (1978). Reconstruction of an object from the modulus of its fourier transform. *Optics letters*, 3(1):27–29.

Fienup, J. R. (1982). Phase retrieval algorithms: a comparison. *Applied optics*, 21(15):2758–2769.

Fujii, N., Fujimoto, K., Michinobu, T., Akada, M., Hill, J. P., Shiratori, S., Ariga, K., and Shigehara, K. (2010). The simplest layer-by-layer assembly structure: Best paired polymer electrolytes with one charge per main chain carbon atom for multilayered thin films. *Macromolecules*, 43(8):3947–3955.

Gai, M., Frueh, J., Tao, T., Petrov, A. V., Petrov, V. V., Shesterikov, E. V., Tverdokhlebov, S. I., and Sukhorukov, G. B. (2017). Polylactic acid nano-and microchamber arrays for encapsulation of small hydrophilic molecules featuring drug release via high intensity focused ultrasound. *Nanoscale*, 9(21):7063–7070.

Gallagher-Jones, M., Bessho, Y., Kim, S., Park, J., Kim, S., Nam, D., Kim, C., Kim, Y., Noh, D. Y., Miyashita, O., et al. (2014). Macromolecular structures probed by combining single-shot free-electron laser diffraction with synchrotron coherent x-ray imaging. *Nature communications*, 5(1):1–9.

Gao, C., Möhwald, H., and Shen, J. C. (2004). Enhanced biomacromolecule encapsulation by swelling and shrinking procedures. *ChemPhysChem*, 5(1):116–120.

García-Alonso, J., Fakhruddin, R. F., and Paunov, V. N. (2010). Rapid and direct magnetization of gfp-reporter yeast for micro-

screening systems. *Biosensors and Bioelectronics*, 25(7):1816–1819.

Georgieva, R., Moya, S., Hin, M., Mitlöhner, R., Donath, E., Kieseewetter, H., Möhwald, H., and Bäuml, H. (2002). Permeation of macromolecules into polyelectrolyte microcapsules. *Biomacromolecules*, 3(3):517–524.

Giewekemeyer, K., Thibault, P., Kalbfleisch, S., Beerlink, A., Kewish, C. M., Dierolf, M., Pfeiffer, F., and Salditt, T. (2010). Quantitative biological imaging by ptychographic x-ray diffraction microscopy. *Proceedings of the National Academy of Sciences*, 107(2):529–534.

Gilchrist, R., Medal, R., Shorey, W. D., Hanselman, R. C., Parrott, J. C., and Taylor, C. B. (1957). Selective inductive heating of lymph nodes. *Annals of surgery*, 146(4):596.

Glaeser, R. M. and Taylor, K. A. (1978). Radiation damage relative to transmission electron microscopy of biological specimens at low temperature: a review. *Journal of microscopy*, 112(1):127–138.

Gomez-Lopera, S., Plaza, R., and Delgado, A. (2001). Synthesis and characterization of spherical magnetite/biodegradable polymer composite particles. *Journal of colloid and interface science*, 240(1):40–47.

Gomzikova, M., Kletukhina, S., Kurbangaleeva, S., and Rizvanov, A. (2018). Evaluation of cytochalasin b-induced membrane vesicles fusion specificity with target cells. *BioMed Research International*, 2018.

Gomzikova, M. O., Zhuravleva, M. N., Vorobev, V. V., Salafutdinov, I. I., Laikov, A. V., Kletukhina, S. K., Martynova, E. V., Tazetdinova, L. G., Ntekim, A. I., Khaiboullina, S. F., et al.

- (2019). Angiogenic activity of cytochalasin b-induced membrane vesicles of human mesenchymal stem cells. *Cells*, 9(1):95.
- Gong, H., Garcia-Turiel, J., Vasilev, K., and Vinogradova, O. I. (2005). Interaction and adhesion properties of polyelectrolyte multilayers. *Langmuir*, 21(16):7545–7550.
- Goya, G., Berquo, T., Fonseca, F., and Morales, M. (2003). Static and dynamic magnetic properties of spherical magnetite nanoparticles. *Journal of applied physics*, 94(5):3520–3528.
- Gromova, O. A., Torshin, I. Y., Maiorova, L. A., Koifman, O., and Salnikov, D. S. (2021). Bioinformatic and chemoneurocytological analysis of the pharmacological properties of vitamin b12 and some of its derivatives. *Journal of Porphyrins and Phthalocyanines*, 25(09):835–842.
- Gupta, A. K. and Curtis, A. S. (2004). Surface modified superparamagnetic nanoparticles for drug delivery: interaction studies with human fibroblasts in culture. *Journal of Materials Science: Materials in Medicine*, 15(4):493–496.
- Gupta, A. K. and Gupta, M. (2005). Synthesis and surface engineering of iron oxide nanoparticles for biomedical applications. *biomaterials*, 26(18):3995–4021.
- Guzmán, E., Ritacco, H., Rubio, J. E., Rubio, R. G., and Ortega, F. (2009). Salt-induced changes in the growth of polyelectrolyte layers of poly (diallyl-dimethylammonium chloride) and poly (4-styrene sulfonate of sodium). *Soft Matter*, 5(10):2130–2142.
- Hamley, I. (2003). Nanotechnology with soft materials. *Angewandte Chemie International Edition*, 42(15):1692–1712.
- Han, Y., Shchukin, D., Yang, J., Simon, C. R., Fuchs, H., and Möhwald, H. (2010). Biocompatible protein nanocontainers for controlled drugs release. *Acs Nano*, 4(5):2838–2844.
- He, Q., Cui, Y., and Li, J. (2009). Molecular assembly and

application of biomimetic microcapsules. *Chemical Society Reviews*, 38(8):2292–2303.

Hebert, M. F. (2013). Impact of pregnancy on maternal pharmacokinetics of medications. *Clinical pharmacology during pregnancy*, pages 17–39.

Hirsch, R. (2004). *Exploring colour photography: a complete guide*. Laurence King Publishing.

Holland, B. T., Blanford, C. F., and Stein, A. (1998). Synthesis of macroporous minerals with highly ordered three-dimensional arrays of spheroidal voids. *Science*, 281(5376):538–540.

Hoshi, T., Akase, S., and Anzai, J.-i. (2002). Preparation of multilayer thin films containing avidin through sugar-lectin interactions and their binding properties. *Langmuir*, 18(18):7024–7028.

Huang, S.-H., Liao, M.-H., and Chen, D.-H. (2003). Direct binding and characterization of lipase onto magnetic nanoparticles. *Biotechnology Progress*, 19(3):1095–1100.

Huang, X., Nelson, J., Kirz, J., Lima, E., Marchesini, S., Miao, H., Neiman, A. M., Shapiro, D., Steinbrener, J., Stewart, A., et al. (2009). Soft x-ray diffraction microscopy of a frozen hydrated yeast cell. *Physical review letters*, 103(19):198101.

Ikeda, A., Hatano, T., Shinkai, S., Akiyama, T., and Yamada, S. (2001). Efficient photocurrent generation in novel self-assembled multilayers comprised of [60] fullerene-cationic homooxalix [3] arene inclusion complex and anionic porphyrin polymer. *Journal of the American Chemical Society*, 123(20):4855–4856.

Ilavsky, J., Zhang, F., Andrews, R. N., Kuzmenko, I., Jemian, P. R., Levine, L. E., and Allen, A. J. (2018). Development of combined microstructure and structure characterization facility

- for in situ and operando studies at the advanced photon source. *Journal of applied crystallography*, 51(3):867–882.
- Iler, R. (1966). Multilayers of colloidal particles. *Journal of colloid and interface science*, 21(6):569–594.
- Itoh, Y., Matsusaki, M., Kida, T., and Akashi, M. (2004). Preparation of biodegradable hollow nanocapsules by silica template method. *Chemistry letters*, 33(12):1552–1553.
- Jiang, H., Ramunno-Johnson, D., Song, C., Amirbekian, B., Kohmura, Y., Nishino, Y., Takahashi, Y., Ishikawa, T., and Miao, J. (2008). Nanoscale imaging of mineral crystals inside biological composite materials using x-ray diffraction microscopy. *Physical review letters*, 100(3):038103.
- Jiang, H., Song, C., Chen, C.-C., Xu, R., Raines, K. S., Fahimian, B. P., Lu, C.-H., Lee, T.-K., Nakashima, A., Urano, J., et al. (2010). Quantitative 3d imaging of whole, unstained cells by using x-ray diffraction microscopy. *Proceedings of the National Academy of Sciences*, 107(25):11234–11239.
- Jiang, H., Xu, R., Chen, C.-C., Yang, W., Fan, J., Tao, X., Song, C., Kohmura, Y., Xiao, T., Wang, Y., et al. (2013). Three-dimensional coherent x-ray diffraction imaging of molten iron in mantle olivine at nanoscale resolution. *Physical review letters*, 110(20):205501.
- Jordan, A., Scholz, R., Maier-Hauff, K., Johannsen, M., Wust, P., Nadobny, J., Schirra, H., Schmidt, H., Deger, S., Loening, S., et al. (2001). Presentation of a new magnetic field therapy system for the treatment of human solid tumors with magnetic fluid hyperthermia. *Journal of magnetism and magnetic materials*, 225(1-2):118–126.
- Katagiri, K., Hamasaki, R., Ariga, K., and Kikuchi, J.-i. (2002a).

- Layer-by-layer self-assembling of liposomal nanohybrid “cerasome” on substrates. *Langmuir*, 18(17):6709–6711.
- Katagiri, K., Hamasaki, R., Ariga, K., and Kikuchi, J.-i. (2002b). Layered paving of vesicular nanoparticles formed with cerasome as a bioinspired organic- inorganic hybrid. *Journal of the American Chemical Society*, 124(27):7892–7893.
- Khalafalla, S. and Reimers, G. (1980). Preparation of dilution-stable aqueous magnetic fluids. *IEEE Transactions on Magnet-ics*, 16(2):178–183.
- Köhler, K., Shchukin, D. G., Möhwald, H., and Sukhorukov, G. B. (2005). Thermal behavior of polyelectrolyte multilayer microcapsules. 1. the effect of odd and even layer number. *The Journal of Physical Chemistry B*, 109(39):18250–18259.
- Kolesnikova, T. A., Gorin, D. A., Fernandes, P., Kessel, S., Khomutov, G. B., Fery, A., Shchukin, D. G., and Möhwald, H. (2010). Nanocomposite microcontainers with high ultrasound sensitivity. *Advanced Functional Materials*, 20(7):1189–1195.
- Koo, H. Y., Lee, H.-J., Kim, J. K., and San Choi, W. (2010). Uv-triggered encapsulation and release from polyelectrolyte microcapsules decorated with photoacid generators. *Journal of Materials Chemistry*, 20(19):3932–3937.
- Kotov, N. (1999). Layer-by-layer self-assembly: the contribution of hydrophobic interactions. *Nanostructured Materials*, 12(5-8):789–796.
- Kotov, N. A., Dekany, I., and Fendler, J. H. (1995). Layer-by-layer self-assembly of polyelectrolyte-semiconductor nanoparticle composite films. *The Journal of Physical Chemistry*, 99(35):13065–13069.
- Kyrikou, I. and Briassoulis, D. (2007). Biodegradation of agri-

cultural plastic films: a critical review. *Journal of Polymers and the Environment*, 15(2):125–150.

Lankalapalli, S. and Kolapalli, V. (2009). Polyelectrolyte complexes: A review of their applicability in drug delivery technology. *Indian journal of pharmaceutical sciences*, 71(5):481.

Lee, H., Kepley, L. J., Hong, H. G., and Mallouk, T. E. (1988). Inorganic analogs of langmuir-blodgett films: adsorption of ordered zirconium 1, 10-decanebisphosphonate multilayers on silicon surfaces. *Journal of the American Chemical Society*, 110(2):618–620.

Lee, J. S. and Feijen, J. (2012). Polymersomes for drug delivery: design, formation and characterization. *Journal of controlled release*, 161(2):473–483.

Leja, K. and Lewandowicz, G. (2010). Polymer biodegradation and biodegradable polymers-a review. *Polish Journal of Environmental Studies*, 19(2).

Lima, E., Wiegart, L., Pernot, P., Howells, M., Timmins, J., Zontone, F., and Madsen, A. (2009). Cryogenic x-ray diffraction microscopy for biological samples. *Physical Review Letters*, 103(19):198102.

Liu, Y., Wang, A., and Claus, R. O. (1997). Layer-by-layer electrostatic self-assembly of nanoscale  $Fe_3O_4$  particles and polyimide precursor on silicon and silica surfaces. *Applied Physics Letters*, 71(16):2265–2267.

Lu, C., Luo, C., and Cao, W. (2003). Self-assembly of a covalently attached magnetic film from diazoresin and  $Fe_3O_4$  nanoparticles. *Journal of Materials Chemistry*, 13(2):382–384.

Lu, Z., Prouty, M. D., Guo, Z., Golub, V. O., Kumar, C. S., and Lvov, Y. M. (2005). Magnetic switch of permeability for poly-



- electrolyte microcapsules embedded with  $\text{Co}@ \text{Au}$  nanoparticles. *Langmuir*, 21(5):2042–2050.
- Lu, Z., Wang, G., Zhuang, J., and Yang, W. (2006). Effects of the concentration of tetramethylammonium hydroxide peptizer on the synthesis of  $\text{Fe}_3\text{O}_4/\text{SiO}_2$  core/shell nanoparticles. *Colloids and Surfaces A: Physicochemical and Engineering Aspects*, 278(1-3):140–143.
- Lübbe, A. S., Alexiou, C., and Bergemann, C. (2001). Clinical applications of magnetic drug targeting. *Journal of Surgical Research*, 95(2):200–206.
- Lucas, N., Bienaime, C., Belloy, C., Queneudec, M., Silvestre, F., and Nava-Saucedo, J.-E. (2008). Polymer biodegradation: Mechanisms and estimation techniques—a review. *Chemosphere*, 73(4):429–442.
- Luke, D. R. (2004). Relaxed averaged alternating reflections for diffraction imaging. *Inverse problems*, 21(1):37.
- Lvov, Y., Antipov, A. A., Mamedov, A., Möhwald, H., and Sukhorukov, G. B. (2001). Urease encapsulation in nanoorganized microshells. *Nano Letters*, 1(3):125–128.
- Lvov, Y., Ariga, K., Ichinose, I., and Kunitake, T. (1995a). Assembly of multicomponent protein films by means of electrostatic layer-by-layer adsorption. *Journal of the American Chemical Society*, 117(22):6117–6123.
- Lvov, Y., Ariga, K., Ichinose, I., and Kunitake, T. (1995b). Layer-by-layer architectures of concanavalin A by means of electrostatic and biospecific interactions. *Journal of the Chemical Society, Chemical Communications*, (22):2313–2314.
- Lvov, Y., Ariga, K., Ichinose, I., and Kunitake, T. (1996). Formation of ultrathin multilayer and hydrated gel from montmorillonite and linear polycations. *Langmuir*, 12(12):3038–3044.

Lvov, Y., Ariga, K., and Kunitake, T. (1994). Layer-by-layer assembly of alternate protein/polyion ultrathin films. *Chemistry Letters*, 23(12):2323–2326.

Lvov, Y., Ariga, K., Onda, M., Ichinose, I., and Kunitake, T. (1997). Alternate assembly of ordered multilayers of  $\text{SiO}_2$  and other nanoparticles and polyions. *Langmuir*, 13(23):6195–6203.

Lvov, Y., Ariga, K., Onda, M., Ichinose, I., and Kunitake, T. (1999). A careful examination of the adsorption step in the alternate layer-by-layer assembly of linear polyanion and polycation. *Colloids and Surfaces A: Physicochemical and Engineering Aspects*, 146(1-3):337–346.

Lvov, Y., Onda, M., Ariga, K., and Kunitake, T. (1998). Ultrathin films of charged polysaccharides assembled alternately with linear polyions. *Journal of Biomaterials Science, Polymer Edition*, 9(4):345–355.

Maiorova, L. A., Erokhina, S. I., Pisani, M., Barucca, G., Marcaccio, M., Koifman, O. I., Salnikov, D. S., Gromova, O. A., Astolfi, P., Ricci, V., et al. (2019). Encapsulation of vitamin B12 into nanoengineered capsules and soft matter nanosystems for targeted delivery. *Colloids and Surfaces B: Biointerfaces*, 182:110366.

Mamedov, A., Ostrander, J., Aliev, F., and Kotov, N. A. (2000). Stratified assemblies of magnetite nanoparticles and montmorillonite prepared by the layer-by-layer assembly. *Langmuir*, 16(8):3941–3949.

Marchesini, S. (2007). Invited article: A unified evaluation of iterative projection algorithms for phase retrieval. *Review of Scientific Instruments*, 78(1):011301.

Marchesini, S., He, H., Chapman, H. N., Hau-Riege, S. P., Noy, A., Howells, M. R., Weierstall, U., and Spence, J. C. (2003). X-

ray image reconstruction from a diffraction pattern alone. *Physical Review B*, 68(14):140101.

Mendenhall, G. D., Geng, Y., and Hwang, J. (1996). Optimization of long-term stability of magnetic fluids from magnetite and synthetic polyelectrolytes. *Journal of colloid and interface science*, 184(2):519–526.

Merrill, E. W. and Salzman, E. W. (1983). Polyethylene oxide as a biomaterial. *ASAIO journal*, 6(2):60–64.

Miao, J., Charalambous, P., Kirz, J., and Sayre, D. (1999). Extending the methodology of x-ray crystallography to allow imaging of micrometre-sized non-crystalline specimens. *Nature*, 400(6742):342–344.

Miao, J., Chen, C.-C., Song, C., Nishino, Y., Kohmura, Y., Ishikawa, T., Ramunno-Johnson, D., Lee, T.-K., and Risbud, S. H. (2006). Three-dimensional gan- ga 2 o 3 core shell structure revealed by x-ray diffraction microscopy. *Physical review letters*, 97(21):215503.

Miao, J., Hodgson, K. O., Ishikawa, T., Larabell, C. A., LeGros, M. A., and Nishino, Y. (2003). Imaging whole escherichia coli bacteria by using single-particle x-ray diffraction. *Proceedings of the National Academy of Sciences*, 100(1):110–112.

Miao, J., Ishikawa, T., Johnson, B., Anderson, E. H., Lai, B., and Hodgson, K. O. (2002). High resolution 3d x-ray diffraction microscopy. *Physical review letters*, 89(8):088303.

Miao, J., Ishikawa, T., Robinson, I. K., and Murnane, M. M. (2015). Beyond crystallography: Diffractive imaging using coherent x-ray light sources. *Science*, 348(6234):530–535.

Miao, J., Nishino, Y., Kohmura, Y., Johnson, B., Song, C., Risbud, S. H., and Ishikawa, T. (2005). Quantitative image re-

construction of gan quantum dots from oversampled diffraction intensities alone. *Physical review letters*, 95(8):085503.

Miao, J., Sandberg, R. L., and Song, C. (2011). Coherent x-ray diffraction imaging. *IEEE Journal of selected topics in quantum electronics*, 18(1):399–410.

Miao, J., Sayre, D., and Chapman, H. (1998). Phase retrieval from the magnitude of the fourier transforms of nonperiodic objects. *JOSA A*, 15(6):1662–1669.

Moghimi, S. M., Hunter, A. C., and Murray, J. C. (2001). Long-circulating and target-specific nanoparticles: theory to practice. *Pharmacological reviews*, 53(2):283–318.

Moya, S., Dähne, L., Voigt, A., Leporatti, S., Donath, E., and Möhwald, H. (2001). Polyelectrolyte multilayer capsules templated on biological cells: core oxidation influences layer chemistry. *Colloids and Surfaces A: Physicochemical and Engineering Aspects*, 183:27–40.

Moya, S., Donath, E., Sukhorukov, G. B., Auch, M., Bäuml, H., Lichtenfeld, H., and Möhwald, H. (2000). Lipid coating on polyelectrolyte surface modified colloidal particles and polyelectrolyte capsules. *Macromolecules*, 33(12):4538–4544.

Muñoz Javier, A., Kreft, O., Semmling, M., Kempter, S., Skirtach, A. G., Bruns, O. T., del Pino, P., Bedard, M. F., Rädler, J., Käs, J., et al. (2008). Uptake of colloidal polyelectrolyte-coated particles and polyelectrolyte multilayer capsules by living cells. *Advanced materials*, 20(22):4281–4287.

Najafi, F. and Sarbolouki, M. N. (2003). Biodegradable micelles/polymersomes from fumaric/sebacic acids and poly(ethylene glycol). *Biomaterials*, 24(7):1175–1182.

Narayanan, T. (2014). Small-angle scattering. *Structure from diffraction methods*, pages 259–324.

- Narayanan, T. and Konovalov, O. (2020). Synchrotron scattering methods for nanomaterials and soft matter research. *Materials*, 13(3):752.
- Narayanan, T., Wacklin, H., Konovalov, O., and Lund, R. (2017). Recent applications of synchrotron radiation and neutrons in the study of soft matter. *Crystallography Reviews*, 23(3):160–226.
- Nermt, M. (1988). Cryotechniques in biological electron microscopy: Edited by ra steinbrecht and k. zierold springer verlag, berlin (1987), 108 figures, 297 pages.
- Neu, B., Voigt, A., Mitlöhner, R., Leporatti, S., Gao, C., Donath, E., Kiesewetter, H., Möhwald, H., Meiselman, H., and Bäuml, H. (2001). Biological cells as templates for hollow microcapsules. *Journal of microencapsulation*, 18(3):385–395.
- Neuberger, T., Schöpf, B., Hofmann, H., Hofmann, M., and Von Rechenberg, B. (2005). Superparamagnetic nanoparticles for biomedical applications: possibilities and limitations of a new drug delivery system. *Journal of Magnetism and Magnetic materials*, 293(1):483–496.
- Newton, M. C., Leake, S. J., Harder, R., and Robinson, I. K. (2010). Three-dimensional imaging of strain in a single zno nanorod. *Nature materials*, 9(2):120–124.
- Ngwuluka, N. C., Ocheke, N. A., and Aruoma, O. I. (2014). Naturapolyceutics: the science of utilizing natural polymers for drug delivery. *polymers*, 6(5):1312–1332.
- Nishino, Y., Takahashi, Y., Imamoto, N., Ishikawa, T., and Maeshima, K. (2009). Three-dimensional visualization of a human chromosome using coherent x-ray diffraction. *Physical review letters*, 102(1):018101.
- Otsuka, H., Nagasaki, Y., and Kataoka, K. (2003). Pegylated

- nanoparticles for biological and pharmaceutical applications. *Advanced drug delivery reviews*, 55(3):403–419.
- Pankhurst, Q. A., Connolly, J., Jones, S. K., and Dobson, J. (2003). Applications of magnetic nanoparticles in biomedicine. *Journal of physics D: Applied physics*, 36(13):R167.
- Panyam, J. and Labhasetwar, V. (2003). Biodegradable nanoparticles for drug and gene delivery to cells and tissue. *Advanced drug delivery reviews*, 55(3):329–347.
- Pastorino, L., Erokhina, S., and Erokhin, V. (2013). Smart nano-engineered polymeric capsules as ideal pharmaceutical carriers. *Current Organic Chemistry*, 17(1):58–64.
- Pastorino, L., Erokhina, S., Ruggiero, C., Erokhin, V., and Petrini, P. (2015). Fabrication and characterization of chitosan and pectin nanostructured multilayers. *Macromolecular Chemistry and Physics*, 216(10):1067–1075.
- Patra, J. K., Das, G., Fraceto, L. F., Campos, E. V. R., del Pilar Rodriguez-Torres, M., Acosta-Torres, L. S., Diaz-Torres, L. A., Grillo, R., Swamy, M. K., Sharma, S., et al. (2018). Nano based drug delivery systems: recent developments and future prospects. *Journal of nanobiotechnology*, 16(1):1–33.
- Pavlov, A. M., Sapelkin, A. V., Huang, X., P'ng, K. M., Bushby, A. J., Sukhorukov, G. B., and Skirtach, A. G. (2011). Neuron cells uptake of polymeric microcapsules and subsequent intracellular release. *Macromolecular bioscience*, 11(6):848–854.
- Pershan, P. S. and Schlossman, M. (2012). *Liquid surfaces and interfaces: synchrotron x-ray methods*. Cambridge University Press.
- Petrov, A. I., Volodkin, D. V., and Sukhorukov, G. B. (2005). Protein—calcium carbonate coprecipitation: a tool for protein encapsulation. *Biotechnology progress*, 21(3):918–925.

- Petukhov, A. V., Meijer, J.-M., and Vroege, G. J. (2015). Particle shape effects in colloidal crystals and colloidal liquid crystals: Small-angle x-ray scattering studies with microradian resolution. *Current opinion in colloid and interface science*, 20(4):272–281.
- Peyratout, C. S. and Daehne, L. (2004). Tailor-made polyelectrolyte microcapsules: from multilayers to smart containers. *Angewandte Chemie International Edition*, 43(29):3762–3783.
- Pfeifer, M. A., Williams, G. J., Vartanyants, I. A., Harder, R., and Robinson, I. K. (2006). Three-dimensional mapping of a deformation field inside a nanocrystal. *Nature*, 442(7098):63–66.
- Plaetzer, K., Krammer, B., Berlanda, J., Berr, F., and Kiesslich, T. (2009). Photophysics and photochemistry of photodynamic therapy: fundamental aspects. *Lasers in medical science*, 24(2):259–268.
- Pratsinis, S. E. and Vemury, S. (1996). Particle formation in gases: a review. *Powder technology*, 88(3):267–273.
- Qiu, X., Leporatti, S., Donath, E., and Möhwald, H. (2001). Studies on the drug release properties of polysaccharide multilayers encapsulated ibuprofen microparticles. *Langmuir*, 17(17):5375–5380.
- Radt, B., Smith, T. A., and Caruso, F. (2004). Optically addressable nanostructured capsules. *Advanced Materials*, 16(23–24):2184–2189.
- Razack, S. A., Suresh, A., Sriram, S., Ramakrishnan, G., Sadanandham, S., Veerasamy, M., Nagalamadaka, R. B., and Sahadevan, R. (2020). Green synthesis of iron oxide nanoparticles using hibiscus rosa-sinensis for fortifying wheat biscuits. *SN Applied Sciences*, 2(5):1–9.

- Reiffel, J. A. (2000). Formulation substitution and other pharmacokinetic variability: underappreciated variables affecting antiarrhythmic efficacy and safety in clinical practice. *The American journal of cardiology*, 85(10):46–52.
- Reimer, P. and Weissleder, R. (1996). Development and experimental use of receptor-specific mr contrast media. *Der Radiologe*, 36(2):153–163.
- Richman, E. K. and Hutchison, J. E. (2009). The nanomaterial characterization bottleneck.
- Riggio, C., Calatayud, M. P., Hoskins, C., Pinkernelle, J., Sanz, B., Torres, T. E., Ibarra, M. R., Wang, L., Keilhoff, G., Goya, G. F., et al. (2012). Poly-L-lysine-coated magnetic nanoparticles as intracellular actuators for neural guidance. *International journal of nanomedicine*, 7:3155.
- Robinson, I. and Harder, R. (2009). Coherent x-ray diffraction imaging of strain at the nanoscale. *Nature materials*, 8(4):291–298.
- Robinson, I., Libbert, J., Vartanyants, I., Pitney, J., Smilgies, D., Abernathy, D., and Grübel, G. (1999). Coherent x-ray diffraction imaging of silicon oxide growth. *Physical Review B*, 60(14):9965.
- Robinson, I. K., Vartanyants, I. A., Williams, G., Pfeifer, M., and Pitney, J. (2001). Reconstruction of the shapes of gold nanocrystals using coherent x-ray diffraction. *Physical review letters*, 87(19):195505.
- Rodenburg, J. M., Hurst, A., Cullis, A. G., Dobson, B. R., Pfeiffer, F., Bunk, O., David, C., Jefimovs, K., and Johnson, I. (2007). Hard-x-ray lensless imaging of extended objects. *Physical review letters*, 98(3):034801.
- Rodriguez, J. A., Xu, R., Chen, C.-C., Huang, Z., Jiang, H.,



- Chen, A. L., Raines, K. S., Pryor Jr, A., Nam, D., Wiegart, L., et al. (2015). Three-dimensional coherent x-ray diffractive imaging of whole frozen-hydrated cells. *IUCrJ*, 2(5):575–583.
- Roggan, A., Friebel, M., Dörschel, K., Hahn, A., and Mueller, G. J. (1999). Optical properties of circulating human blood in the wavelength range 400–2500 nm. *Journal of biomedical optics*, 4(1):36–46.
- Rolland, J. P., Maynor, B. W., Euliss, L. E., Exner, A. E., Denison, G. M., and DeSimone, J. M. (2005). Direct fabrication and harvesting of monodisperse, shape-specific nanobiomaterials. *Journal of the American Chemical Society*, 127(28):10096–10100.
- Roy, S., Parks, D., Seu, K., Su, R., Turner, J., Chao, W., Anderson, E., Cabrini, S., and Kevan, S. (2011). Lensless x-ray imaging in reflection geometry. *Nature Photonics*, 5(4):243–245.
- Rozhina, E., Danilushkina, A., Akhatova, F., Fakhrullin, R., Rozhin, A., and Batasheva, S. (2021). Biocompatibility of magnetic nanoparticles coating with polycations using a549 cells. *Journal of Biotechnology*, 325:25–34.
- Rudge, S., Kurtz, T., Vessely, C. R., Catterall, L., and Williamson, D. (2000). Preparation, characterization, and performance of magnetic iron–carbon composite microparticles for chemotherapy. *Biomaterials*, 21(14):1411–1420.
- Sayre, D. (1980). Prospects for long-wavelength x-ray microscopy and diffraction. In *Imaging Processes and Coherence in Physics*, pages 229–235. Springer.
- Sayre, D., Chapman, H., and Miao, J. (1998). On the extendibility of x-ray crystallography to noncrystals. *Acta Crystallographica Section A: Foundations of Crystallography*, 54(2):232–239.

- Schneider, G. (1998). Cryo x-ray microscopy with high spatial resolution in amplitude and phase contrast. *Ultramicroscopy*, 75(2):85–104.
- Schneider, G. and Decher, G. (2004). From functional core/shell nanoparticles prepared via layer-by-layer deposition to empty nanospheres. *Nano Letters*, 4(10):1833–1839.
- Schuetz, P. and Caruso, F. (2003). Copper-assisted weak polyelectrolyte multilayer formation on microspheres and subsequent film crosslinking. *Advanced Functional Materials*, 13(12):929–937.
- Schütt, W., Grüttner, C., Häfeli, U., Zborowski, M., Teller, J., Putzar, H., and Schümichen, C. (1997). Applications of magnetic targeting in diagnosis and therapy—possibilities and limitations: a mini-review. *Hybridoma*, 16(1):109–117.
- Seaberg, M. D., Zhang, B., Gardner, D. F., Shanblatt, E. R., Murnane, M. M., Kapteyn, H. C., and Adams, D. E. (2014). Tabletop nanometer extreme ultraviolet imaging in an extended reflection mode using coherent fresnel ptychography. *Optica*, 1(1):39–44.
- Serizawa, T., Hamada, K.-i., and Akashi, M. (2004). Polymerization within a molecular-scale stereoregular template. *Nature*, 429(6987):52–55.
- Serizawa, T., Hamada, K.-i., Kitayama, T., Fujimoto, N., Hatada, K., and Akashi, M. (2000). Stepwise stereocomplex assembly of stereoregular poly (methyl methacrylate) s on a substrate. *Journal of the American Chemical Society*, 122(9):1891–1899.
- Shapiro, D., Thibault, P., Beetz, T., Elser, V., Howells, M., Jacobsen, C., Kirz, J., Lima, E., Miao, H., Neiman, A. M., et al. (2005). Biological imaging by soft x-ray diffraction mi-

croscopy. *Proceedings of the National Academy of Sciences*, 102(43):15343–15346.

Shapiro, D. A., Yu, Y.-S., Tyliczszak, T., Cabana, J., Celestre, R., Chao, W., Kaznatcheev, K., Kilcoyne, A. D., Maia, F., Marchesini, S., et al. (2014). Chemical composition mapping with nanometre resolution by soft x-ray microscopy. *Nature Photonics*, 8(10):765–769.

Shchukin, D. G., Radtchenko, I. L., and Sukhorukov, G. B. (2003). Micron-scale hollow polyelectrolyte capsules with nano-sized magnetic  $Fe_3O_4$  inside. *Materials Letters*, 57(11):1743–1747.

Shen, Q., Bazarov, I., and Thibault, P. (2004). Diffractive imaging of nonperiodic materials with future coherent x-ray sources. *Journal of synchrotron radiation*, 11(5):432–438.

Shenoy, D. B., Antipov, A. A., Sukhorukov, G. B., and Möhwald, H. (2003). Layer-by-layer engineering of biocompatible, decomposable core-shell structures. *Biomacromolecules*, 4(2):265–272.

Shimazaki, Y., Mitsuishi, M., Ito, S., and Yamamoto, M. (1998). Preparation and characterization of the layer-by-layer deposited ultrathin film based on the charge-transfer interaction in organic solvents. *Langmuir*, 14(10):2768–2773.

Si, Y., Chen, M., and Wu, L. (2016). Syntheses and biomedical applications of hollow micro-/nano-spheres with large-through-holes. *Chemical Society Reviews*, 45(3):690–714.

Silverman, B. L., Blethen, S. L., Reiter, E. O., Attie, K. M., Neuwirth, R. B., and Ford, K. M. (2002). A long-acting human growth hormone (nutropin depot®): efficacy and safety following two years of treatment in children with growth hormone

deficiency. *Journal of Pediatric Endocrinology and Metabolism*, 15(Supplement):715–722.

Sinha, V. R. and Kumria, R. (2001). Polysaccharides in colon-specific drug delivery. *International journal of pharmaceuticals*, 224(1-2):19–38.

Skirtach, A. G., Antipov, A. A., Shchukin, D. G., and Sukhorukov, G. B. (2004). Remote activation of capsules containing ag nanoparticles and ir dye by laser light. *Langmuir*, 20(17):6988–6992.

Skirtach, A. G., Dejugnat, C., Braun, D., Susha, A. S., Rogach, A. L., Parak, W. J., Möhwald, H., and Sukhorukov, G. B. (2005). The role of metal nanoparticles in remote release of encapsulated materials. *Nano Letters*, 5(7):1371–1377.

Skirtach, A. G. and Kreft, O. (2009). Stimuli-sensitive nanotechnology for drug delivery. In *Nanotechnology in drug delivery*, pages 545–578. Springer.

Skirtach, A. G., Munoz Javier, A., Kreft, O., Köhler, K., Piera Alberola, A., Möhwald, H., Parak, W. J., and Sukhorukov, G. B. (2006). Laser-induced release of encapsulated materials inside living cells. *Angewandte Chemie International Edition*, 45(28):4612–4617.

Song, C., Bergstrom, R., Ramunno-Johnson, D., Jiang, H., Paterson, D., De Jonge, M. D., McNulty, I., Lee, J., Wang, K. L., and Miao, J. (2008a). Nanoscale imaging of buried structures with elemental specificity using resonant x-ray diffraction microscopy. *Physical review letters*, 100(2):025504.

Song, C., Jiang, H., Mancuso, A., Amirbekian, B., Peng, L., Sun, R., Shah, S. S., Zhou, Z. H., Ishikawa, T., and Miao, J. (2008b). Quantitative imaging of single, unstained viruses with coherent x rays. *Physical review letters*, 101(15):158101.

- Stadler, L.-M., Gutt, C., Autenrieth, T., Leupold, O., Rehbein, S., Chushkin, Y., and Grübel, G. (2008). Hard x ray holographic diffraction imaging. *Physical review letters*, 100(24):245503.
- Steinbüchel, A. (2005). Non-biodegradable biopolymers from renewable resources: perspectives and impacts. *Current opinion in biotechnology*, 16(6):607–613.
- Stockton, W. and Rubner, M. (1997). Molecular-level processing of conjugated polymers. 4. layer-by-layer manipulation of polyaniline via hydrogen-bonding interactions. *Macromolecules*, 30(9):2717–2725.
- Such, G. K., Quinn, J. F., Quinn, A., Tjipto, E., and Caruso, F. (2006). Assembly of ultrathin polymer multilayer films by click chemistry. *Journal of the American Chemical Society*, 128 29:9318–9.
- Sui, Z. and Schlenoff, J. B. (2004). Phase separations in pH-responsive polyelectrolyte multilayers: charge extrusion versus charge expulsion. *Langmuir*, 20(14):6026–6031.
- Sukhishvili, S. A. and Granick, S. (2000). Layered, erasable, ultrathin polymer films. *Journal of the American Chemical Society*, 122(39):9550–9551.
- Sukhorukov, G. B., Brumen, M., Donath, E., and Möhwald, H. (1999). Hollow polyelectrolyte shells: exclusion of polymers and donnan equilibrium. *The Journal of Physical Chemistry B*, 103(31):6434–6440.
- Sukhorukov, G. B., Donath, E., Davis, S., Lichtenfeld, H., Caruso, F., Popov, V. I., and Möhwald, H. (1998a). Stepwise polyelectrolyte assembly on particle surfaces: a novel approach to colloid design. *Polymers for Advanced Technologies*, 9(10-11):759–767.
- Sukhorukov, G. B., Donath, E., Lichtenfeld, H., Knippel, E.,

Knippel, M., Budde, A., and Möhwald, H. (1998b). Layer-by-layer self assembly of polyelectrolytes on colloidal particles. *Colloids and Surfaces A: physicochemical and engineering aspects*, 137(1-3):253–266.

Sun, T., Jiang, Z., Strzalka, J., Ocola, L., and Wang, J. (2012). Three-dimensional coherent x-ray surface scattering imaging near total external reflection. *Nature Photonics*, 6(9):586–590.

Takahashi, Y., Nishino, Y., Tsutsumi, R., Kubo, H., Furukawa, H., Mimura, H., Matsuyama, S., Zettsu, N., Matsubara, E., Ishikawa, T., et al. (2009). High-resolution diffraction microscopy using the plane-wave field of a nearly diffraction limited focused x-ray beam. *Physical Review B*, 80(5):054103.

Takahashi, Y., Nishino, Y., Tsutsumi, R., Zettsu, N., Matsubara, E., Yamauchi, K., and Ishikawa, T. (2010a). High-resolution projection image reconstruction of thick objects by hard x-ray diffraction microscopy. *Physical Review B*, 82(21):214102.

Takahashi, Y., Zettsu, N., Nishino, Y., Tsutsumi, R., Matsubara, E., Ishikawa, T., and Yamauchi, K. (2010b). Three-dimensional electron density mapping of shape-controlled nanoparticle by focused hard x-ray diffraction microscopy. *Nano Letters*, 10(5):1922–1926.

Tamargo, J., Le Heuzey, J.-Y., and Mabo, P. (2015). Narrow therapeutic index drugs: a clinical pharmacological consideration to flecainide. *European journal of clinical pharmacology*, 71(5):549–567.

Tartaj, P., del Puerto Morales, M., Veintemillas-Verdaguer, S., González-Carreño, T., and Serna, C. J. (2003). The preparation of magnetic nanoparticles for applications in biomedicine. *Journal of physics D: Applied physics*, 36(13):R182.

Tepper, T., Ilievski, F., Ross, C., Zaman, T., Ram, R., Sung,

- S., and Stadler, B. (2003). Magneto-optical properties of iron oxide films. *Journal of applied physics*, 93(10):6948–6950.
- Thibault, P., Dierolf, M., Menzel, A., Bunk, O., David, C., and Pfeiffer, F. (2008). High-resolution scanning x-ray diffraction microscopy. *Science*, 321(5887):379–382.
- Timko, B. P., Dvir, T., and Kohane, D. S. (2010). Remotely triggerable drug delivery systems. *Advanced materials*, 22(44):4925–4943.
- Tiwari, G., Tiwari, R., and Sriwastawa, B. (2012). L bhati, s pandey, saurabh k bannerjee. *Drug delivery systems: An updated review, International Journal of Pharmaceutical Investigation*, 2:2–11.
- Trevor, A. J., Katzung, B. G., Masters, S. B., and Kruidering-Hall, M. (2010). *Pharmacology examination and board review*. McGraw-Hill Medical New York, NY, USA:.
- Tripathi, A., Mohanty, J., Dietze, S. H., Shpyrko, O. G., Ship-ton, E., Fullerton, E. E., Kim, S. S., and McNulty, I. (2011). Dichroic coherent diffractive imaging. *Proceedings of the National Academy of Sciences*, 108(33):13393–13398.
- Tzvetkov, G., Graf, B., Fernandes, P., Fery, A., Cavalieri, F., Paradossi, G., and Fink, R. H. (2008). In situ characterization of gas-filled microballoons using soft x-ray microspectroscopy. *Soft Matter*, 4(3):510–514.
- Uhrich, K. E., Cannizzaro, S. M., Langer, R. S., and Shakesheff, K. M. (1999). Polymeric systems for controlled drug release. *Chemical Reviews-Columbus*, 99(11):3181–3198.
- Villegas, V. A. R., Ramírez, J. I. D. L., Guevara, E. H., Sicairos, S. P., Ayala, L. A. H., and Sanchez, B. L. (2020). Synthesis and characterization of magnetite nanoparticles for photocatalysis of

- nitrobenzene. *Journal of Saudi Chemical Society*, 24(2):223–235.
- Vollath, D. (2013). *Nanoparticles-nanocomposites-nanomaterials: An introduction for beginners*. John Wiley and Sons.
- Volodkin, D. V., Larionova, N. I., and Sukhorukov, G. B. (2004a). Protein encapsulation via porous caco3 microparticles templating. *Biomacromolecules*, 5(5):1962–1972.
- Volodkin, D. V., Petrov, A. I., Prevot, M., and Sukhorukov, G. B. (2004b). Matrix polyelectrolyte microcapsules: new system for macromolecule encapsulation. *Langmuir*, 20(8):3398–3406.
- Wang, X., Feng, J., Bai, Y., Zhang, Q., and Yin, Y. (2016). Synthesis, properties, and applications of hollow micro/nanostructures. *Chemical reviews*, 116(18):10983–11060.
- Wang, Y., Jacobsen, C., Maser, J., and Osanna, A. (2000). Soft x-ray microscopy with a cryo scanning transmission x-ray microscope: II. tomography. *Journal of Microscopy*, 197(1):80–93.
- Wanunu, M., Vaskevich, A., Cohen, S. R., Cohen, H., Arad-Yellin, R., Shanzer, A., and Rubinstein, I. (2005). Branched coordination multilayers on gold. *Journal of the American Chemical Society*, 127(50):17877–17887.
- Widder, K. J., Morris, R. M., Poore, G. A., Howard, D. P., and Senyei, A. E. (1983). Selective targeting of magnetic albumin microspheres containing low-dose doxorubicin: total remission in yoshida sarcoma-bearing rats. *European Journal of Cancer and Clinical Oncology*, 19(1):135–139.
- Widder, K. J., Senyei, A. E., and Scarpelli, D. G. (1978). Magnetic microspheres: a model system for site specific drug delivery



in vivo. *Proceedings of the Society for Experimental Biology and Medicine*, 158(2):141–146.

Wilkinson, J. (2003). Nanotechnology applications in medicine. *Medical device technology*, 14(5):29–31.

Williams, G., Pfeifer, M., Vartanyants, I., and Robinson, I. (2003). Three-dimensional imaging of microstructure in au nanocrystals. *Physical review letters*, 90(17):175501.

Williams, G., Quiney, H., Dhal, B., Tran, C., Nugent, K. A., Peele, A., Paterson, D., and De Jonge, M. (2006). Fresnel coherent diffractive imaging. *Physical review letters*, 97(2):025506.

Xu, K., Sun, W., Shao, Y., Wei, F., Zhang, X., Wang, W., and Li, P. (2018). Recent development of peakforce tapping mode atomic force microscopy and its applications on nanoscience. *Nanotechnology Reviews*, 7(6):605–621.

Xu, R., Salha, S., Raines, K. S., Jiang, H., Chen, C.-C., Takahashi, Y., Kohmura, Y., Nishino, Y., Song, C., Ishikawa, T., et al. (2011). Coherent diffraction microscopy at spring-8: instrumentation, data acquisition and data analysis. *Journal of synchrotron radiation*, 18(2):293–298.

Yan, Y., Such, G. K., Johnston, A. P., Best, J. P., and Caruso, F. (2012). Engineering particles for therapeutic delivery: prospects and challenges. *ACS nano*, 6(5):3663–3669.

Yashchenok, A. M., Bratashov, D. N., Gorin, D. A., Lomova, M. V., Pavlov, A. M., Sapelkin, A. V., Shim, B. S., Khomutov, G. B., Kotov, N. A., Sukhorukov, G. B., et al. (2010a). Carbon nanotubes on polymeric microcapsules: Free-standing structures and point-wise laser openings. *Advanced Functional Materials*, 20(18):3136–3142.

Yashchenok, A. M., Delcea, M., Videnova, K., Jares-Erijman,

- E. A., Jovin, T. M., Konrad, M., Moehwald, H., and Skirtach, A. G. (2010b). Enzyme reaction in the pores of  $\text{CaCO}_3$  particles upon ultrasound disruption of attached substrate-filled liposomes. *Angewandte Chemie International Edition*, 49(44):8116–8120.
- Yu, J.-H., Lee, C.-W., Im, S.-S., and Lee, J.-S. (2003). Structure and magnetic properties of  $\text{SiO}_2$  coated  $\text{Fe}_2\text{O}_3$  nanoparticles synthesized by chemical vapor condensation process.
- Zborowski, M., Moore, L. R., Sun, L., and Chalmers, J. J. (1997). Continuous-flow magnetic cell sorting using soluble immunomagnetic label. In *Scientific and Clinical Applications of Magnetic Carriers*, pages 247–260. Springer.
- Zelikin, A. N., Li, Q., and Caruso, F. (2006). Degradable polyelectrolyte capsules filled with oligonucleotide sequences. *Angewandte Chemie International Edition*, 45(46):7743–7745.
- Zhang, Y., Chan, H. F., and Leong, K. W. (2013). Advanced materials and processing for drug delivery: the past and the future. *Advanced drug delivery reviews*, 65(1):104–120.
- Zuo, J., Vartanyants, I., Gao, M., Zhang, R., and Nagahara, L. (2003). Atomic resolution imaging of a carbon nanotube from diffraction intensities. *Science*, 300(5624):1419–1421.

---

## LIST OF PUBLICATIONS

1. Erokhina, S., L. Pastorino, D. Di Lisa, A. G. Kiiamov, D. A. Tayurskii, S. Iannotta, V. Erokhin, and **A. R. Faizullina**. "3D structure reconstruction of nanoengineered polymeric capsules using Coherent X-Ray diffraction imaging." *MethodsX* 8 (2021): 101230.  
<https://doi.org/10.1016/j.mex.2021.101230>
2. Erokhina, S., L. Pastorino, D. Di Lisa, Airat Gazinurovich Kiiamov, **A. R. Faizullina**, Dmitrii Al'bertovich Tayurskii, S. Iannotta, and V. Erokhin. "Coherent X-ray diffraction imaging of nanoengineered polymeric capsules." *JETP Letters* 106, no. 8 (2017): 540-543.  
<https://doi.org/10.1134/S0021364017200036>
3. Erokhina, S., L. Pastorino, D. Di Lisa, Airat Gazinurovich Kiiamov, **A. R. Faizullina**, Dmitrii Al'bertovich Tayurskii, S. Iannotta, and V. Erokhin. "Coherent X-ray diffraction imaging of nanoengineered polymeric capsules." *Pis'ma v ZhETF*, 106, no. 8 (2017): 521–522.  
<https://doi.org/10.7868/S0370274X17200115>
4. Blokhin, Dmitriy S., **Adeliya R. Fayzullina**, Andrei V.

Filippov, Farida Kh Karataeva, and Vladimir V. Klochkov. "Spatial structure of fibrinopeptide B in water solution with DPC micelles by NMR spectroscopy." *Journal of Molecular Structure* 1102 (2015): 91-94.

<https://doi.org/10.1016/j.molstruc.2015.08.059>

5. **Faizullina, Adeliia R.**, Dmitriy S. Blokhin, Aleksandra M. Kusova, and Vladimir V. Klochkov. "Investigation of the effect of transition metals (MN, CO, GD) on the spatial structure of fibrinopeptide B by NMR spectroscopy." *Journal of Molecular Structure* 1204 (2020): 127484.

<https://doi.org/10.1016/j.molstruc.2019.127484>

## **ACKNOWLEDGEMENT**

Throughout the writing of this thesis I have received a great deal of support and assistance.

Firstly, I would like to thank my supervisor, Dr. Victor Erokhin, whose expertise was invaluable in formulating the research questions and methodology. His insightful feedback pushed me to sharpen my thinking and brought my work to a higher level. Without his assistance and dedicated involvement in every step throughout the process, this paper would have never been accomplished. I would like to thank you very much for your support and understanding over these past years.

I am sincerely grateful to Dr. Svetlana Erokhina for the valuable guidance throughout my studies. I do appreciate your support and all the opportunities and advice I was given meanwhile my stay and work in Parma. I am grateful her limitless talents, unparalleled enthusiasm, energy, and personal care.

I would like to acknowledge my colleagues from IMEM – CNR for their wonderful collaboration and help. I would particularly like to single out Dr. Salvatore Iannotta. He provided me with the tools that I needed to choose the right direction and successfully complete my thesis. Huge thanks to Dr. Silvia Battistoni, Dr. Valentina Ricci, Dr. Francesca Rossi. Many thanks to Dr. Laura Pastorino from University of Genoa for her advices and suggestions.

I would like to thank my lab mates and friends: Regina and Roman for their support and for a good time. I also want to

thank Stefania Boi for her help in the experiment and for the fun time we have spent together. Also, I want to thank all my Parma's friends Giulia and Simona for being a significant part of this long and sometimes difficult experience far from home and for being lovely friends and neighbors. My gratitude also goes to my wonderful friend Olga, who has supported me over the past few years even despite the distance between us.

Last but not least I am extremely grateful to my parents for their love, prayers, caring and sacrifices for educating and preparing me for my future. You are always there for me. Finally, I could not have completed this thesis without the support of my sister, Dilyara for the keen interest shown to complete this thesis successfully.

I would like to thank the evaluators. Their valuable comments made it possible to provide the work in an improved form.

Finally, my thanks go to all the people who have supported me to complete the research work directly or indirectly.

**Adeliia**